

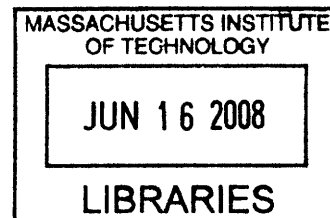
Reversible Stimulus-Responsive Polymers for the Control of the Surface Interfacial and Nanomechanical Properties

by

Miao Ye

M.S. Chemical Engineering
Tsinghua University, China, 2002

B.S. Polymers Science and Engineering
Beijing University of Chemical Technology, China, 1999



ARCHIVES

Submitted to the Department of Materials Science and Engineering in Partial
Fulfillment of the Requirements for the Degree of

Doctor of Philosophy in Materials Science and Engineering

at the

MASSACHUSETTS INSTITUTE OF TECHNOLOGY

February 2008

© 2008 Massachusetts Institute of Technology. All Rights Reserved.

Author.....

Department of Materials Science and Engineering
January 17th, 2008

Certified by.....

Christine Ortiz
Associate Professor of Materials Science and Engineering
Thesis Supervisor

Accepted by.

Samuel M. Allen
POSCO Professor of Physical Metallurgy
Chairman, Departmental Committee on Graduate Students

Reversible Stimulus-Responsive Polymers for the Control of the Surface Interfacial and Nanomechanical Properties

by

Miao Ye

Submitted to the Department of Materials Science and Engineering
on January 17th, 2008 in Partial Fulfillment of the
Requirements for the Degree of Doctor of Philosophy in
Materials Science and Engineering

Abstract

Surfaces with reversible stimulus-responsive properties have great potential for a wide variety of applications, such as transport, separation, and detection of biomolecules, controlled adhesion, friction, and lubrication in microfluidic systems, and force or displacement generation in micro- and nanoscale devices. Surface bound stimulus-responsive polymers are ideal candidates for above applications due to their conformational sensitivity to many stimuli with controlled molecular weight, composition, architecture and topology. In this thesis, one particular class of stimulus-responsive polymers, pH-sensitive comb-type graft copolymers with ionizable main chain segments was investigated. Mono(end)-functional thiol-terminated poly(methacrylic acid-g-ethylene glycol) (HS-poly(MAA-g-EG)) with three different macromolecular architectures (number average molecular weight, $M_n = 27K$, PEG graft density, PEG(%) = 7.7%, backbone contour length, $L_{\text{contour}} = 41.1$ nm; $M_n = 15K$, PEG(%) = 8.8%, $L_{\text{contour}} = 22.1$ nm; $M_n = 17K$, PEG(%) = 1.9%, $L_{\text{contour}} = 39.8$ nm) have been synthesized via atomic transfer radical polymerization and characterized by 1H NMR, GPC and FT-IR.

Stimulus responsive surfaces were prepared via chemically end-attached "brush-brushes" formed by chemisorption of the copolymers on Au substrates. Chemically specific high resolution force spectroscopy (HRFS) was carried out with probe tips (end radius ~50 nm) functionalized with $HS(CH_2)_{10}COOH$ (a carboxy-terminated self-assembling monolayer or COOH-SAM) to measure the normal nanoscale interaction forces, F , as a function of probe-tip sample separation distance, D , in a series of aqueous buffer solutions of varied pH (=4-9) and constant ionic strength (IS=0.005M NaCl). The higher PEG grafting density surfaces (27K, 15K) exhibited the unique property of "nanomechanical switching" with pH, i.e. the normal intersurface force inverted from net repulsive (high pH, ionized uncomplexed side chains) to net attractive (low pH, side-chain/main-chain hydrogen bonding complexation). The 17K polymer brushes did not exhibit nanomechanical switching and maintained a slightly repulsive intersurface force at low pH.

Surface plasmon resonance (SPR) was employed to assess the adsorption of human serum albumin (HSA) to these poly(MAA-g-EG) brushes in aqueous buffer solutions of varying pH. Polymers with a higher grafting density of hydrophilic PEG side chains and

longer polymer backbones showed much less HSA adsorption at high pH and more protein adsorption at low pH. Surprisingly, HSA adsorption was found to be greatly amplified at intermediate pH6 (~1.4-1.8 × greater than that of the hydrophobic state of polymer layers at pH4). Higher PEG grafting density and a longer polymer backbone demonstrated larger protein adsorption amplification at pH6, which may be due to increased molecular mobility/disorder at a metastable state of the conformational transition.

For the lateral force interaction between the end-grafted polymer layers and a probe tip (nominal radius ~ 50 nm) functionalized with OH-SAM ($\text{HS}(\text{CH}_2)_{11}\text{OH}$), as pH decreased, both the 27K and 17K polymer layers exhibit an abrupt change in lateral proportionality coefficient (ratio of lateral force to normal force) between pH7.1 and pH6 with larger lateral proportionality coefficients, $\mu \sim 0.63-0.89$ at pH 4-6 and decreased $\mu \sim 0.12-0.34$ at pH 7.1-9. The 27K polymer had relatively higher μ values at pH < 6 (0.89 ± 0.19) but smaller μ at pH > 7.1 (0.21 ± 0.04) than the 17K polymer, indicating that a more dramatic change in lateral force coefficient is expected for stimulus-responsive graft copolymers with higher side chain grafting densities.

Thesis Supervisor: Christine Ortiz

Title: Associate Professor of Materials Science and Engineering

Acknowledgements

First of all, I would like to express my deep gratitude to my parents, particularly my father, who had passed away before I was about to graduate. Like all parents who have high expectations on their children, they always encourage and support me in the progress of my life. It was regret for him not seeing my finishing PhD program. He would be happy and proud to see where I stand today. To my mother, who has done so much for me, there are no words can carry my thankfulness.

I would like to like to thank many other people for their encouragements, help and support during my days at MIT. Without them, my life, studying and research experience in the pursuit of the doctorate degree wouldn't have been as colorful and enjoyable as it was. To Professor Christine Ortiz, my advisor and mentor: Her support and guidance on my study and research at MIT is of great help and value. I was influenced tremendously by her endless enthusiasm and endeavor in both research and teaching. Her advisory on my thesis research always pushes me to see new angles in the research direction. Her careful revisions and comments on my manuscripts of papers and reports helped me greatly hone my scientific writing skills. I am grateful for all the things she has done for me and the whole research group.

Among all my friends at MIT, the officers and members of the MIT Chinese Students and Scholars Association provided a great amount of help and services to many Chinese students like me to make our life and study at MIT easier and more rewarding. In particular, I am greatly indebted to the friendship I have made with Andy Yu Wang, Yuhua Hu, Xuemin Chi, Song Gao. Without their company, I wouldn't have accomplished my first half-marathon, first down-hill skiing on dark-diamond trails and many more first-time experiences. It was a lot of fun hanging out with them and they will be treasured in my memory forever.

To my friends at the Department of Materials Science and Engineering and Ortiz Research Group members and alumni, I would like to thank to Ming Tang, Dong Zhang, Delphine Dean, Lin Han, Laurel Ng, Jennifer Vandiver, Celia Macias, Jonathan Tejada (UROP), Jane Yoon (UROP), Emily Chen (UROP) and Fredrick Porter (UROP). Discussions with Ming Tang have always been informative on my understanding of thermodynamics, quantum mechanics, solid state physics and ceramics materials. Ortiz group members and alumni offered me kindly and generous help on AFM and MFP training, data modeling, experiments troubleshooting or contributed to some work presented in this thesis.

Finally, I would like to thank to my thesis committee members: Professor Paula T. Hammond, Professor Michael F. Rubner and Professor Anne Mayes. Their guidance and suggestions were very helpful and enlightening.

Contents

Chapter 1 Introduction	18
1.1 Background.....	18
1.2 Objective.....	22
1.3 Overview.....	24
Chapter 2 Synthesis of Mono(thiol)-Terminated Poly(methacrylic acid- <i>g</i> -ethylene glycol)	25
2.1 Introduction.....	25
2.2 Materials and Experiments.....	27
2.3 Characterizations.....	30
2.4 Results and Discussion.....	31
2.5 Conclusions.....	39
Chapter 3 Conformational Transition of End-Grafted Poly(methacrylic acid- <i>g</i> -ethylene glycol) Polymer Layer on Planar Substrate	40
3.1 Introduction.....	40
3.2 Methods.....	41
3.2.1 Sample Preparation.....	41
3.2.2 Contact Mode Atomic Force Microscopy in pH Buffer Solutions....	42
3.3 Results and Discussion.....	44
3.4 Conclusions.....	53
Chapter 4 Nanomechanical Switching in Normal Intersurface Interactions of	

End-Grafted Poly(methacrylic acid-g-ethylene glycol) Polymer Layer on Planar Substrate	55
4.1 Introduction.....	55
4.2 Methods.....	56
4.2.1 Sample Preparation.....	56
4.2.2 High Resolution Force Spectroscopy (HRFS).....	58
4.3 Results and Discussion.....	61
4.3.1 HRFS on Approach.....	61
4.3.2 HRFS on Retract.....	70
4.3.3 Comparison between HRFS on Approach and Predictions of a Poisson-Boltzmann Based Theoretical Model for Electrostatic Forces.....	76
4.4 Conclusions.....	83

Chapter 5 Nanomechanical Switching in Lateral Intersurface Interactions of End-Grafted Poly(methacrylic acid-g-ethylene glycol) Polymer

Layers on Planar Substrate	85
5.1 Introduction.....	85
5.2 Methods.....	86
5.2.1 Sample Preparation.....	86
5.2.2 Lateral Force Spectroscopy.....	86
5.3 Results and Discussion.....	89
Lateral Intersurface Interactions Using a Nanosized Probe Tip.....	89
5.4 Conclusions.....	96

Chapter 6 Human Serum Albumin (HSA) Adsorption on End-Grafted

Poly(methacrylic acid-g-ethylene glycol) Polymer Layer	98
6.1 Introduction.....	98
6.2 Methods.....	99
6.2.1 Materials and Sample Preparation.....	99

6.2.2 Surface Plasmon Resonance.....	99
6.3 Results and Discussion.....	100
6.3.1 HSA Adsorption Triggered by pH.....	100
6.3.2 HSA Adsorption Amplification at Intermediate pH.....	104
6.4 Conclusions.....	105
 Appendix Au Nanoparticles functionalized with HS-Poly(methacrylic acid- g-ethylene glycol)	 107
References	111

Figures

1.1	<i>Molecular Force Probe (MFP) from Asylum Research, Inc</i>	21
1.2	Schematic depiction of “Nanoscale Valves” and reversible “switch” under stimulus.....	23
1.3	a) Displacement of nanoscale devices; (b) Stimulus-responsive structures.....	23
2.1	Schematic of a conformational transition of a chemically end-grafted stimulus-responsive side-chain graft copolymer (insets show molecular interactions for poly(MAA- <i>g</i> -EG)). The bar extending from the methyl group of methacrylic acid to the methylene group of PEG stands for hydrophobic interaction while the dashed line between -COOH and -O- represents H-bonding, which shows the collapsed conformation of the end-grafted polymer layers is due to the H-bonding and further stabilized by the intramolecular hydrophobic interaction in acidic aqueous media.....	26
2.2	Atom transfer radical polymerization chemical reaction scheme for synthesis of mono(thiol)-terminated poly(methacrylic acid- <i>g</i> -ethylene glycol) or HS-poly(MAA- <i>g</i> -EG).....	29
2.3	¹ H nuclear magnetic resonance (NMR) spectra in methanol- <i>d</i> ₄ of (a) protected mono(thiol)-terminated poly(<i>tert</i> -butyl methacrylate- <i>g</i> -ethylene glycol) or poly(<i>tert</i> -BMA- <i>g</i> -EG) _{20K} , (b) mono(thiol)-terminated HS-poly(<i>tert</i> -BMA- <i>g</i> -EG) _{20K} , and (c) mono(thiol)-terminated poly(methacrylic acid- <i>g</i> -ethylene glycol) or HS-poly(MAA- <i>g</i> -EG) _{15K} . The numerical subscript in the abbreviated polymer name labels refer to the number average molecular weight, <i>M</i> _n , of the graft	

	copolymer in g/mol (as measured by ^1H NMR) and “K” is an abbreviation for 1000. The peak numbers labeled in each NMR spectrum correspond to the protons labeled in the chemical structure insets at the top of each NMR spectrum.....	34
2.4	Schematics of mono(thiol)-terminated poly(methacrylic acid- <i>g</i> -ethylene glycol) or HS-poly(MAA- <i>g</i> -EG) graft copolymers synthesized in this study with contour length dimensions for PMAA (poly(methacrylic acid)) backbone, PEG (poly(ethylene glycol)) side chains, and PEG side chain density drawn approximately to scale. The schematics are not meant to indicate the actual spatial distribution of PEG side chains along the MAA backbone or the conformation of the polymer chains. The numerical subscript in the abbreviated polymer name labels refer to the number average molecular weight, M_n , of the graft copolymer in g/mol (as measured by ^1H nuclear magnetic resonance) and “K” is an abbreviation for 1000.....	37
2.5	Fourier transform infrared (FTIR) spectra of (a)after hydrolysis, mono(thiol)-terminated poly(methacrylic acid- <i>g</i> -ethylene glycol) or HS-poly(MAA- <i>g</i> -EG) _{27K} and (b) before hydrolysis, mono(thiol)-terminated poly(<i>tert</i> butyl methacrylate- <i>g</i> -ethylene glycol) or HS-poly(<i>tert</i> -BMA- <i>g</i> -EG) _{35K} . The numerical subscript in the abbreviated polymer name labels refer to the number average molecular weight, M_n , of the graft copolymer in g/mol (as measured by ^1H nuclear magnetic resonance) and “K” is an abbreviation for 1000.....	38
3.1	(a) Side view schematic of height measurement using atomic force microscope contact mode imaging on micro contact printed surface of graft copolymer and hydroxyl-terminated self-assembled monolayer (OH-SAM) where R_{tip} is the probe tip end radius, and (b) schematic of top view of microcontact printed surface.....	43
3.2	Advancing contact angles of gold (zero hours) and chemically end-grafted poly(methacrylic acid- <i>g</i> -ethylene glycol) or poly(MAA- <i>g</i> -EG) _{27K} polymer layers as a function of chemisorption incubation time. The numerical subscript in the abbreviated polymer name labels refer to the number average molecular weight,	

	M_n , of the graft copolymer in g/mol as measured by ^1H nuclear magnetic resonance and “K” is an abbreviation for 1000. Hi-lo bars represent one standard deviation. The number of measurements taken was on three different locations of the polymer layers for each incubation time.....	45
3.3	AFM contact mode height images of micro-contact printed samples of end-grafted poly(methacrylic acid- <i>g</i> -ethylene glycol) or poly(MAA- <i>g</i> -EG) _{15K} layers (inside the line patterns) and a hydroxy-terminated self-assembling monolayer (OH-SAM, outside the line patterns) and as a function of pH (ionic strength = 0.001M) taken with an OH-SAM functionalized probe tip. The minimum possible normal imaging force was employed. The numerical subscript in the abbreviated polymer name labels refer to the number average molecular weight, M_n , of the graft copolymer in g/mol as measured by ^1H nuclear magnetic resonance and “K” is an abbreviation for 1000.....	47
3.4	Heights of end-grafted poly(methacrylic acid- <i>g</i> -ethylene glycol) or poly(MAA- <i>g</i> -EG) polymer layers relative to a hydroxy-terminated self-assembling monolayer measured by contact mode atomic force microscopy at the lowest possible imaging force as a function of pH in 0.005M buffered aqueous solution on micro-contact printed samples. Hi-lo bars represent one standard deviation. Heights are the average of eight scan lines per image.....	48
3.5	Heights of end-grafted poly(methacrylic acid- <i>g</i> -ethylene glycol) or poly(MAA- <i>g</i> -EG) polymer layers relative to a hydroxy-terminated self-assembling monolayer measured by contact mode atomic force microscopy as a function of normal imaging force in 0.005M buffered aqueous solution on micro-contact printed samples. Hi-lo bars represent one standard deviation. Heights are the average of eight scan lines per image. (a) pH9 and (b) pH4.....	50
4.1	Schematic illustration of the pH-stimulated conformational change of poly(methacrylic acid- <i>g</i> -ethylene glycol) or poly(MAA- <i>g</i> -EG) polymer via high resolution force spectroscopy measurement on the polymer layer chemically end-attached to Au by probe tip. The scale is based on the data of the 15K polymer	

and the probe tip radius is set as 50 nm. X stands for -COOH groups. Y stands for O atoms.....59

4.2 Averaged nanomechanical data measured on approach between a probe tip functionalized with a carboxy-terminated self-assembling monolayer or COOH-SAM (HS-(CH₂)₁₀COOH, probe tip end radius, R_{tip} ~50 nm) and chemically end-grafted poly(methacrylic acid-*g*-ethylene glycol) or poly(MAA-*g*-EG) layers as a function of pH at a constant ionic strength of 0.005M. Hi-lo bars represent one standard deviation for $n=60$ experiments; (a) 27K, (b) 15K, and (c) 17K. The inset schematic does not represent the actual conformation of the polymer (as this is changing with pH).....62-64

4.3 Averaged nanomechanical data measured on approach between a probe tip functionalized with a carboxy-terminated self-assembling monolayer or COOH-SAM (HS-(CH₂)₁₀COOH, probe tip end radius, R_{tip} ~50 nm) and COOH-SAM (HS-(CH₂)₁₀COOH) as a function of pH at a constant ionic strength of 0.005M. Hi-lo bars represent one standard deviation for $n=60$ experiments.....66

4.4 Nanoscale compressive stress vs. strain plot calculated from nanomechanical data measured on approach between a probe tip functionalized with a carboxyl-terminated self-assembling monolayer and chemically end-grafted poly(methacrylic acid-*g*-ethylene glycol) or poly(MAA-*g*-EG) layers at pH9 and a constant ionic strength of 0.005M. Hi-lo bars represent one standard deviation.....68

4.5 Force versus [1-Normalized Height] derived from Height versus Force measurement via contact mode AFM, where left- and right- error bars represent the standard deviation of eight scan lines in height measurement. The probe tip was functionalized with a hydroxyl-terminated self-assembling monolayer. The AFM imaging was conducted at pH9 and a constant ionic strength of 0.005M.....69

- 4.6 Nanomechanical data measured on retract between a probe tip functionalized with a carboxyl-terminated self-assembling monolayer (HS-(CH₂)₁₀COOH, probe tip end radius, $R_{tip} \sim 50$ nm) and chemically end-grafted poly(methacrylic acid-g-ethylene glycol) or poly(MAA-g-EG) layers as a function of pH at a constant ionic strength of 0.005M. (a) Nanoscale adhesion force (maximum force exhibited on retraction) normalized by the probe tip end-radius where the hi-low bars represent one standard deviation and (b) Percentage of retraction curves exhibiting adhesion ($n= 60$ experiments).....71
- 4.7 Nanomechanical data measured on retract between a probe tip functionalized with a carboxyl-terminated self-assembling monolayer and a chemically end-grafted poly(methacrylic acid-g-ethylene glycol) or poly(MAA-g-EG) layers at pH4 and a constant ionic strength of 0.005M (probe tip end radius, $R_{tip} \sim 50$ nm). Typical individual curves are shown.....72
- 4.8 Probability histograms for nanoscale adhesion between a probe tip functionalized with a carboxyl-terminated self-assembling monolayer and a chemically end-grafted poly(methacrylic acid-g-ethylene glycol) or poly(MAA-g-EG)_{27K} layer as a function of pH and a constant ionic strength of 0.005M. (a) 27K, (b) 15K, and (c) 17K. Hi-lo bars represent one standard deviation for $n= 60$ experiments.....73-75
- 4.9 Comparison of the theoretical predictions of Poisson-Boltzmann based electrostatic double layer surface and volume charge models with nanomechanical data on approach of a probe tip functionalized with a carboxyl-terminated self-assembling monolayer (HS-(CH₂)₁₀COOH, probe tip end radius, $R_{tip} \sim 50$ nm) and chemically end-grafted poly(methacrylic acid-g-ethylene glycol)_{27K} layers at (a) pH9 (model parameters were estimated as detailed in the Supplementary Materials section and fixed to $\sigma_{tip} = \sigma_{COO^-}$ (C/m²) = -0.021, $\sigma_{sub} = \sigma_{polymer}$ (C/m²) = -1.2992, $\rho_{sub} = \rho_{polymer}$ (C/m³) = -4.64×10^7) (b) pH6 ($\sigma_{tip} = \sigma_{COO^-}$ (C/m²) = -0.01596, $\sigma_{sub} = \sigma_{polymer}$ (C/m²) = -0.98738, $\rho_{sub} = \rho_{polymer}$ (C/m³) = -4.91×10^7), (c) pH5 ($\sigma_{tip} = \sigma_{COO^-}$ (C/m²) = -0.00504, $\sigma_{sub} = \sigma_{polymer}$ (C/m²) = -0.31224) and a

constant ionic strength of 0.005M (see Supplementary Material for details of calculations). Experimental data represents averages of $n= 60$ experiments.....77-78

5.1 Lateral Force Microscopy images of chemically end-grafted 17K poly(MAA-g-EG) layers obtained via contact mode AFM on micro-contact printed samples at scan angle = 90° under normal force ~ 4 nN in aqueous buffer solutions of pH 9 - pH 4 and IS=0.005M. The nanosized probe tip was -OH functionalized.....91

5.2 Lateral force versus normal force of the chemically end-grafted 17K, 27K poly(MAA-g-EG) layers via contact mode AFM on micro-contact printed samples at scan angle = 90° in aqueous buffer solutions of pH 9-4 (IS=0.005M) using -OH functionalized probe tip. Every data point represents the mean and standard deviation of 16 independent lateral signal loops under a fixed normal load.....93

5.3 Lateral force versus height of the chemically end-grafted 17K, 27K poly(MAA-g-EG) layers via contact mode AFM on micro-contact printed samples at scan angle = 90° in aqueous buffer solutions of pH 9-4 (IS=0.005M) using -OH functionalized probe tip. Every data point represents the mean and standard deviation of 16 independent lateral signal loops under a fixed normal load.....94

5.4 Lateral proportionality coefficients of the chemically end-grafted 17K and 27K poly(MAA-g-EG) layers via contact mode AFM on micro-contact printed samples at scan angle = 90° in aqueous buffer solutions of pH 9-4 (IS=0.005M) using -OH functionalized probe tip.....96

6.1 Typical SPR response of HSA adsorption on the end-grafted poly(MAA-g-EG) surfaces at different pH: (a)27K, (b)15K, (c)17K and average SPR response of HSA adsorption as a function of pH on the 27K, 15K and 17K polymer surfaces (d). Baselines are all zeroed in (a), (b) and (c). Hi-low bars in (d) represent one standard deviation for four different experiments.....102

6.2	Average surface plasmon resonance response for human serum albumin adsorption as a function of pH on the 27K, 15K and 17K end-grafted poly(MAA-g-EG) substrate and COOH-SAM (HS(CH ₂) ₁₀ COOH) on Au as a function of pH (IS =0.005 M). Hi-low bars represent one standard deviation for four different experiments.....	103
A1	TEM images of (a) 5 nm Au nanoparticles and (b) 10 nm Au nanoparticles.....	108
A2	Hydrodynamic size of Au nanoparticles (nominal size 20 nm) capped with 17K poly(methacrylic acid-g-ethylene glycol) copolymer in aqueous buffer solutions of pH9 – pH4 at IS = 0.005M.....	109
A3	TEM images of (a) 5 nm Au nanoparticles and (b) 15K polymer-capped nm Au nanoparticles.....	110

List of Tables

- 2.1 Parameters describing the macromolecular architecture of the thiol-protected poly(*tert* butyl methacrylate-*g*-ethylene glycol) or poly(*tert*-BMA-*g*-EG) graft copolymers as determined by ^1H nuclear magnetic resonance (NMR) in methanol- d_4 and gel permeation chromatography (GPC) in tetrahydrofuran (THF). The numerical subscript in the abbreviated polymer name labels refer to the number-average molecular weight, M_n , of the graft copolymer in g/mol and “K” is an abbreviation for 1000, M_w is the weight average molecular weight measured by GPC, MW_{PEG} is the known molecular weight of each PEG chain, The PEG graft density (%) is defined as N_{PEG} divided by the total number of backbone monomers, N_{PEG} is the average number of PEG chains per poly(*tert*-BMA) or PMAA chain, DP_n is the number-average degree of polymerization, EG/*tert*-BMA (mole ratio) is calculated as the $DP_n(\text{EG})/DP_n(\text{tert-BMA})= DP_n(\text{EG})/DP_n(\text{MAA})$, and L_{contour} is the average contour length calculated from the known molecular weights assuming *ttt* conformations for the PMAA and *ttg* conformations for the PEG. The M_n of corresponding thiol-terminated poly(methacrylic acid-*g*-ethylene glycol) or HS-poly(MAA-*g*-EG) copolymers were calculated after removal of the *tert*-butyl groups and replacement with H atoms.....35
- 3.1 Summary of swelling factors for heights of poly(acrylic acid) or PAA and poly(methacrylic acid) or PMAA end-anchored* or chemically end-grafted[†] weak polyelectrolyte layers as a function of pH compared to poly(methacrylic acid-*g*-ethylene glycol) or poly(MAA-*g*-EG) reported in this paper where the swelling factor, s , is defined as the maximum height divided by the minimum height, Γ is the grafting density (chains/nm²), DP_n is the number average degree of

polymerization, and μCP is micro contact printing. s for the poly(MAA-*g*-EG) was calculated with the addition of 1.4 nm to each of the heights since the reported values (Fig. 9) were relative to the $\text{SH}(\text{CH}_2)_{11}\text{OH}$ self-assembling monolayer.[¶] The DP_n in Konradi, et al. was not reported but expected to be very large since the collapsed height of the layer at low pH was ~ 600 nm.....52

4.1 Characterization data of thiol-terminated poly(methacrylic acid-*g*-ethylene glycol) or HS-poly(MAA-*g*-EG) comb-type graft copolymers as determined by ^1H nuclear magnetic resonance (NMR), as reported previously. The numerical subscript in the abbreviated polymer name labels refer to the number-average molecular weight, M_n , in g/mol and “K” is an abbreviation for 1000, the poly(ethylene glycol) or PEG graft density (%) is defined as N_{PEG} divided by the total number of backbone monomers where N_{PEG} is the average number of PEG chains per poly(methacrylic acid) or PMAA chain, and L_{contour} is the average contour length calculated from the known molecular weights assuming *ttt* conformations for the PMAA and *ttg* conformations for the PEG, which is known to exist in aqueous solution. The schematics of the polymers are not meant to indicate the actual conformation. The packing density and contact angle of the chemically end-grafted polymer layers are also given.....57

4.2 Fixed parameters in the surface charge and volume charge models used to predict the interaction force versus distance when a probe tip ($R_{\text{tip}} \sim 50\text{nm}$) functionalized with a carboxyl-terminated self-assembling monolayer approaches a chemically end-grafted poly(methacrylic acid-*g*-ethylene glycol) or poly(MAA-*g*-EG) layer at pH9, pH6, and pH5 and a constant ionic strength of 0.005M. $\sigma_{\text{tip}} = \sigma_{\text{COO}^-}$ is the tip surface charge density due to the COO^- -SAM determined by equation (a), $\sigma_{\text{sub}} = \sigma_{\text{polymer}}$ (C/m^2) is the substrate surface charge density due to the polymer layer (C/m^2) determined by equation (b) in the surface charge model, and $\rho_{\text{sub}} = \rho_{\text{polymer}}$ is the volume charge density (C/m^3) in the volume charge model which is determined by equation (c) above.....81

Chapter 1

Introduction

1.1 Background

Surfaces with dynamically controlled reversible stimulus-responsive interfacial properties have great promise in a variety of applications including, for example; drug delivery, transport, separation, and detection of biomolecules, directed cellular function, controlled adhesion, friction, and lubrication in microfluidics, force generation in micro- and nanoscale devices, and varying bulk mechanical properties of hierarchical materials. Surface bound or confined stimulus-responsive polymers are ideal for such applications given the fact that their conformational sensitivity to a wide variety of parameters (e.g. solvent quality, pH, ionic strength, type of salt, light, temperature, and electrical potentials) can be tailored by molecular weight, composition, architecture, and topology; and devices based on entropy of chains, surface energies and specific segmental interactions can be readily made[1, 2]. Research in this area has been focused on wettability, for example; use of a 16-(mercapto)hexadecanoic acid self-assembling monolayer (SAM) which exhibits a reversible conformational transition in response to an electrical potential[3], end-grafted poly(N-isopropylacrylamide) "brushes" which are temperature sensitive [4], and pH and ionic strength dependent effects that arise from polyelectrolytic electrostatic interactions [5]. Of particular interest, are polymers which exhibit sudden and dramatic changes in molecular conformation, so as to act as switches for the above mentioned applications.

Polymer Complexes System of PMAA and PEG

It is well known that polymers with complementary binding sites can be aggregated in solution to form polymer complexes, which has been intensively studied over the past decades because of their great importance from both a fundamental and practical point of view; and they are also regarded as simple models of the complicated biological macromolecular assemblies [6, 7]. Among the work on polymer complexes, complexes system of poly(methacrylic acid) (PMAA) and poly(ethylene glycol) (PEG) has been well characterized or studied both experimentally and theoretically. It is well known that noncovalent intermolecular interactions can occur between poly(methacrylic acid) (PMAA) and poly(ethylene glycol) (PEG). The carboxylic groups of PMAA are pH sensitive in aqueous solution and can reversibly switch between being charged or protonated as pH varies. If either free (ungrafted) PEG or copolymerized poly(MAA-g-EG) macromolecules exist in the aqueous solution, they can form intermolecular or intramolecular polymer complexes via hydrogen-bonding in the acidic condition [8]. This complex is thought to be further stabilized by hydrophobic interactions between the $-CH_3$ groups of PMAA and the hydrophobic segments of PEG. When pH arises passing a certain value, the carboxylic acid groups of PMAA will become deprotonated and negatively charged, which then lose its capability to form hydrogen bonds and hence, the interpolymer complex is destroyed. It is also known that PMAA and PEG are hydrophilic expanded coils when uncomplexed, while the complex collapse into a hydrophobic globule. Similar hydrogen-bonding complexes form in systems of poly(acrylic acid) (PAA) and poly(ethylene oxide) (PEO) or other poly-bases.

Enormous research has been done on the PMAA/PAA and PEG/POE or other bases in the cross-linked state, the blend system or the copolymer system with a wide variety of physical, spectroscopic and compositional techniques. For example, study on the conformational transitions in polyelectrolyte gels of PMAA and PEO [9]; a semiquantitative theoretical model for reversible polymer complexes stabilized through hydrogen bonds like PAA/poly-base system [10]; potentiometric study of the influence of uncomplexable groups in the copolymer chain on complex formation [11]; complex-forming interpenetrating polymer networks of polyoxyethylene/PAA systems [12-14]; the

equilibrium and kinetics study of PAA/polyoxyethylene or poly(vinyl pyrrolidone) [15]; IR study on poly(styrene-co-MAA) with polytetrahydrofuran [16]; poly(MAA-g-EO) microspheres [17]; cross-linked star polymers of PMAA/PEG with varying architecture [18] ; preparation, characterization and biological and medical applications of poly(MAA-g-EG) hydrogels [19-28]; study on blends of PEG and PAA [14]; PAA/PEG in water solution [29]; hydrophobic interactions in PMAA/PEG complexes [30]; PMAA/PVP complexes [31]; self-assembly multilayer of PMAA, PAA, PEO and PVP [32] and thermodynamic study on macromolecular complexes [33].

Even though the cross-linked poly(MAA-g-EG) have been investigated intensively so far, this copolymer has never been explored in the form of brushes before. As more opportunities are emerging in the field of surface-stimulus-responsive materials, poly(MAA-g-EG) can be a great option to make reversible stimulus-responsive surface.

Generally, there are two ways to make polymer brushes to be covalently tethered to a planar substrate, which includes “grafting to” and “grafting from” approaches[34]. In order to prepare a series of polymers with varying macromolecular structures enabling the structure-stimulus-responsive property relationship, we adopt “grafting to” approach, which means preformed, end-functionalized polymers are tethered to a suitable substrate under appropriate conditions to form polymer brushes. Our group has successfully synthesized thiol-ended poly(2-hydroxyl methacrylate-g-ethylene glycol) previously [35]. Therefore the synthesis of HS-poly(MAA-g-EG) will start based on our previous catalyst/ligand/initiator system via atomic transfer radical polymerization method (ATRP).

After thiol-ended graft copolymer of HS-poly(MAA-g-EG) was synthesized, it was characterized by a variety of techniques and instruments, which include Varian Unity-300, Varian Mercury-300, Varian Inova-501 NMR spectroscopy, Dawn GPC from Wyatt Technology with Waters 510 HPLC pump and Waters 410 differential refractometer, BI-200SM light scattering(LS) goniometer from Brookhaven Instruments Corporation and Nicolet Magna 860 Fourier Transform Infra-Red Spectrometer to measure the molecular weight, confirm the chemical composition and calculate the grafting density of the copolymer.

Then, polymer brushes were prepared on gold coated silicon wafer using HS-

poly(MAA-g-EG). The kinetics of chemisorption was assessed via contact angle measurements. The information of surface chemical composition was collected via X-ray photoelectron spectroscopy (Kratos AXIS Ultra Imaging X-ray photoelectron spectrometer). The film thickness in the dry and wet state was collected from spectroscopic ellipsometry by measuring the polarization state variation of the incident light beam.

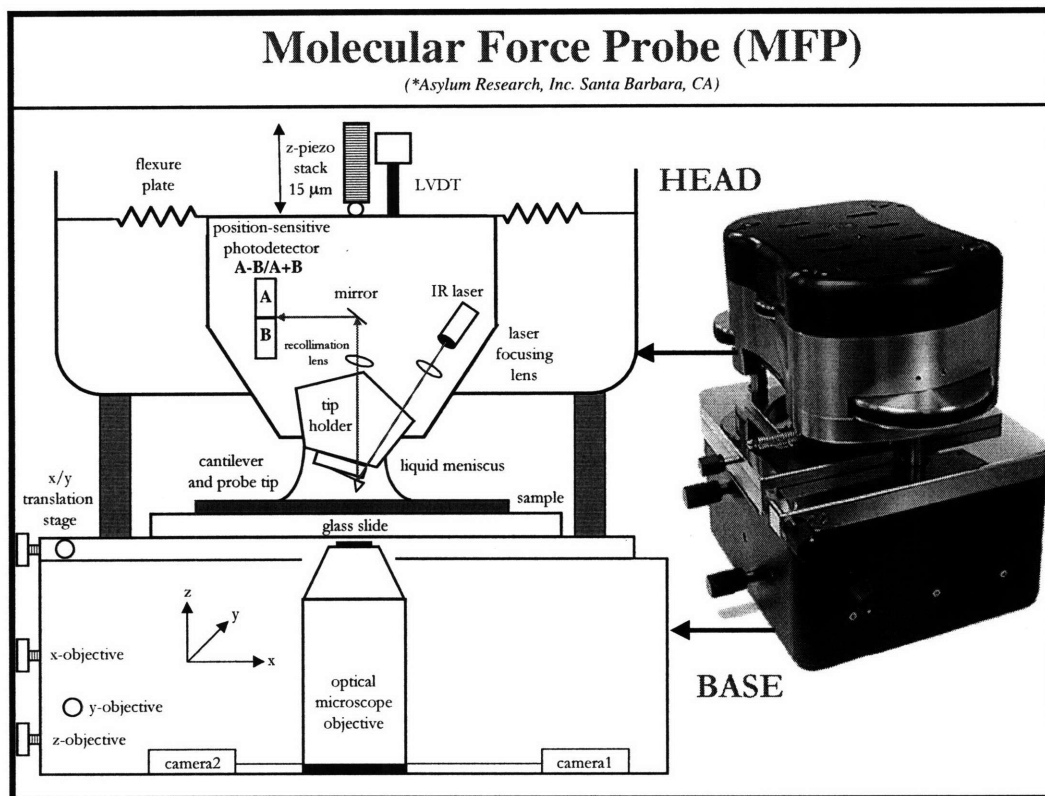


Figure 1.1 *Molecular Force Probe (MFP) from Asylum Research, Inc*

Chemically Specific High Resolution Force Spectroscopy (HRFS): a 1-D Molecular Force Probe (MFP) by *Asylum Research, Inc* is specifically designed and optimized to measure molecular stretching force at high resolution(**Figure 1.1**). The tip is usually functionalized with chemical species of interest. The force between the tip and the sample surface is derived from the deflection of the cantilever at the magnitude of pN (10^{-12} N). Since the force versus separation distance is measured in fluid, the

conformational transition of polymer brush will result in the sudden change of the surface charge distribution and wetting property, which can be pinned down by the differences in the pattern or magnitude of the force before and after the conformational transition with appropriate chemically modified tip.

Atomic Force Microscopy Imaging: a *Digital Instruments* Nanoscope IIIA System Controller with Multimode Atomic Force Microscope (AFM) is capable of contact, tapping, and force modulation imaging modes in air and fluids, as well as standard HRFS, which can measure topography by sliding the probe tip across the sample surface or tapping the sample surface with an oscillating tip.

The surface interfacial properties and nanomechanical testing results were analyzed and could be used to guide the tuning of chemical structure, molecular weight, grafting density, side chain length and topography of the polymeric system to manipulate and optimize the response rate and mechanism.

1.2 Objective

Inspired by those pioneering research on surface-responsive polymer materials, we have designed and synthesized a polymeric system that not only can undergo sudden dramatic changes over a small range of stimuli (e.g. pH), but also has specific end-functional group capable of chemisorbing onto the gold substrate, which allows for nanomechanical testing and correlating the structure-stimulus responsive properties at nanoscale. Such polymeric system is not only for control of microscopic interfacial properties, such as wettability, but also for control of local nanomechanical properties (e.g. the specific form of the intersurface potential) which is also critical to all of the above mentioned applications. The specific type of architecture chosen was that of end-functionalized, side-chain graft copolymers in which the side chains exhibit pH and ionic strength dependent noncovalent complexation with the main chains and the end-functional group are used for covalent attachment to surfaces. Changes in the stimulus-responsive nature of the interfacial and nanomechanical properties can be imparted via variations in the length, density, and type of side chains.

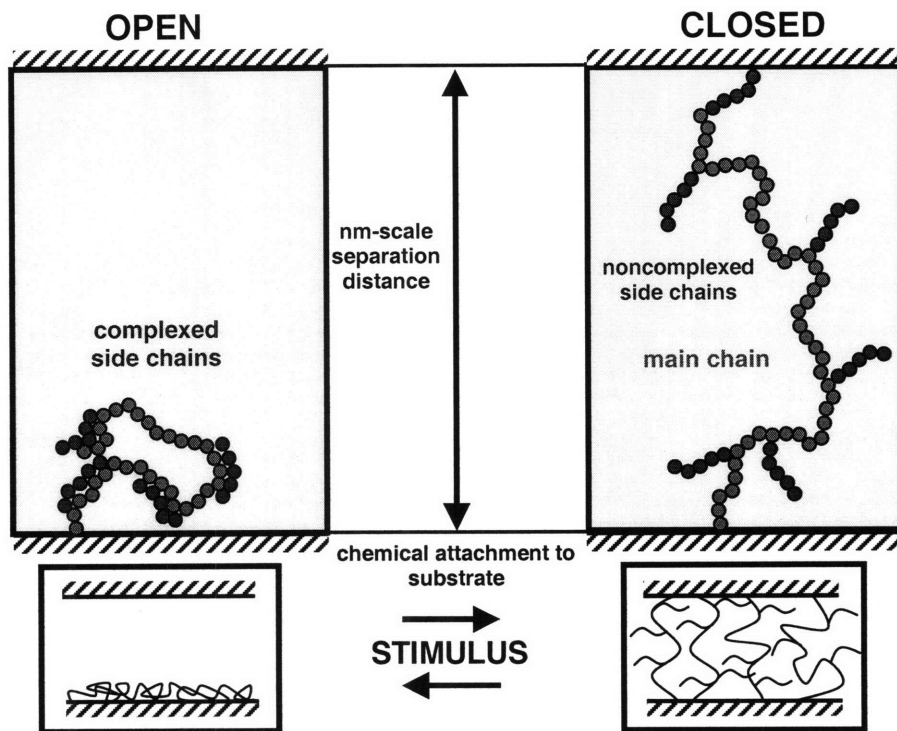


Figure 1.2 Schematic depiction of “Nanoscale Valves”, reversible “switch” under stimulus.

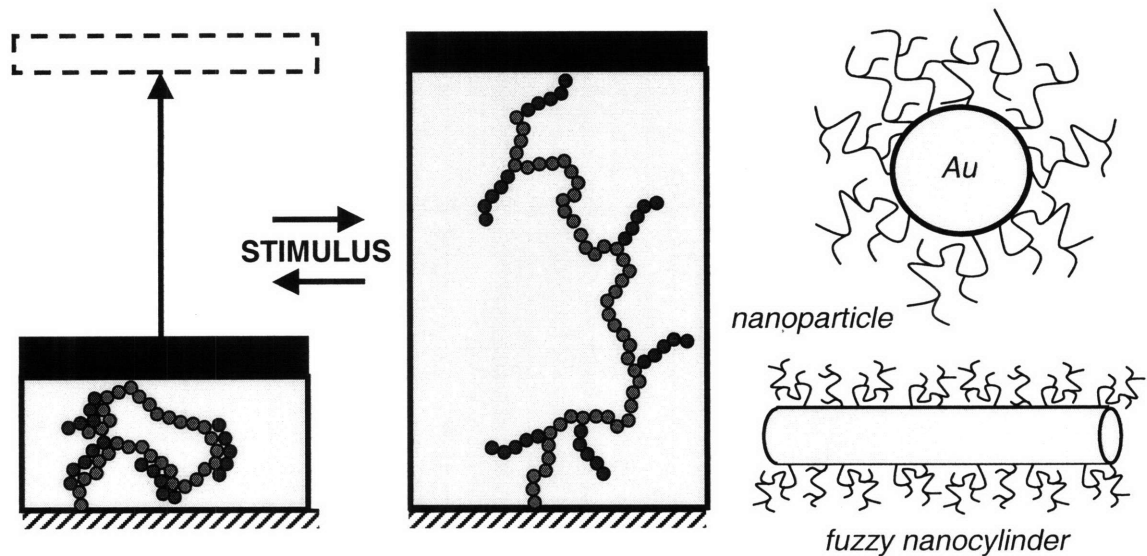


Figure 1.3 (a) Displacement of nanoscale devices; (b) Stimulus-responsive structures.

The polymers are chemisorbed to surfaces in monolayer brush-like form as monitored by the technique of contact angle measurement, characterized by atomic force microscopy imaging, X-ray photoelectron spectroscopy, and spectroscopic ellipsometry, and its interfacial properties are assessed via contact angle measurements and chemically specific high-resolution force spectroscopy (HRFS) in order to formulate structure-property relationships. The polymers may be of great potential use in nanoscale devices or stimulus-responsive nanoscale structures in the future, which can generate nanoscale forces/displacements as well as controlling single molecular elasticity, surface charge and other surface properties (e.g. adhesion, friction and wetting) (**Figure 1.2 and 1.3**).

1.3 Overview

The thesis is structured as follows. Chapter 1 provides the background and objective of the stimulus-responsive polymer systems, particularly poly(methacrylic acid) and poly(ethylene glycol) system, and the control of surface interfacial and nanomechanical properties through the chemisorption of such copolymers onto planar substrates. Chapter 2 describes the synthesis of mono(thiol)-terminated poly(methacrylic acid-g-ethylene glycol). Chapter 3 demonstrates the conformational transition of end-grafted poly(methacrylic acid-g-ethylene glycol) polymer Layers on planar substrate measured by contact mode atomic force microscopy. Chapter 4 and chapter 5 discusses the nanomechanical switching of end-grafted poly(methacrylic acid-g-ethylene glycol) polymer layers on planar substrate in normal intersurface interactions and lateral intersurface interactions respectively. Chapter 6 describes the adsorption of human serum albumin (HSA) on end-grafted poly(methacrylic acid-g-ethylene glycol) polymer layers.

Chapter 2

Synthesis of Mono(thiol)-Terminated Poly(methacrylic acid-*g*-ethylene glycol)

2.1 Introduction

In this chapter, we reported the synthesis of comb-type graft copolymers of poly(methacrylic acid-*g*-ethylene glycol) or poly(MAA-*g*-EG) in mono(thiol)end-functionalized form, which were then chemically end-grafted to planar substrates to prepare surface-bound stimulus responsive "brush-brushes" (**Figure 2.1**). Comb-like side-chain graft copolymers, also called molecular bottle brushes, cylindrical brushes, or polymacromonomers, are branched macromolecules composed of an array of side chains attached to a main chain backbone. Many types have been synthesized (see for example[36-39]) and also exist in biology; e.g. cartilage aggrecan[40] and epithelial mucins.[41] The synthesis and stimulus responsive nature of poly(MAA-*g*-EG) without end-functionalization has been reported previously by free radical polymerization[8, 42, 43] and by atom transfer radical polymerization (ATRP).[44] Since many of the potential applications described previously necessitate polymers bound to surfaces in a well defined manner, the methodology presented here for end-functionalization and chemical end-grafting of poly(MAA-*g*-EG) provides a technologically important model system that then can be used for studies of macromolecular surface properties, such as nanoscale

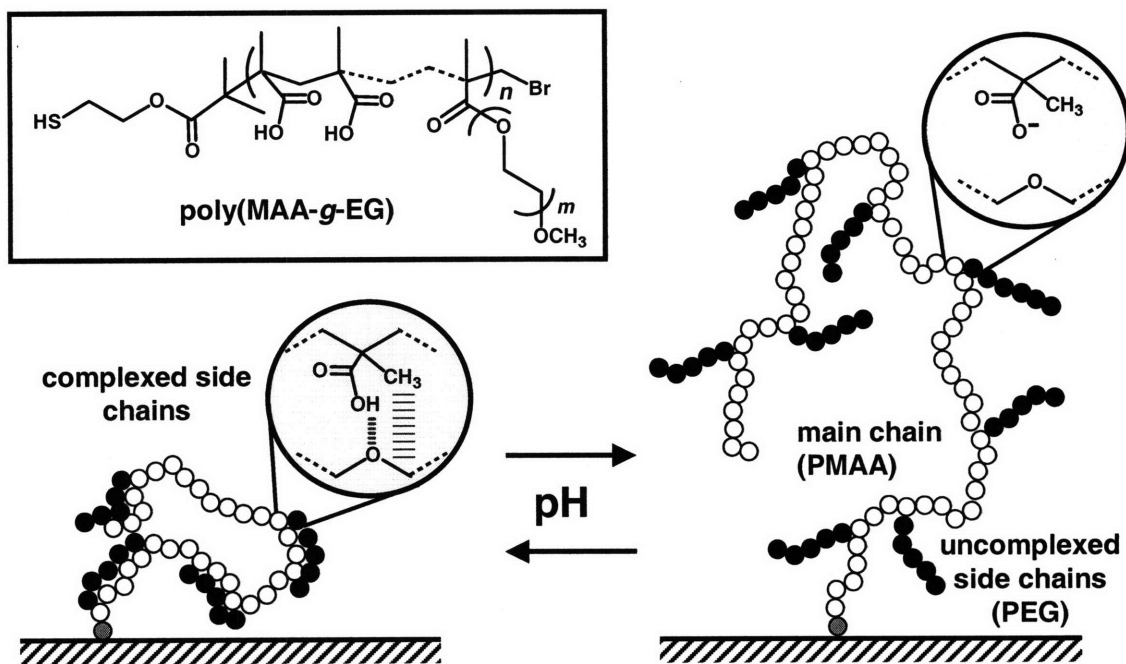


Figure 2.1 Schematic of a conformational transition of a chemically end-grafted stimulus-responsive side-chain graft copolymer (insets show molecular interactions for poly(MAA-g-EG)). [8, 42, 43] The bar extending from the methyl group of methacrylic acid to the methylene group of PEG stands for hydrophobic interaction while the dashed line between -COOH and -O- represents H-bonding, which shows the collapsed conformation of the end-grafted polymer layers is due to the H-bonding and further stabilized by the intramolecular hydrophobic interaction in acidic aqueous media.

conformation and wettability. We are particularly interested in employing these end-grafted poly(MAA-*g*-EG) layers for precise control of normal and lateral nanomechanical surface properties (i.e. the form of the attractive or repulsive intersurface potential, the lateral proportionality coefficient between normal and shear forces) both of which will be described in chapter 4 and 5. In addition, end-grafted systems with unique macromolecular architectures, such as combs, are expected to undergo interesting new stimulus responsive and nanomechanical behavior at high enough surface grafting densities due to lateral intermolecular interactions and confinement (for example, between PEG side chains of the poly(MAA-*g*-EG)), which are expected to stiffen the layer. This concept is employed in cartilage aggrecan via glycosaminoglycan side chain interactions and has important physiological consequences.[45, 46] Experiments which probe the nanoscale stimulus responsiveness of end-grafted poly(MAA-*g*-EG) also have the potential to provide important fundamental scientific information on the molecular origins of the unique macroscopic equilibrium swelling behavior of crosslinked hydrogels based on this graft copolymer.[22]

Three mono(thiol)end-functionalized poly(MAA-*g*-EG) with varying macromolecular architecture were synthesized by combining protecting group chemistry[35] with ATRP, i.e. using an alternate initiator[47-49] than that reported previously.[44] The number average molecular weights of these polymers were 15K, 27K, and 17K with side chain graft densities ~8-9% of the total main chain backbone monomers (EG/MAA molar ratio~2) for the 15K and 27K and a side chain graft density of 1.9% (EG/MAA molar ratio~0.4) for the 17K. Characterization was achieved by gel permeation chromatography (GPC), ¹H nuclear magnetic resonance (NMR), and Fourier transform infrared spectroscopy (FTIR).

2.2 Materials and Experiments

Materials

2,4-dinitrofluorobenzene (99%), 2-mercaptoethanol (98%), 2-bromoisobutyryl bromide (98%), *tert*-butyl methacrylate (BMA) (98%), poly(ethylene glycol) methyl

ether methacrylate (MW~1100, 23 EG monomers long), triethylamine (99.5%), chloroform (99.8% A.C.S. Reagent), toluene (99.8%, HPLC grade), 2,2'-dipyridyl (99%), copper(I) bromide (99.999%), chloroform-*d* (100.0%), methanol-*d*₄(99.8%), tris (hydroxymethyl) aminomethane (Tris), 4-morpholineethanesulfonic acid monohydrate (MES), acetic and formic acid were all purchased from Sigma-Aldrich. All water used for solutions, rinsing, and storage was deionized (DI, pH 5.6) (18MΩ·cm resistance). N-type Silicon wafers with 100 orientation were purchased from Crystaltek. Chromium was purchased from R.D. Mathis and gold (99%) was purchased from J & J Materials. All the other chemicals were used as received from commercial suppliers.

Synthesis of HS-poly(*tert*-BMA-*g*-EG)

The synthesis of the thiol-protected initiator: 2-(2,4-dinitrophenylthio)ethyl 2-bromo-2-methyl propionate (DEBPM) was performed as described previously.[35] In a typical polymerization (**Figure 2.2**), a 250 ml three-neck round bottom flask was equipped with a condenser, argon inlet and paddle stirrer. 0.078 g (0.0005 mol) of 2,2'-dipyridyl and 0.029 g (0.0002 mol) of CuBr were added to the mixture of 14.2 g (0.1 mol) of *tert*-butyl methacrylate, 1.1 g (0.001 mol) of poly(ethylene glycol) methyl ether methacrylate (MW~1100) and 12.0 g of methanol. Then, 0.078 g (0.0002 mol) of 2-(2,4-dinitrophenylthio) ethyl 2-bromo-2-methylpropionate was added into the solution. The solution was purged with Argon to remove oxygen. The ratio of catalyst/initiator/ligand was 1/1/2.5. The molar ratio of *tert*-butyl methacrylate and poly(ethylene glycol) methyl ether methacrylate was 100:1. The solution was heated to 40°C and maintained at this temperature with stirring under argon for 17 h in the synthesis of the 15K polymer. The amount of the initiator, ligand and catalyst were doubled in the synthesis of the 17K polymer while the molar ratio of *tert*-butyl methacrylate and poly(ethylene glycol) methyl ether methacrylate was 50:1 and the reaction temperature was 60°C in the synthesis of the 27K polymer. The crude thiol-protected polymer was obtained in solid form and purified by dissolving in hot methanol, cooling, and precipitating in DI water. The polymer was then filtered and dried in a vacuum oven at 50°C overnight. Then, the thiol-protected polymer was rinsed again with DI water, petroleum ether, cyclohexane,

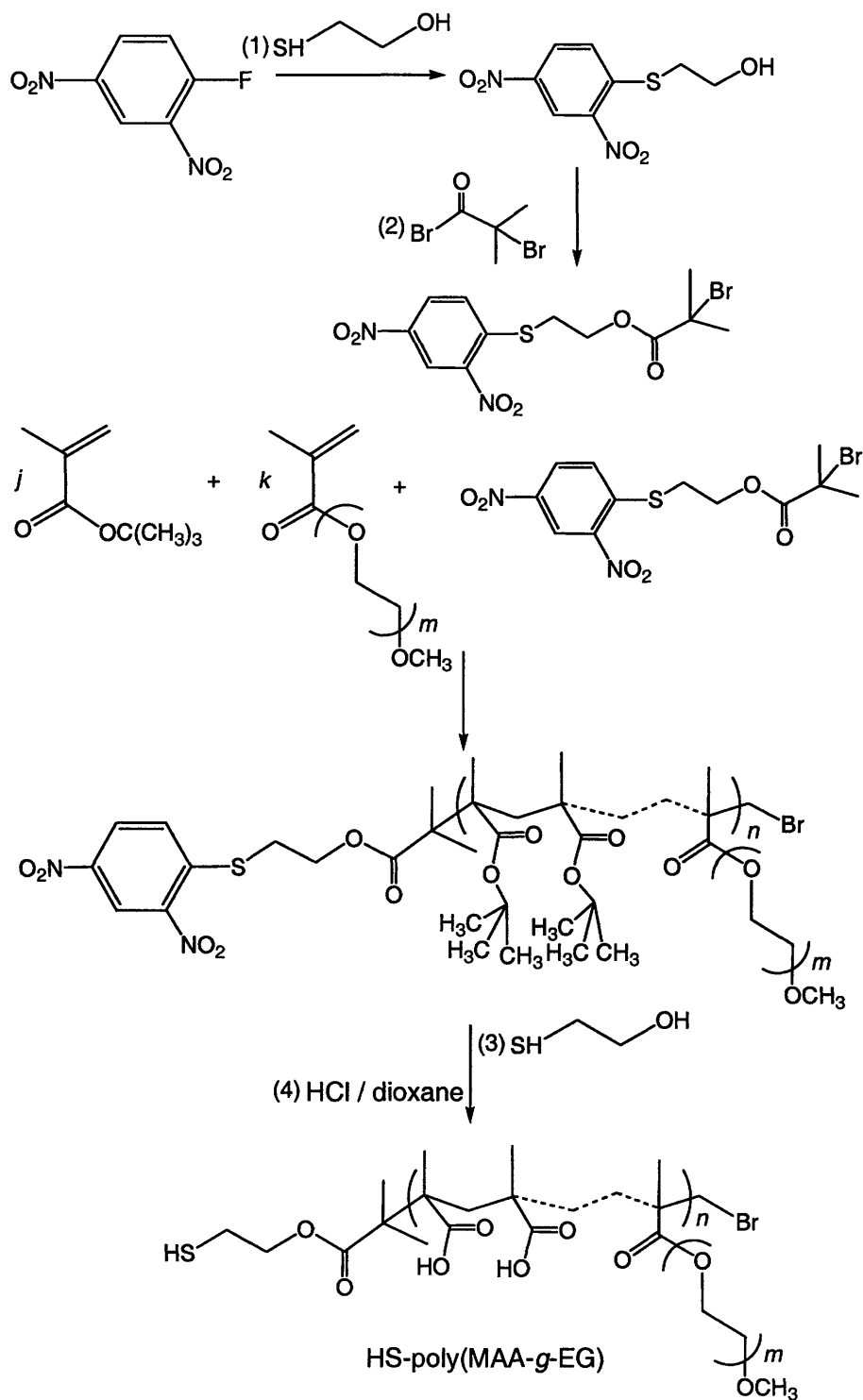


Figure 2.2 Atom transfer radical polymerization chemical reaction scheme for synthesis of mono(thiol)-terminated poly(methacrylic acid-g-ethylene glycol) or HS-poly(MAA-g-EG).

and filtered and dried in a vacuum oven at 50°C overnight. In a 20 mL borosilicate glass scintillation vial, 1.00 g of thiol-protected polymer, 5.2 g of mercaptoethanol, 0.1 g of triethylamine and 0.8 g of DI water were added and stirred by a magnetic stirrer at room temperature for 17 h. The polymer was then precipitated by adding DI water, filtered, and dried in a vacuum oven at 50°C overnight. For further purification, the HS-poly(*tert*-BMA-*g*-EG) was dissolved in methanol and fractioned by adding water or petroleum ether. The polymer was filtered and dried at 50°C in a vacuum oven overnight to yield HS-poly(*tert*-BMA-*g*-EG).

Conversion of HS-poly(*tert*-BMA-*g*-EG) to HS-poly(MAA-*g*-EG)

The cleavage of the *tert*-BMA groups of the HS-poly(*tert*-BMA-*g*-EG) was achieved by treatment with an HCl solution in dioxane. In a 50 mL single-neck round bottom flask 0.6 g of HS-poly(*tert*-BMA-*g*-EG) were suspended in 20 mL dioxane. 3 mL of a concentrated HCl solution (37%) were added and the mixture was magnetically stirred at 80°C for 5 h. Then, most of the solvent was evaporated, the polymer was precipitated and rinsed with cyclohexane, and then dried at 50°C in a vacuum oven overnight to yield HS-poly(MAA-*g*-EG).

2.3 Characterizations

GPC was taken using DAWN from Wyatt Technology, a Waters 510 HPLC pump and Waters 410 Differential Refractometer to measure the weight average molecular weight, M_w , and the molecular weight distribution. The calibration curves for polystyrene and poly(methyl methacrylate) were determined in tetrahydrofuran (THF). The polymers were prepared in a 5 mg/mL solution of THF. ^1H NMR spectra were obtained on Varian Unity-300 and Varian Mercury-300 in chloroform- d_4 or methanol- d_4 . The chemical shifts (δ) of hydrogen atoms of chloroform- d_4 or methanol- d_4 were used for reference. From the integrated peak areas corresponding to protons of the protecting end-group and the characteristic chemical groups of the poly(ethylene glycol) or PEG and PMAA, the number average molecular weight, M_n and grafting density of the copolymer were

calculated, as described previously.[35, 50] FTIR spectra were obtained on Nicolet Magna 860 Fourier Transform Infrared Spectrometer in air. The polymers were mixed with KBr and compressed into pellets. Both the copolymer and KBr were dried in vacuum oven at 50 °C overnight to remove moisture before running FTIR. Qualitative (visual) solubility assessment was performed after mixing 0.005g of the polymers with ~10 ml of buffer solutions (pH4 formate, pH5 acetate, pH6 MES and pH 7.1-9 Tris (hydroxymethyl) aminomethane) (Tris) and stirring for ~ 1 h.

2.4 Results and Discussion

Synthesis : Initiator and Polymer Characterization

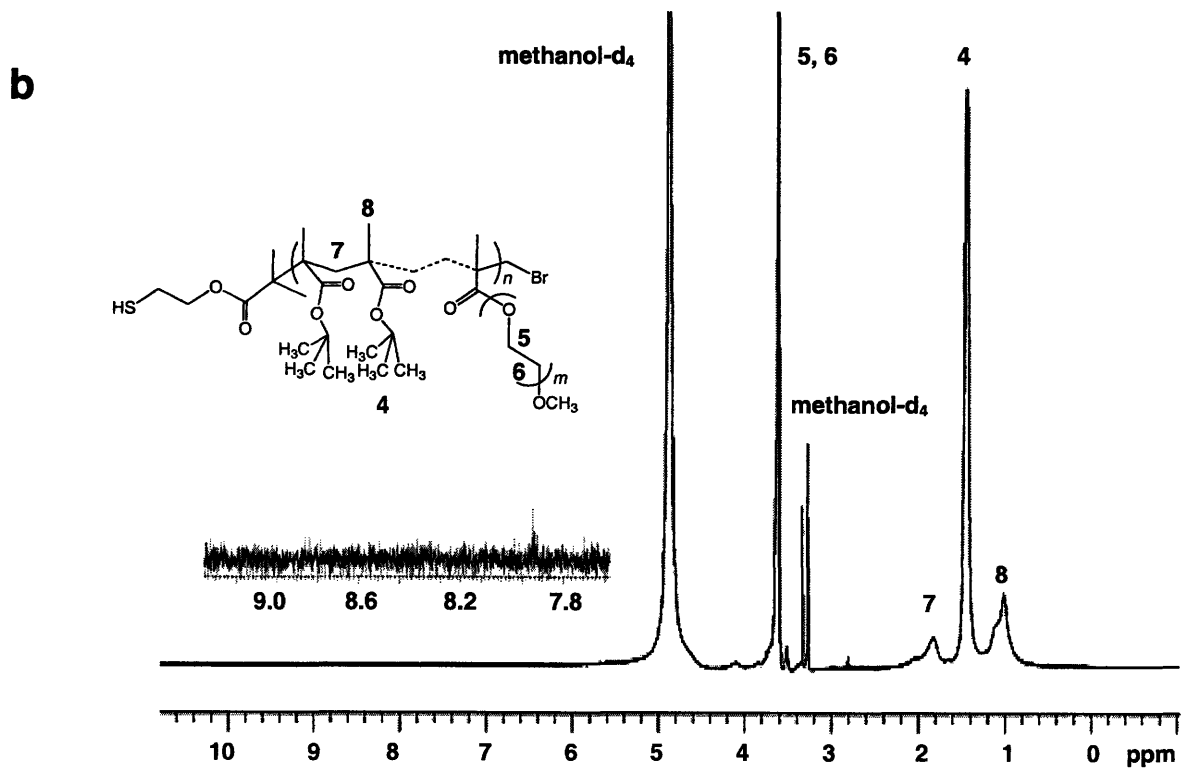
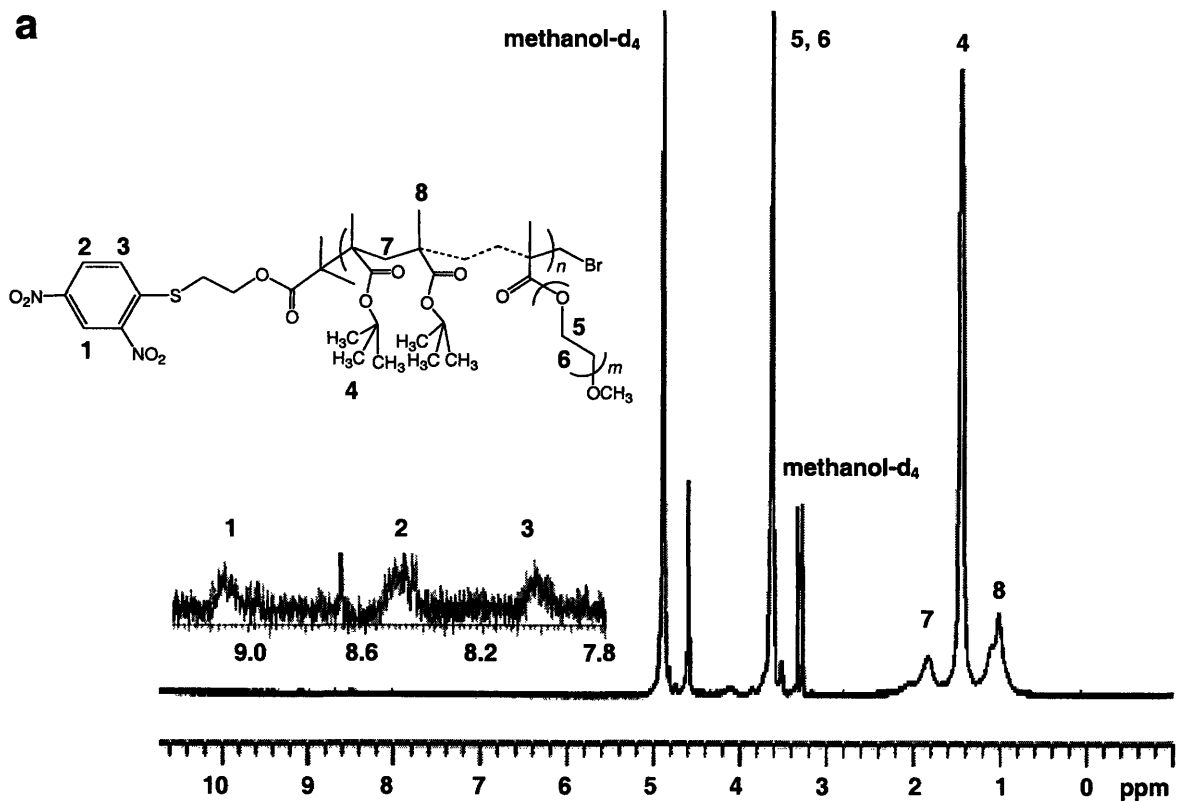
The synthesis of poly(MAA-g-EG) without end-functionalization has been reported previously by free radical polymerization[8, 42, 43] and by ATRP.[44] To our knowledge the synthesis of thiol (end)-functionalized poly(MAA-g-EG) has never been reported before. It is known that controlled polymerization of methacrylic acid via ATRP is difficult because the acid monomers can poison the catalysts by coordinating to the transition metal and nitrogen-containing ligands can be protonated interfering with the metal complexation ability.[51] Alternatively PMAA can be obtained by polymerization of protected polymers such as *tert*-butyl methacrylate (*t*BMA). Reported ATRP formulation for polymerization of *t*BMA includes methyl 2-bromopropionate (initiator) and Cu(I)Br/*N,N,N',N'',N'''*-pentamethyldiethylenetriamine (PMDETA) or 2,2'-bipyridine (bpy) (catalyst) in bulk, methanol or methanol/water mixture;[52] *p*-toluenesulfonyl chloride (*p*-TsCl) (initiator) and Cu(I)Cl/ *N,N,N',N'',N'''*-hexamethyltriethylenetetramine (HMTETA) (catalyst) in 50% vol. anisole[53] or methyl ethyl ketone (MEK).[54] ATRP formulation for polymerization of poly(ethylene glycol) methyl ether methacrylate (PEGMEM) can be Cu(I)Cl/bpy or pyridyl methanimine-based ligands with various initiators in water;[55, 56] a water soluble bromo-capped oligo(ethylene glycol) based alkyl initiator, Cu(I)Br with bpy, PMDETA, or HMTETA in water;[57] 1,2-dihydroxypropane-3-oxy-(2-bromo-2-methylpropionyl) (initiator) and Cu(I)Br/*N*-(*n*-alkyl)-2-pyridylmethanimine in water;[58] ethyl 2-bromoisobutyrate

(EtBriBu) or *p*-TsCl (initiator) and Cu(I)Br/4,4'-Di(5-nonyl)-2,2'-bipyridyne (dNbpy) (catalyst) in toluene or THF.[59]

Block copolymers of poly(ethylene glycol)-*b*-poly(*t*BMA) were also reported to be synthesized via ATRP using PEG macroinitiator and Cu(I)Br/PMDETA in bulk[60] or THF.[44, 61] Block copolymers of poly(ethylene glycol) with *n*-butyl methacrylate were prepared using PEG macroinitiator and Cu(I)Br/HMTETA in bulk;[62] poly(methyl methacrylate-co-poly(ethylene glycol) monomethacrylate) was synthesized using TsCl and CuBr/dNbpy in cyclohexanol or diphenyl ether.[63]

As a multicomponent system, initiator, catalyst including ligands, solvent and temperature of an ATRP reaction must all be taken into consideration. Based on the thiol protective group chemistry utilized[48] and our previous work on the ATRP synthesis of thiol end-functionalized poly(2-hydroxyethyl methacrylate-*g*-ethylene glycol),[35] we chose the current ATRP formulation and obtained the thiol functionalized comb-type .

¹H NMR, GPC, and Solubility. The structure of the initiator, 2-(2,4-dinitrophenylthio)ethyl 2-bromo-2-methyl propionate, was verified by ¹H NMR (chloroform-*d*, δ): 9.11-9.10 (d, 1H), 8.48-8.44 (dd, 1H), 7.84-7.81 (d, 1H), 4.50-4.45 (t, 2H), 3.43-3.38 (t, 2H), and 1.96 (s, 6H) (*spectrum not shown*). **Figure 2.3a** shows the ¹H NMR spectrum of the Protected thiol-functionalized poly(*tert*-BMA-*g*-EG) in methanol-*d*₄. The three peaks at δ 9.08, 8.54 and 8.03 were attributed to the protons at positions 1, 2 and 3 from the 2,4-dinitrophenyl protecting group as shown in the chemical structure inset of **Figure 2.3a**. The integrated areas of the peaks corresponding to positions 1, 2, and 3 were found to be approximately equivalent. The peaks at δ 4.87 and 3.31 correspond to methanol-*d*₄. The peak at δ 4.6 was probably from the impurities in the raw materials of *tert*-butyl methacrylate. The peak at δ 3.61 was attributed to the protons at positions 5 and 6 from the PEG graft side chains. The peak at δ 1.44 was attributed to the protons at position 4 from the methyl groups of *tert*-butyl methacrylate segments,[54] and the peaks at δ 1.9 and 1.0 were attributed to the protons from the methyl and methylene groups on the backbone. The peak at δ 4.7 may come from the protons on the C=C bonds of some residual monomers which still remained after purification. **Table 2.1** shows the results of calculations to determine the macromolecular architectural parameters from the



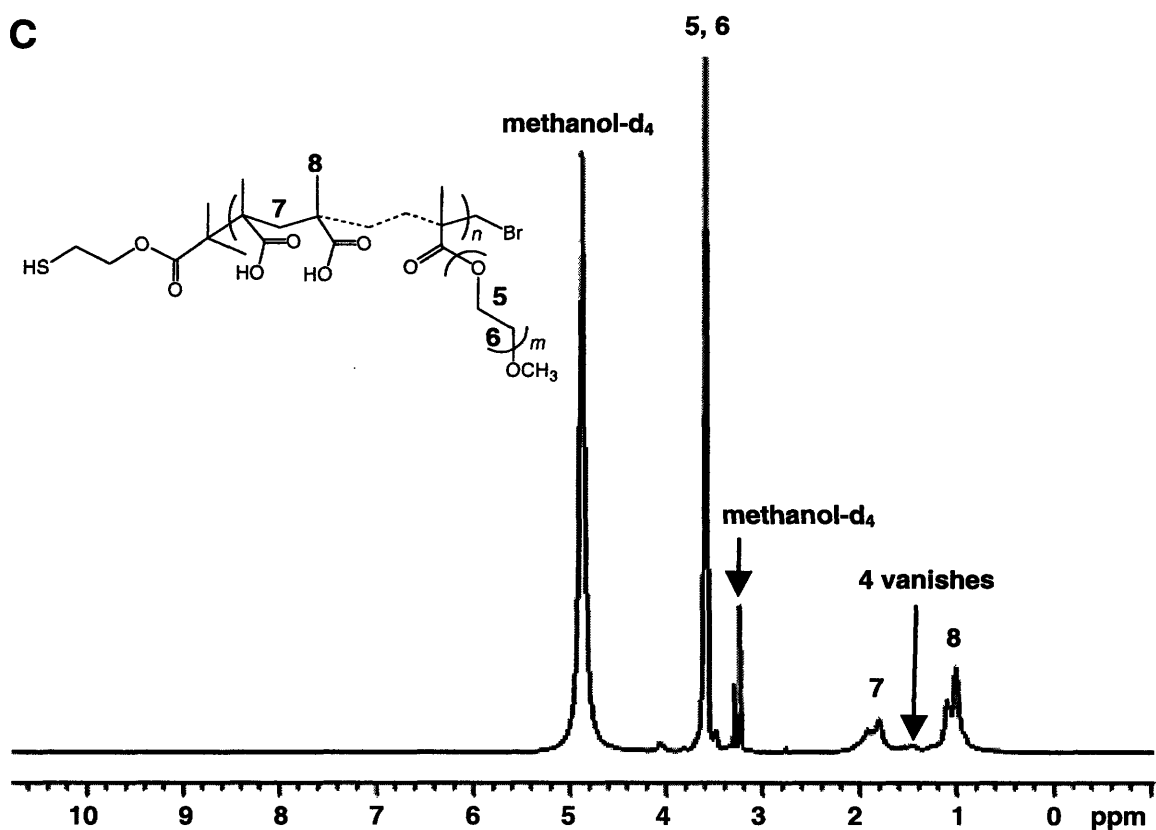


Figure 2.3 ^1H nuclear magnetic resonance (NMR) spectra in methanol- d_4 of (a) protected mono(thiol)-terminated poly(*tert*-butyl methacrylate-*g*-ethylene glycol) or poly(*tert*-BMA-*g*-EG)_{20K}, (b) mono(thiol)-terminated HS-poly(*tert*-BMA-*g*-EG)_{20K}, and (c) mono(thiol)-terminated poly(methacrylic acid-*g*-ethylene glycol) or HS-poly(MAA-*g*-EG)_{15K}. The numerical subscript in the abbreviated polymer name labels refer to the number average molecular weight, M_n , of the graft copolymer in g/mol (as measured by ^1H NMR) and “K” is an abbreviation for 1000. The peak numbers labeled in each NMR spectrum correspond to the protons labeled in the chemical structure insets at the top of each NMR spectrum.

	Thiol-Protected poly(<i>tert</i> -BMA- <i>g</i> - EG) _{20K}	Thiol-Protected poly(<i>tert</i> -BMA- <i>g</i> - EG) _{35K}	Thiol-Protected poly(<i>tert</i> -BMA- <i>g</i> - EG) _{25K}
¹ H NMR (methanol- <i>d</i> ₄)			
M _n	19900	35200	25300
EG/ <i>tert</i> -BMA (mole ratio)	2.2	1.9	0.4
PEG graft density (%)	8.8	7.7	1.9
M _n (<i>t</i> BMA)	11400	21300	22000
DP _n (<i>tert</i> BMA)	80	150	155
M _n (EG)	8500	13800	3300
DP _n (EG)	176	286	67
MW _{PEG} (each side chain)	~1100	~1100	~1100
N _{PEG}	7.8	12.6	3.0
L _{contour} , main chain (nm)	22.1	41.1	39.8
L _{contour} , side chain (nm)	6.7	6.7	6.7
M _n after hydrolysis (calculated)	15400 (HS-poly(MAA- <i>g</i> - EG) _{15K})	26800 (HS-poly(MAA- <i>g</i> - EG) _{27K})	16600 (HS-poly(MAA- <i>g</i> - EG) _{17K})
GPC (THF)			
M _w	12700	16800	13200
M _w /M _n	1.189	1.178	1.262
Solubility (aqueous solution)	complete dissolution : pH 6-9 swell : pH4-5 swell	complete dissolution : pH 6-9 pH4-5 swell	Complete dissolution : pH6-9 partial dissolution : pH5 swell : pH4

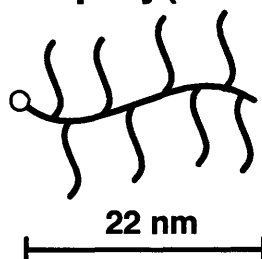
Table 2.1 Parameters describing the macromolecular architecture of the thiol-protected poly(*tert* butyl methacrylate-*g*-ethylene glycol) or poly(*tert*-BMA-*g*-EG) graft copolymers as determined by ¹H nuclear magnetic resonance (NMR) in methanol-*d*₄ and gel permeation chromatography (GPC) in tetrahydrofuran (THF). The numerical subscript in the abbreviated polymer name labels refer to the number-average molecular weight, M_n, of the graft copolymer in g/mol and “K” is an abbreviation for 1000, M_w is the weight average molecular weight measured by GPC, MW_{PEG} is the known molecular weight of each PEG chain, The PEG graft density (%) is defined as N_{PEG} divided by the total number of backbone monomers, N_{PEG} is the average number of PEG chains per poly(*tert*-BMA) or PMAA chain, DP_n is the number-average degree of polymerization, EG/*tert*-BMA (mole ratio) is calculated as the DP_n(EG)/DP_n(*tert*-BMA)=DP_n(EG)/DP_n(MAA), and L_{contour} is the average contour length calculated from the known molecular weights assuming *ttt* conformations for the PMAA and *ttg* conformations for the PEG. The M_n of corresponding thiol-terminated poly(methacrylic acid-*g*-ethylene glycol) or HS-poly(MAA-*g*-EG) copolymers were calculated after removal of the *tert*-butyl groups and replacement with H atoms.

NMR data (performed as described previously[35, 50]) compared with GPC data. The molecular weights were found to be 20K, 25K, and 35K with PEG graft densities of 8.8, 1.7, and 1.9%, respectively corresponding to EG/*tert*-BMA mole ratios of 2.2, 1.9, and 0.4. The estimated average contour lengths of the main chain backbone (calculated from the molecular weights) for the three polymers were ~ 22 nm (20K), 41 nm (35K), and 40 nm (25K) (assuming *ttt* backbone conformations) and for the PEG side chains ~ 7 nm (assuming *ttg* backbone conformations, which is known to exist in aqueous solution[64]).

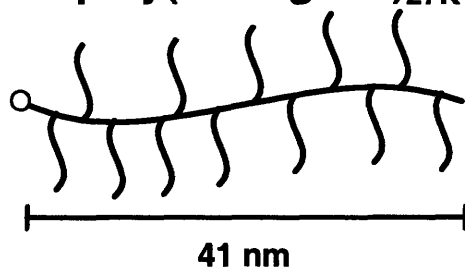
After removal of the 2-(2,4-dinitrophenyl) protecting group, the characteristic end group peaks at positions 1, 2 and 3 vanished as shown in **Figure 2.3b**, while the peaks corresponding to PEG graft side chains and *tert*-butyl methacrylate segments still remained. When the *tert*-butyl methacrylate groups were replaced with carboxylic groups after the hydrolysis, the characteristic peak of *tert*-butyl methacrylate segments at δ 1.44 vanished, while the peak of PEG graft side chains at δ 3.61 still remained (**Figure 2.3c**). These results verified the success of the selective hydrolysis reaction, which was consistent with other reports[44]. The molecular weights of the poly(MAA-*g*-EG) graft copolymers were calculated to be 15K, 27K, and 17K (**Table 2.1**). A schematic illustration of the copolymers drawn to scale is given in **Figure 2.4**.

FTIR. The FTIR spectra of HS-poly(*tert*-BMA-*g*-EG)_{35K} and HS-poly(MAA-*g*-EG)_{27K} (before and after hydrolysis) were obtained to additionally confirm the success of hydrolysis. As shown in **Figure 2.5**, after hydrolysis a broad peak is observed at 2500~3500 cm⁻¹ due to the formation of hydrogen bonding,[65, 66] which is not possible for the HS-poly(*tert*-BMA-*g*-EG). In the spectrum of HS-poly(*tert*-BMA-*g*-EG), 2978 cm⁻¹ was attributed to the asymmetric stretching of -CH₃; 1724 cm⁻¹ was the stretching of C=O in the carbonyl group of *tert*-BMA; 1394 cm⁻¹ and 1368 cm⁻¹ was due to the bending of -CH₃ group, which are the characteristic absorptions of *tert*-butyl group,[67] 1276 cm⁻¹ and 1251 cm⁻¹ were the stretching of -C-C-O of PEG and 1140 cm⁻¹ was attributed to the stretching of C-O.

HS-poly(MAA-*g*-EG)_{15K}



HS-poly(MAA-*g*-EG)_{27K}



HS-poly(MAA-*g*-EG)_{17K}

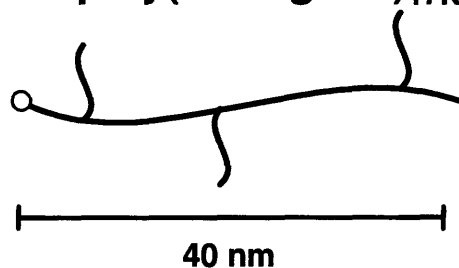


Figure 2.4 Schematics of mono(thiol)-terminated poly(methacrylic acid-*g*-ethylene glycol) or HS-poly(MAA-*g*-EG) graft copolymers synthesized in this study with contour length dimensions for PMAA (poly(methacrylic acid)) backbone, PEG (poly (ethylene glycol)) side chains, and PEG side chain density drawn approximately to scale. The schematics are not meant to indicate the actual spatial distribution of PEG side chains along the MAA backbone or the conformation of the polymer chains. The numerical subscript in the abbreviated polymer name labels refer to the number average molecular weight, M_n , of the graft copolymer in g/mol (as measured by ^1H nuclear magnetic resonance) and “K” is an abbreviation for 1000.

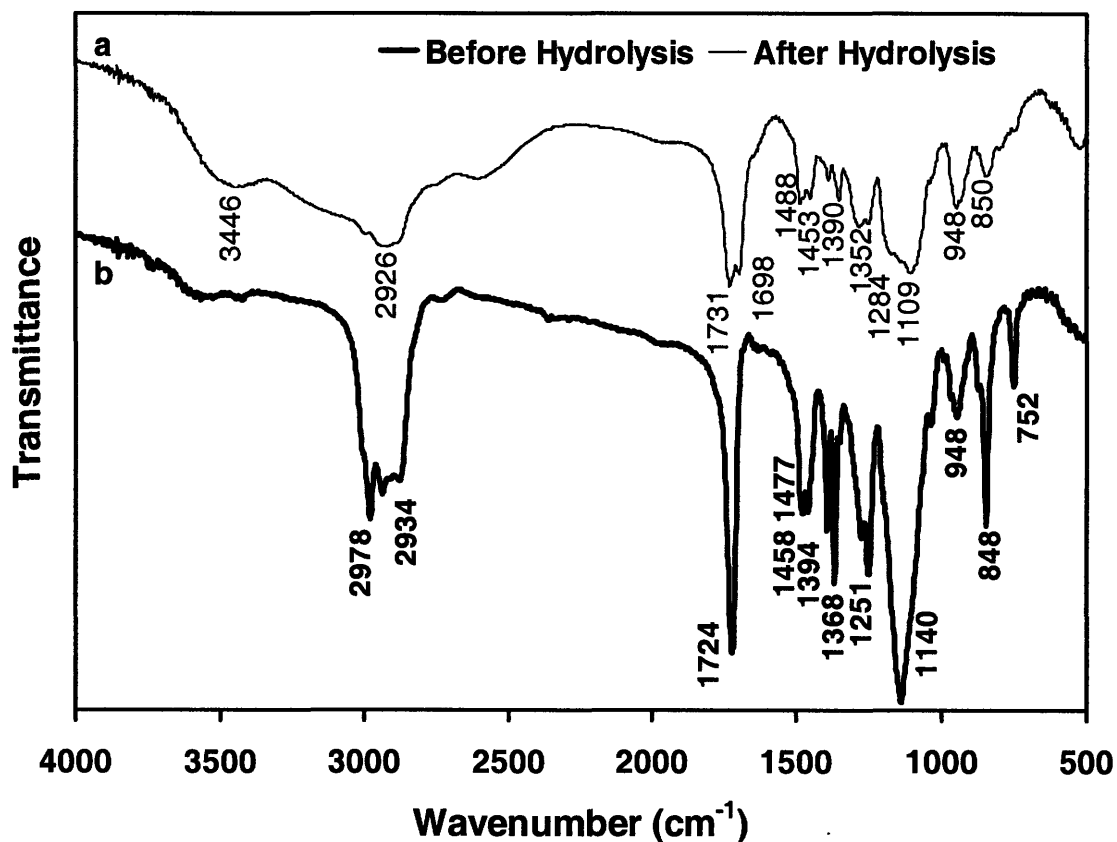


Figure 2.5 Fourier transform infrared (FTIR) spectra of (a) after hydrolysis, mono(thiol)-terminated poly(methacrylic acid-*g*-ethylene glycol) or HS-poly(MAA-*g*-EG)_{27K} and (b) before hydrolysis, mono(thiol)-terminated poly(*tert* butyl methacrylate-*g*-ethylene glycol) or HS-poly(*tert*-BMA-*g*-EG)_{35K}. The numerical subscript in the abbreviated polymer name labels refer to the number average molecular weight, M_n , of the graft copolymer in g/mol (as measured by ^1H nuclear magnetic resonance) and “K” is an abbreviation for 1000.

By treatment with HCl in dioxane the *tert*-butyl groups were removed to form free carboxylic acid groups. Besides considerable absorption due to the –OH stretching of hydrogen bonding at 2500~3500 cm⁻¹, the C=O absorption peak of the MAA groups split into two peaks: 1731 cm⁻¹ and 1698 cm⁻¹, which has been seen in poly(styrene-*co*-MAA)[16] and poly(MAA-*g*-EG).[17] From FTIR studies on complexes of PMAA gel with PEG,[26] the 1731 cm⁻¹ would be attributed to the C=O absorption peak affected by the formation of the hydrogen bonding between PMAA and PEG side chains and the 1698 cm⁻¹ would be attributed to the C=O absorption peak affected by the formation of the hydrogen bonding between two carboxylic groups of PMAA on the backbone. The FTIR spectrum of HS-poly(MAA-*g*-EG) also shows there was still absorptions in the region of 1394 cm⁻¹ ~1368 cm⁻¹, though the peak positions shifted slightly. Since there were –CH₃ groups remaining on the backbone after the hydrolysis, 1390 cm⁻¹ and 1353 cm⁻¹ were attributed to symmetric bending vibrations of –CH₃ groups under the influence of acid dimers or formation of hydrogen bonding.

Solubility. The 27K and 15K polymers were observed to dissolve completely in pH 6, 7.1, 8 and 9 and swelled in pH 4 and 5 aqueous solutions. The 17K polymers dissolved completely in pH 6, 7.1, 8 and 9, partially dissolved in pH5, and swelled in pH 4.

2.5 Conclusions

A series of mono(thiol)-terminated poly(methacrylic acid-*g*-ethylene glycol) have been synthesized via atom transfer radical polymerization method. The end-functionalized comb-type copolymers were characterized by GPC, ¹H NMR and FTIR, which results indicate the molecular structures designed were attained successfully. The varying macromolecular architectures are as follows by decreasing molecular weight by ~2× and side chain graft density by ~4×. The number average molecular weight, M_n = 27K, PEG graft density, PEG(%) = 7.7%, backbone contour length, L_{contour} = 41.1 nm; M_n = 15K, PEG(%) = 8.8%, L_{contour} = 22.1 nm; M_n = 17K, PEG(%) = 1.9%, L_{contour} = 39.8 nm.

Chapter 3

Conformational Transition of End-Grafted Poly(methacrylic acid-g-ethylene glycol) Polymer Layer on Planar Substrate

3.1 Introduction

Study on polymer complexes of copolymer poly(MAA-g-EG) in solution has been reported in literature, for example, high molecular weight poly(MAA-g-EG) polymers (~700-800K) free in solution show a dramatic conformational transition in aqueous solution from a collapsed hydrophobic intrapolymer complex at low pH to an expanded hydrophilic coil at high pH that is essentially completed for pH > 6.0 and is amplified compared to the poly(methacrylic acid) or PMAA homopolymer.[43]

In this chapter, three mono(thiol)end-functionalized poly(MAA-g-EG) copolymers with varying macromolecular architecture were chemically end-grafted to planar Au-coated substrates using a "grafting to" chemisorption technique (which yielded a polymer layer with molecular surface separation distances of ~ 3-4 nm) and then characterized by contact angle measurements to monitor the kinetics of chemisorption and assess wettability. Samples were prepared via the technique of micro-contact printing[68] where patterned surfaces with micrometer-sized areas of the end-grafted polymers were surrounded by areas of a neutral hydroxyl-terminated self-assembled monolayer (OH-SAM). The relative graft copolymer layer height was measured as a function of pH in

aqueous solution using these patterned samples by contact mode atomic force microscopy (AFM) imaging,[46] thus providing direct information on the nature of the pH-dependent conformational transition.

3.2 Methods

3.2.1 Sample Preparation

End-Grafting of HS-poly(MAA-g-EG) to Planar Surfaces

Au-coated silicon substrates were prepared as previously described[69] and cleaned using a piranha solution (98% H_2SO_4 / 30% H_2O_2 , volume ratio 3:1) for 10 min followed by copious rinsing with water, acetone, and methanol. Any terminal disulfide bonds formed by the $-\text{SH}$ end groups of HS-poly(MAA-g-EG) were reduced to a thiol group by diluting polymer to 200 $\mu\text{g}/\text{mL}$ of methanol solution in 0.1 mM dithiothreitol (DTT, Sigman Aldrich) and incubating under continuous stirring for 1 h. After removal of the excess reactants using centrifugal filters (Centricon, Millipore, 3000 MW cutoff), the Au substrates were immersed in 0.4 mg/mL of the polymer solution in methanol for times ranging between 3 and 72 h. The end-grafted poly(MAA-g-EG) surfaces were rinsed with acetone, methanol, and water thoroughly before experimentation.

Characterization of End-Grafted poly(MAA-g-EG)

Advancing contact angles for the end-grafted poly(MAA-g-EG) layers were measured using droplets of ~ 0.5 ml DI H_2O (pH5.6) and a VCA2000 Video Contact Angle system. The contact angle reported is the average of measurements on three different sample locations.

The micro-contact printed samples were gently dried in a stream of nitrogen and imaged using contact mode AFM and an OH-SAM functionalized cantilever probe tip in ambient conditions to measure the relative height in air using similar procedures as described in chapter 3.2.2 for the wet heights.

The polymer layer thickness in air was also measured on M-2000D Spectroscopic Ellipsometer (J. A. Woollam Co., Inc.). The change in polarization state of light reflected from the surface of the sample was measured via the ellipsometric values Ψ and Δ versus wavelength (200–1000 nm) at a fixed angle of incidence (70°) between the incoming beam and the sample surface normal. The polymer layer thickness was obtained by fitting the ellipsometry data with a Lorentz oscillator model over the wave length of 400–800 nm. The polymer layer surface was modeled as two layers: gold and the polymer. The thickness was fitted as the value with a mean squared error (MSE) less than five and was the average of the measurements at three different sample locations.

The surface grafting density, Γ (chains/nm²), was calculated from the dry polymer layer height data as follows :

$$\Gamma\left(\frac{\text{chains}}{\text{nm}^2}\right) = \frac{\text{dry height (nm)} \cdot \rho\left(\frac{\text{g}}{\text{nm}^3}\right) \cdot 6.023 \cdot 10^{23} \text{ mol}^{-1}}{M_n\left(\frac{\text{g}}{\text{mol}}\right)}$$

In the dry state, the density of the polymer layer, ρ , was assumed to be the same as its bulk density. The densities of PMAA and PEG are known to be 1.0153 g/cm³ and 1.1135 g/cm³, respectively.[70] The density of the copolymer is assumed to be an additive function of the densities of two compositional homopolymers on a weight basis (~1.07 g/cm³).

3.2.2 Contact Mode Atomic Force Microscopy in pH Buffer Solutions

The polymer layer heights (and hence, macromolecular conformation) were measured in aqueous buffer solutions using micro-contact printed samples[68] in conjunction with contact mode atomic force microscopy imaging.[46] The advantages and disadvantages of this technique have been discussed previously.[46] The patterned samples were prepared with micrometer-sized areas of the end-grafted poly(MAA-g-EG) surrounded by areas of a neutral hydroxyl-terminated self-assembled monolayer (OH-SAM) as shown in **Figure 3.1**. A polydimethylsiloxane stamp with parallel lines 1.5 μm in width was compressed onto piranha (98% H_2SO_4 /30% H_2O_2 , volume ratio 3:1)-cleaned

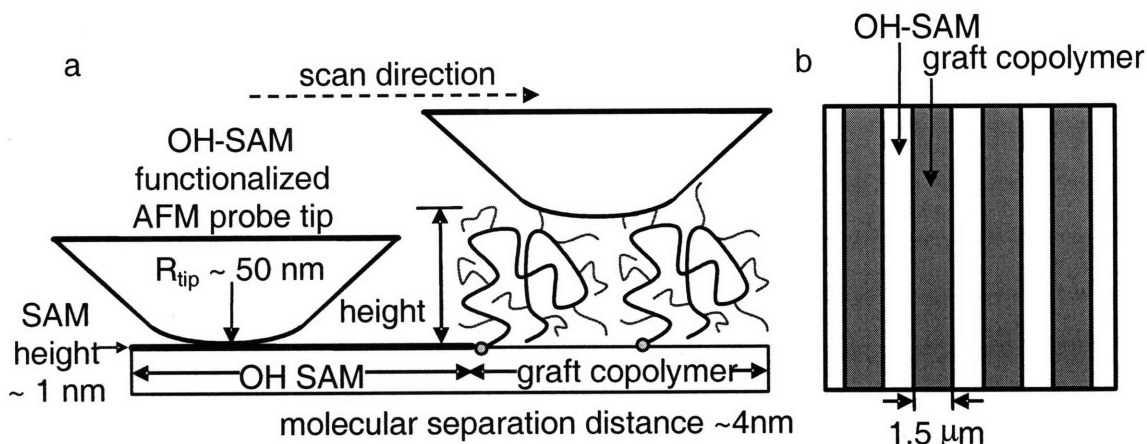


Figure 3.1 (a) Side view schematic of height measurement using atomic force microscope contact mode imaging on micro contact printed surface of graft copolymer and hydroxyl-terminated self-assembled monolayer (OH-SAM) where R_{tip} is the probe tip end radius, and (b) schematic of top view of microcontact printed surface (adapted from[46]).

Au substrates using 1mM ethanol solution of 11-mercaptopundecanol, $HS(CH_2)_{11}OH$ (Sigma-Aldrich), to fill the areas outside of the lines. Then the patterned substrate was immersed into a DTT-treated poly(MAA-g-EG) solution of 0.4 mg/mL for 72 h to allow the polymer to chemisorb to the inner areas of the lines. The samples were rinsed thoroughly with methanol, ethanol, and DI water prior to experimentation. Height maps were taken as a function of pH using these samples by contact mode atomic force microscopy (AFM) imaging in 0.005M ionic strength (IS) buffered aqueous solution as a function of pH. pH 4, pH5 and pH6 buffer solutions were formate, acetate, and MES, respectively, while pH7.1, pH8 and pH9 were Tris. All buffer solutions used sodium chloride to adjust the ionic strength to 0.005M. A Multimode Nanoscope III AFM (Veeco) was used at the lowest normal imaging force possible ~ 200 pN (scan size= $10 \mu m$, scan rate= 1 Hz, 256 datapoints per line scan, and scan angle= 0°) with an OH-SAM functionalized cantilever probe tip prepared in the same manner as for the planar substrate (Veeco, end radius ~ 50 nm, nominal cantilever spring constant, $k \sim 0.06$ N/m). The AFM images were flattened and the polymer heights reported are the relative height between the OH-SAM surface areas outside the patterned lines (which has a height of ~ 1.4 nm in air[71]) and the polymer-functionalized surface areas within the patterned lines. The heights are the average of eight scan lines per image.

3.3 Results and Discussion

Contact Angle Measurements on End-Grafted Poly(MAA-g-EG)

Figure 3.2 shows a dramatic decrease in advancing contact angles for DI water relative to the hydrophobic bare gold substrate ($70\pm 2^\circ$) with chemisorption incubation time for end-grafted poly(MAA-g-EG)_{27K}. The instantaneous advancing contact angles equilibrated after ~48 h of incubation time stabilizing at $32\pm 0.6^\circ$ (27K), $44\pm 2.4^\circ$ (17K), and $47\pm 2.6^\circ$ (15K). To achieve the highest surface grafting density, samples were prepared with an incubation time of 72 h. Receding contact angles were 0° (27K), $5\pm 0.5^\circ$ (17K), and $11\pm 0.6^\circ$ (15K). The large difference in advancing and receding contact angles suggest that the end-grafted poly(MAA-g-EG) exposed its hydrophilic segments to water after dramatically molecular reorganization due to hydration for all three polymers.

Estimation of Packing Density of End-Grafted Poly(MAA-g-EG)

The heights of the polymer layers were measured in air using both the μ CP-contact mode AFM method and spectroscopic ellipsometry to estimate the surface packing density. From the contact mode AFM imaging, the layer thicknesses relative to the OH-SAM were found to be ~0.8 nm (27K), ~1.5 nm (17K) and ~0.3 nm (15K). The height of HS(CH₂)₁₁OH is known to be 1.4 ± 0.1 nm in air.[71] Hence, the dry polymer layer heights were calculated to be ~2.2 nm (27K), ~2.9 nm (17K) and ~1.7 nm (15K), which is similar to the thicknesses obtained from the ellipsometry (2.2 nm for the 27K polymer, 2.0 nm for the 27K polymer and 1.4 nm for the 15K polymer). From the AFM-measured height values, the packing densities were calculated to be $\Gamma\sim 0.053$ chains/nm² or a molecular separation distance of ~4.3 nm (27K), $\Gamma\sim 0.109$ chains/nm² or a molecular separation distance of ~3.1 nm (17K) and $\Gamma\sim 0.071$ chains/nm² or a molecular separation distance of ~3.8 nm (15K). These values are ~2× larger than the radius of gyration of these 1100 g/mol PEG side chains (~ 1.5 nm[72]). However, lateral interactions between

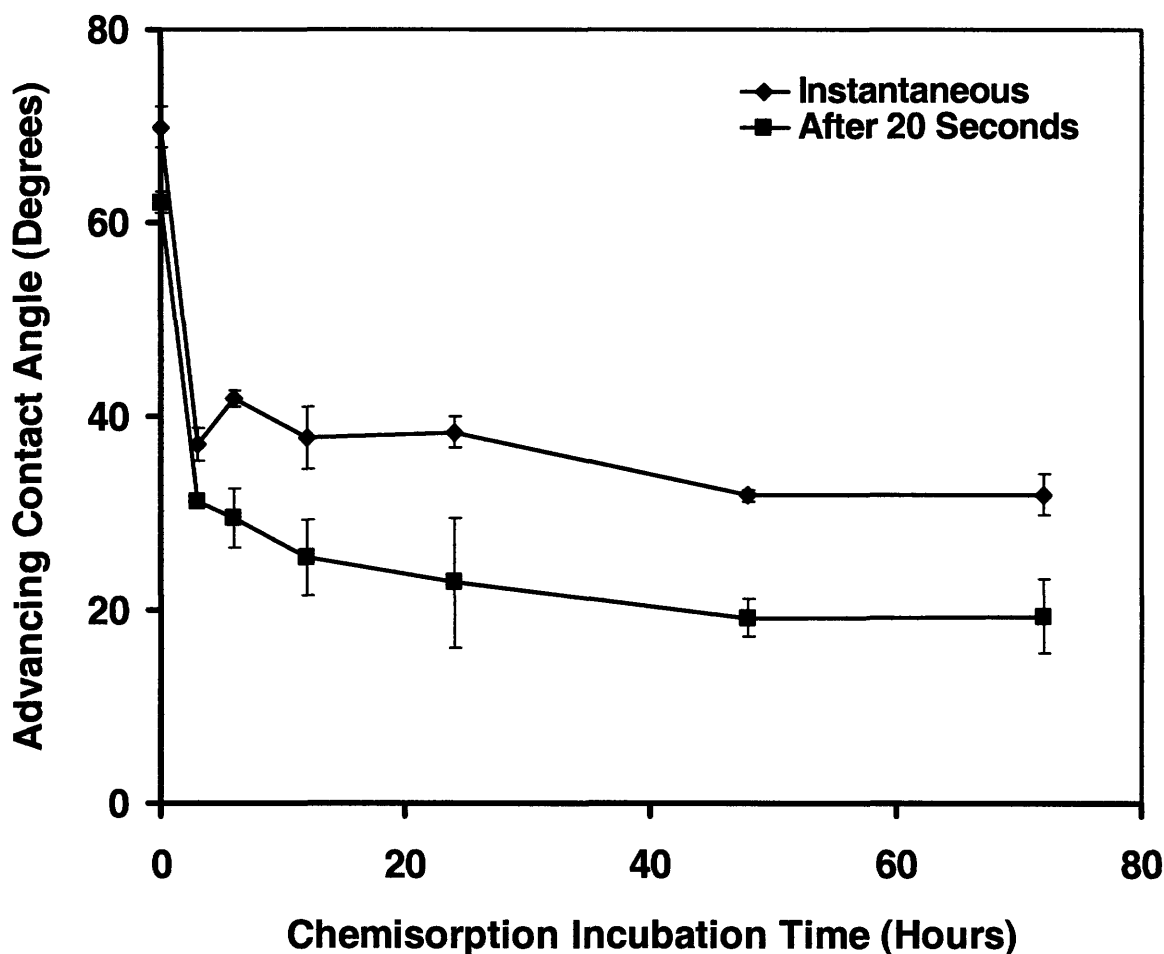


Figure 3.2 Advancing contact angles of gold (zero hours) and chemically end-grafted poly(methacrylic acid-*g*-ethylene glycol) or poly(MAA-*g*-EG)_{27K} polymer layers as a function of chemisorption incubation time. The numerical subscript in the abbreviated polymer name labels refer to the number average molecular weight, M_n , of the graft copolymer in *g*/mol as measured by ¹H nuclear magnetic resonance and “K” is an abbreviation for 1000. Hi-lo bars represent one standard deviation. The number of measurements taken were on three different locations of the polymer layers for each incubation time.

PEG chains are expected at these grafting densities since PEG is known to have longer range repulsive interactions up to $\sim 3\times$ its radius of gyration.[72]

Stimulus-Responsive Conformational Transition of End-Grafted Poly(MAA-g-EG)

Figure 3.3 shows contact mode AFM height images of micro-contact printed 15K (72 h chemisorption incubation time) / OH-SAM surfaces taken under the minimum possible normal forces in a series of buffer solutions with pH 4-9 (ionic strength = 0.005M). These images allow for direct visualization of variations in the polymer conformation, which is quantified in the subsequent height versus pH plot of **Figure 3.4**. At high pH the carboxylic acid groups of PMAA are ionized (negatively charged) and unbound to the PEG chains which are free to participate in hydrogen bonding with water. Both intramolecular electrostatic repulsion and the hydrophilicity of PEG can contribute to a significant coil expansion. At pH9, the height was found to be 8 ± 0.8 nm ($0.36L_{\text{contour}}$) for the 15K, EG/MAA \sim 2.2, 15 ± 0.5 nm ($0.37L_{\text{contour}}$) for the 27K, EG/MAA \sim 1.9, and 9.1 ± 0.4 nm ($0.23L_{\text{contour}}$) for 17K, EG/MAA \sim 0.4 polymers. These results suggest that the relative extension is determined by the side chain graft density where a lower graft density results in a lower relative extension of the main chain backbone. Since a small tare force of up to ~ 200 pN is necessary to attain stable feedback for AFM imaging, some compression of the polymer layer may result and these AFM measured height values may be somewhat less than the true equilibrium polymer heights (depending on the nanoscale compliance of the polymer layer). At high pH values (7-9), the height of the 27K polymer was found to be statistically larger ($p < 0.003$) than the 15K and 17K.

As the pH is reduced, the carboxylate groups of the PMAA become protonated and intrapolymer main-chain side-chain complexation can take place via hydrogen bonding with the PEG -O- groups and is thought to be further stabilized by hydrophobic interactions between the $-\text{CH}_3$ groups of PMAA and the hydrophobic segments of PEG. This leads to a hydrophobic, globular, collapsed conformation. As pH was decreased, the

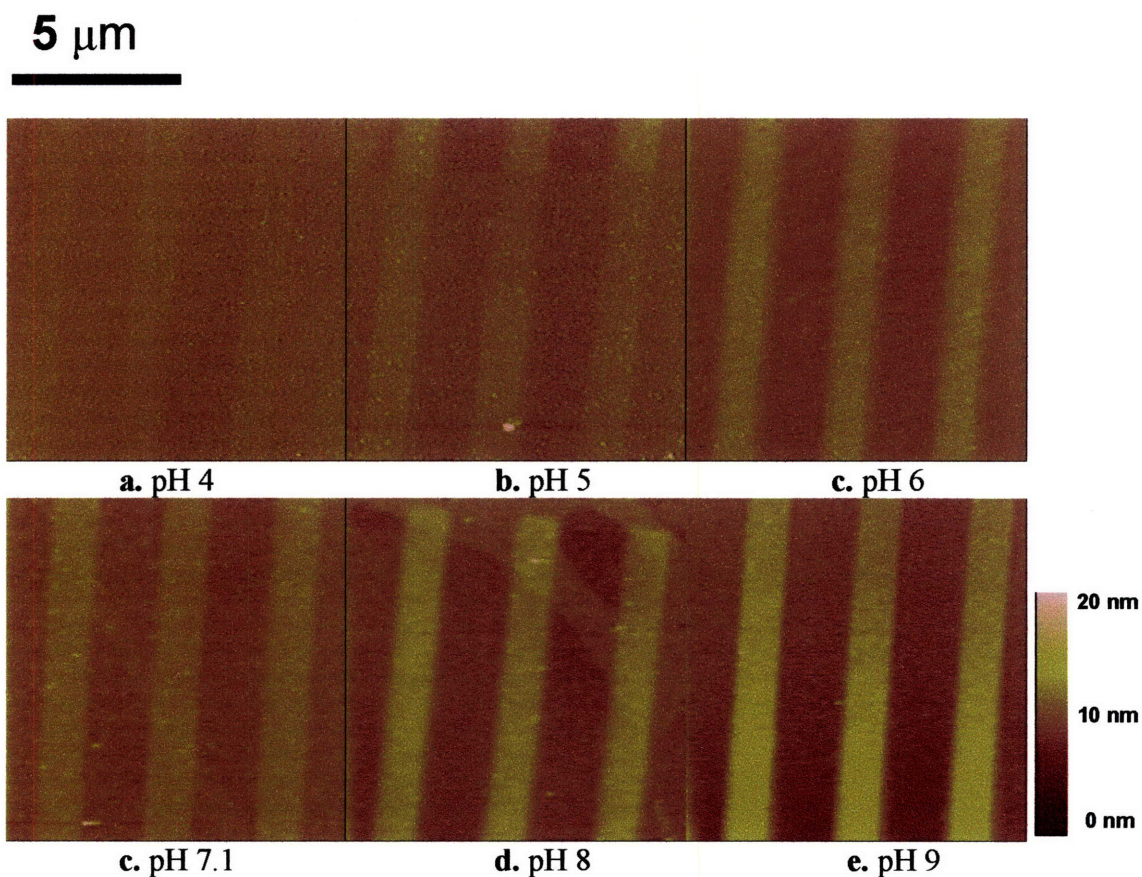


Figure 3.3 AFM contact mode height images of micro-contact printed samples of end-grafted poly(methacrylic acid-*g*-ethylene glycol) or poly(MAA-*g*-EG)_{15K} layers (inside the line patterns) and a hydroxy-terminated self-assembling monolayer (OH-SAM, outside the line patterns) and as a function of pH (ionic strength = 0.001M) taken with an OH-SAM functionalized probe tip. The minimum possible normal imaging force was employed. The numerical subscript in the abbreviated polymer name labels refer to the number average molecular weight, M_n , of the graft copolymer in g/mol as measured by ^1H nuclear magnetic resonance and “K” is an abbreviation for 1000.

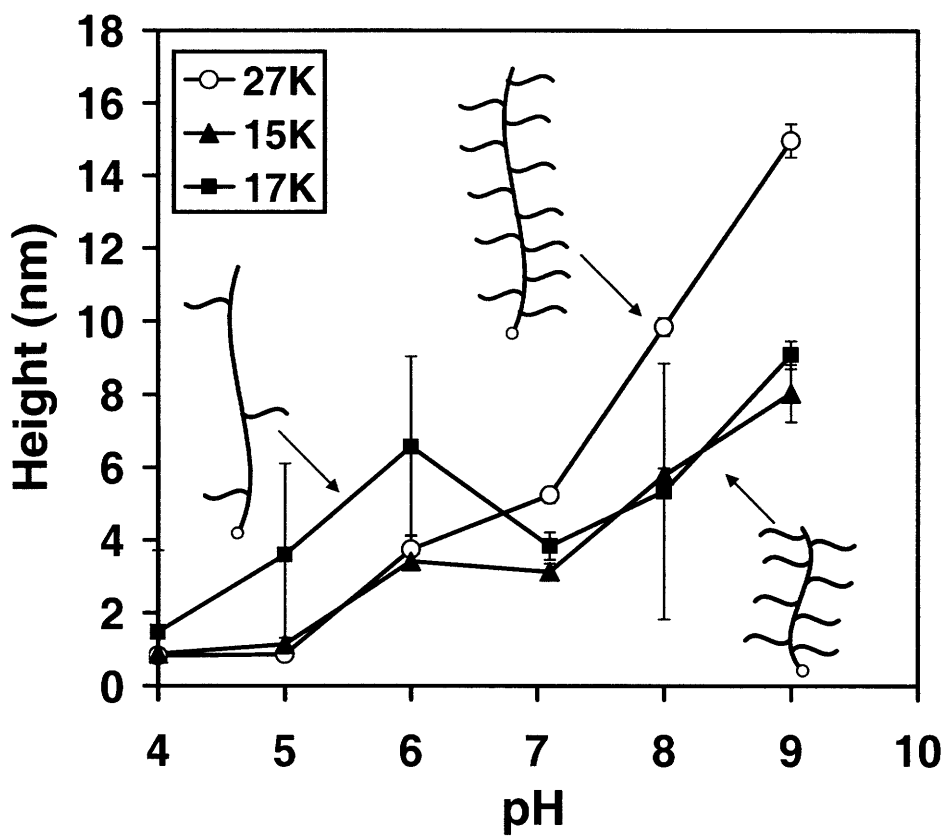
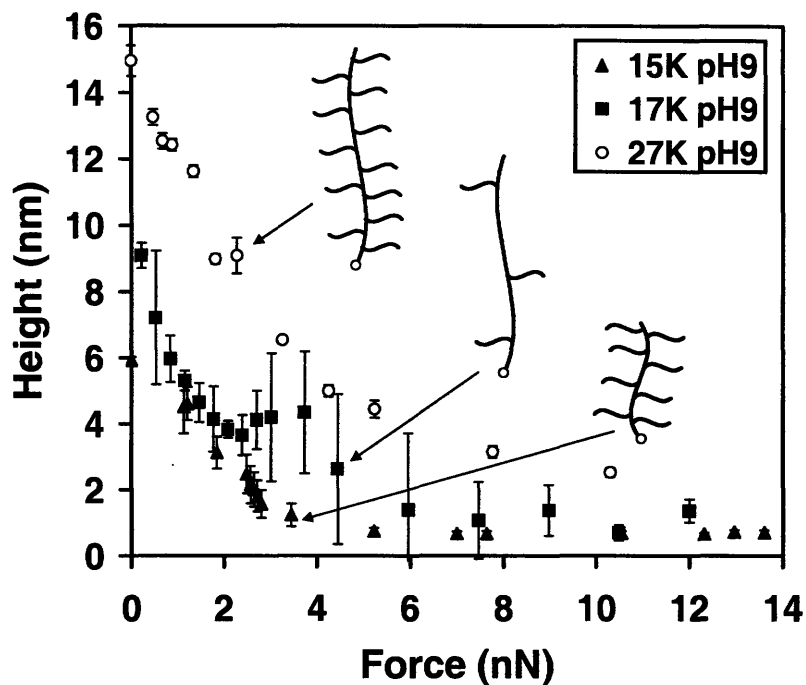


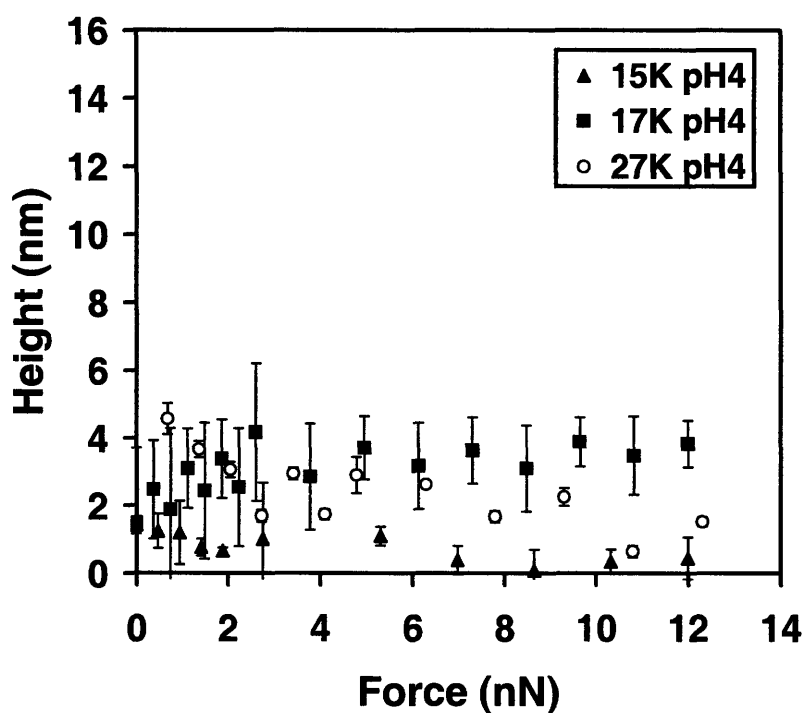
Figure 3.4 Heights of end-grafted poly(methacrylic acid-g-ethylene glycol) or poly(MAA-g-EG) polymer layers relative to a hydroxy-terminated self-assembling monolayer measured by contact mode atomic force microscopy at the lowest possible imaging force as a function of pH in 0.005M buffered aqueous solution on micro-contact printed samples. Hi-lo bars represent one standard deviation. Heights are the average of eight scan lines per image.

AFM-measured height (**Figure 3.4**) was observed to decrease gradually until reaching a minimal value of $\sim 1\text{-}2$ nm at pH 4, indicating that the polymer layer was in a nearly completely flattened state during imaging (height values for all three polymers were statistically similar ($p > 0.01$)). Hence, the expanded to collapsed conformational transition appears to be completed between pH 4-6 which is consistent with the solubility results, reports on high MW ($\sim 700\text{-}800\text{K}$) poly(MAA-*g*-EG) in dilute aqueous solution,[43] and equilibrium swelling of macroscopic crosslinked poly(MAA-*g*-EG) hydrogels.[24] The heights of end-grafted polymer layers as a function of pH also showed that the conformation transition occurred at a lower pH range (pH 4 - 5) for the 17K polymer compared to pH 5 -6 for the 27K and 15K polymer, suggesting that the lower acidic proton binding potential resulting from less hydrogen bonding interactions between PMAA backbone and PEG sidechains shifted the pK_a of end-grafted polymer layers to smaller value. In other words, it is easier for carboxyl groups to release protons through dissociation at a more acidic condition if the polymers have less intramolecular complexation through hydrogen bonding.

The pK_a of high MW poly(MAA-*g*-EG) has been reported between 5.8-6.7 and interestingly light scattering data on these high MW polymers show minimal expansion above pH 6.0, even though further ionization takes place.[43] In our experiment, we do not observe formation of a plateau, only continued expansion up until pH 9 (the highest pH tested), similar to the macroscopic equilibrium swelling behavior of crosslinked poly(MAA-*g*-EG) gels[24] and high molecular weight PMAA brushes.[73, 74] This behavior may be indicative of intermediate conformations which has been suggested previously.[75, 76] While a quantitative comparison with these studies[24, 43] is not possible due to differences in copolymer and PEG MW, solution ionic strength, and sample type (i.e. free, end-grafted, or crosslinked copolymers), it is interesting to note that many qualitatively similar trends emerge. The height of the 17K polymer at lower pH values (5-6) was statistically greater than the 27K or 15K polymer ($p < 0.015$). It is noted that the surfaces are still extremely hydrophilic at pH 5.6 (as indicated by contact angle measurements taken with DI water) when the polymer layers have already collapsed by 70-85% of its expanded height at pH9, suggesting that wettability should have a much more discrete stimulus-responsive nature.



a



b

Figure 3.5 Heights of end-grafted poly(methacrylic acid-*g*-ethylene glycol) or poly(MAA-*g*-EG) polymer layers relative to a hydroxy-terminated self-assembling monolayer measured by contact mode atomic force microscopy as a function of normal imaging force in 0.005M buffered aqueous solution on micro-contact printed samples. Hi-lo bars represent one standard deviation. Heights are the average of eight scan lines per image. (a) pH9 and (b) pH4.

Figure 3.5a is a plot of the heights of the poly(MAA-g-EG) layers measured by contact mode atomic force microscopy as a function of normal imaging force on micro-contact printed samples in buffered aqueous solution of pH9 and ionic strength of 0.005M. A nonlinear decrease in polymer height is observed for both molecular weights with increasing normal force until reaching a plateau value ("incompressible layer height") of < 2 nm at ~10 nN of force. **Figure 3.5b** shows the corresponding data for pH 4 where all three polymers are in a nearly completely collapsed configuration.

(E) End-Grafted Poly(MAA-g-EG) Layers Relative to Other Reported End-Grafted Stimulus-Responsive Macromolecular Systems

One parameter that can be employed to directly characterize the magnitude of the stimulus responsive nature of a particular system is a swelling factor, s , which for end-grafted macromolecular layers exposed to a particular stimulus can be defined as :

$$s = \frac{\text{maximum height}}{\text{minimum height}}$$

where the heights may be taken anywhere throughout the stimulus range. s is expected to depend on Γ and intermolecular interactions, DP_n and polydispersity, macromolecular architecture and intramolecular interactions, and surface curvature. s is also expected to decrease at high grafting densities due to lateral confinement effects and layer stiffening. Values of s have been observed to be exceedingly large (up to 19) for polyelectrolytes attached to curved surfaces (calculated by hydrodynamic thicknesses measured by dynamic light scattering of brush-functionalized particle dispersions), for example; temperature and salt concentration of poly(N-isopropylacrylamide) (PNIPAM),[77] pH and salt concentration dependence of polyacrylic acid or PAA, salt concentration dependence for poly(2-(dimethylamino)ethyl methacrylate) or PDMAEMA[78] and salt concentration dependence of poly(styrene sulfonate) or PSS.[79] Hence, for consistency we will limit further discussion to macromolecules attached to planar surfaces. **Table 3.1** provides a summary of end-grafted or end-anchored PAA[80, 81] and PMAA[73, 74, 82] data reported in the literature compared to the poly(MAA-g-EG) graft copolymers studied here. s values are measured to fall < 3.3 for PAA and PMAA with a wide variety

Polymer	DP _n	Γ (chains/nm ²)	Technique	s	Reference
PAA [†]	49-57	0.1-0.85	ellipsometry	<1.3	Wu, et al.[80]
PAA*	122	0.125-0.38	ellipsometry	<2.35	Currie, et al.[81]
PMAA [†]	300	-	AFM (scratch method)	1.97	Ryan, et al.[82]
PMAA [†]	high [‡]	-	ellipsometry	3.3	Konradi, et al.[73]
PMAA [†]	23,000	0.005-0.16	ellipsometry	1.9-2.5	Zhang, et al.[74]
poly(MAA-g-EG) [†]	80-155	0.053-0.11	AFM (μCP)	3.6-7.3	This study

Table 3.1 Summary of swelling factors for heights of poly(acrylic acid) or PAA and poly(methacrylic acid) or PMAA end-anchored* or chemically end-grafted[†] weak polyelectrolyte layers as a function of pH compared to poly(methacrylic acid-g-ethylene glycol) or poly(MAA-g-EG) reported in this paper where the swelling factor, *s*, is defined as the maximum height divided by the minimum height, Γ is the grafting density (chains/nm²), DP_n is the number average degree of polymerization, and μCP is micro contact printing. *s* for the poly(MAA-g-EG) was calculated with the addition of 1.4 nm[71] to each of the heights since the reported values (Fig. 9) were relative to the SH(CH₂)₁₁OH self-assembling monolayer. [‡] The DP_n in Konradi, et al.[73] was not reported but expected to be very large since the collapsed height of the layer at low pH was ~ 600 nm.

of DP_n and grafting densities while s for the poly(MAA-g-EG) were found to be generally larger at 4.14 (15K), 3.64 (17K), and 7.3 (27K). The swelling factors calculated for the poly(MAA-g-EG) were from low force contact mode AFM imaging of μ CP samples while the majority of the others were measured via ellipsometry. As mentioned before, the former method (AFM) typically will lead to an underestimation of the measured heights, which would in turn lead to an underestimation of s and hence, the trend observed comparing poly(MAA-g-EG) to PAA and PMAA can not be due to differences in the measurement techniques.

To compare these values to other types of stimuli, PAA and PMAA also exhibit a well-known nonmonotonous dependency on salt concentration which exhibits a maximum height between the "osmotic brush" and "salted brush" regimes.[80] Swelling factors as a function of salt concentration for PAA and PMAA are generally larger than for pH dependency of the equivalent systems ($s \sim 1.4-6.4$).[73, 74, 80, 81] Solvent and temperature-dependent swelling factors for end-grafted poly(N-isopropylacrylamide) (PNIPAM) on planar substrates are found to be < 3.2 . [83-86] Other end-tethered stimulus-responsive macromolecular layers reported in the literature (which did not report heights and swelling factors) include; elastin-like polypeptides,[87] semifluorinated polystyrene and poly(methyl acrylate)-based diblock copolymers,[88] binary layers of chemically modified poly(styrene)/poly(methyl acrylate), poly(butyl acrylate) or poly(acrylic acid),[89, 90] and Y-shaped amphiphilic poly(styrene)/poly(acrylic acid).[91, 92] In these systems and some of the others cited above, alternative surface properties have been employed to characterize stimulus responsiveness including wettability,[88, 91, 93] protein adsorption,[87] membrane permeability,[94] nanoscale morphology in air,[88-92] bioadhesion,[86] and more recently, nanomechanical properties.[87, 89, 92]

3.4 Conclusions

The pH-dependent conformational transition (swelling) of stimulus-responsive chemically end-grafted "brush-brushes" of mono thiol(end)-functionalized poly(MAA-g-EG) comb-type graft copolymers was confirmed to take place gradually above pH 4-5

and quantified by contact mode AFM measurements of polymer height on μ CP samples. At pH9, the height of the end-grafted polymer layers was found to be $\sim 0.36L_{\text{contour}}$ for the 15K, EG/MAA ~ 2.2 , $\sim 0.37L_{\text{contour}}$ for the 27K, EG/MAA ~ 1.9 , and $\sim 0.23L_{\text{contour}}$ for 17K, EG/MAA ~ 0.4 polymers. At pH4, the conformational transition resulted in a sharp drop in the polymer layer height to $\sim 0.05\text{-}0.09 L_{\text{contour}}$ for all three copolymers. The nanoscale compressibility as a function of macromolecular architecture and pH was also measured. Polymer layer height vs normal AFM imaging force measured on μ CP samples at pH9 showed a nonlinear relationship and complete compressibility < 1 nm for forces > 10 nN. The 27K polymer was observed to be the least compressible at pH9 and at pH4 all polymers were collapsed and essentially incompressible.

Not only is this advance technologically important for preparing homogeneous and stable stimulus-responsive surfaces, but also provides a system for which the fundamental nanoscale origins of the stimulus responsive nature of such macromolecules can be studied systematically.

Chapter 4

Nanomechanical Switching in Normal Intersurface Interactions of End-Grafted Poly(methacrylic acid-g-ethylene glycol) Polymer Layer on Planar Substrate

4.1 Introduction

Stimulus-responsive surfaces which can dynamically and reversibly capture and release biomacromolecules, such as proteins, hold great potential for bioseparation and sensor systems, as well as the regulated administration of drugs and growth factors for modulation of cellular processes in tissue engineering.[95] Certain active polymers chemically end-attached to surfaces in a well-defined "brush"-like configuration have been shown to possess this capability, for example poly(*N*-isopropylacrylamide)[96] and elastin-like polypeptides.[97] These systems are based on macromolecular conformational transitions leading to an inversion in the intersurface interaction potential from net repulsive (hindering protein adsorption) to net attractive (promoting protein adsorption), what we refer to here as "nanomechanical switching." Such net interaction potentials are typically a superposition of numerous nonspecific repulsive (e.g. electrostatic counterion double layer, steric, hydration, etc.) and attractive (e.g. van der Waals, hydrophobic, H-bonding, ionic, etc.) components that can lead to complicated

functional forms which vary with the strength and range of the constituent interactions.[98]

In this chapter, we focus on a unique stimulus-responsive system, polymer "brush-brushes," which are comb-like side-chain graft copolymers chemically end-attached to surfaces at relatively high packing densities where the noncovalent side-chain main-chain interactions are sensitive to various environmental conditions (e.g. pH, salt concentration, etc.). Here, we show that these systems also undergo nanomechanical switching from a net repulsive (high pH) to a net attractive (low pH) intersurface potential. A series of different macromolecular architectures was shown to modulate both nanomechanical switching properties.

4.2 Methods

4.2.1 Sample Preparation

Materials

HS-poly(MAA-*g*-EG) graft polymers were synthesized and characterized as previously described (Table 4.1).[99] Tris (hydroxymethyl) aminomethane (Tris), 4-morpholineethanesulfonic acid monohydrate (MES), acetic and formic acid were all purchased from Sigma-Aldrich. All water used for solutions, rinsing, and storage was deionized (DI, pH 5.6) (18M Ω ·cm resistance). N-type Silicon wafers with 100 orientation were purchased from Crystaltek. Chromium was purchased from R.D. Mathis and gold (99%) was purchased from J & J Materials. All the other chemicals were used as received from commercial suppliers.

End-grafting of HS-poly(MAA-*g*-EG) to planar surfaces

Au-coated silicon substrates were cleaned using a piranha solution (98% H₂SO₄/30%H₂O₂, volume ratio 3:1) for 10 min followed by copious rinsing with water, acetone, and methanol. Any terminal disulfide bonds formed by the -SH end groups of HS-poly(MAA-*g*-EG) were reduced to a thiol group by diluting polymer to 200 μ g/mL of methanol solution in 0.1 mM dithiothreitol (DTT, Sigma-Aldrich) and incubating under

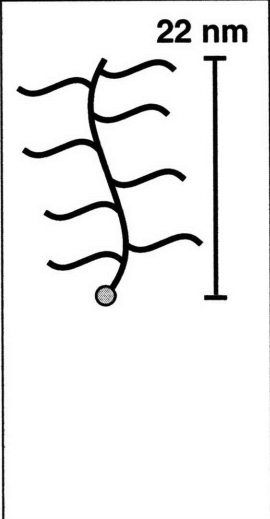
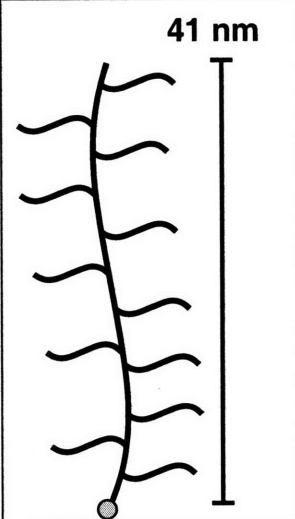
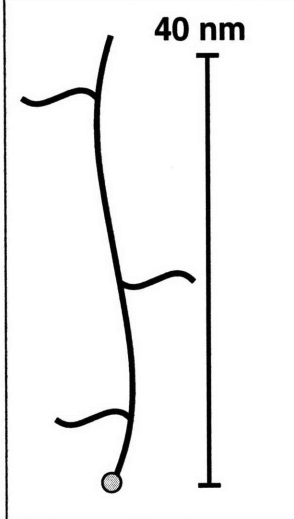
Polymer	HS-poly(MAA-g-EG) _{15K}	HS-poly(MAA-g-EG) _{27K}	HS-poly(MAA-g-EG) _{17K}
M_n (¹ H NMR)	15400	26800	16,600
EG/MAA (mole ratio)	2.2	1.9	0.4
PEG graft density (%)	8.8	7.7	1.9
N_{PEG}	7.8	12.6	3.0
$L_{\text{contour, main chain}}$ (nm)	22.1	41.1	39.8
$L_{\text{contour, side chain}}$ (nm)	6.7	6.7	6.7
Packing density, Γ (molecular separation distance)	0.071 chains/nm ² (~3.8 nm)	0.053 chains/nm ² (~4.3 nm)	0.109 chains/nm ² (~3.1 nm)
Contact angle (DI water, pH5.6)			
Instantaneous advancing	47±2.6°	32±0.6°	44±2.4°
Instantaneous receding	11±0.6°	0°	5±0.5°
Schematic			

Table 4.1. Characterization data of thiol-terminated poly(methacrylic acid-g-ethylene glycol) or HS-poly(MAA-g-EG) comb-type graft copolymers as determined by ¹H nuclear magnetic resonance (NMR), as reported previously.[99] The numerical subscript in the abbreviated polymer name labels refer to the number-average molecular weight, M_n , in g/mol and “K” is an abbreviation for 1000, the poly(ethylene glycol) or PEG graft density (%) is defined as N_{PEG} divided by the total number of backbone monomers where N_{PEG} is the average number of PEG chains per poly(methacrylic acid) or PMAA chain, and L_{contour} is the average contour length calculated from the known molecular weights assuming *ttt* conformations for the PMAA and *ttg* conformations for the PEG, which is known to exist in aqueous solution.[64] The schematics of the polymers are not meant to indicate the actual conformation. The packing density and contact angle of the chemically end-grafted polymer layers are also given.

continuous stirring for 1 h. After removal of the excess reactants using centrifugal filters (Centricon, Millipore, 3000 MW cutoff), the Au substrates were immersed in 0.4 mg/mL of the polymer solution in methanol for 72 h. The end-grafted poly(MAA-g-EG) surfaces were rinsed with acetone, methanol, and deionized water thoroughly before experimentation.

4.2.2 High Resolution Force Spectroscopy (HRFS)

The nanomechanical properties of these three poly(MAA-g-EG) monolayers were measured in aqueous buffer solutions of different pH at constant salt concentration (ionic strength, IS) using the technique of chemically specific high-resolution force spectroscopy. A single Au-coated[69] Si_3N_4 V-shaped cantilevers with square-pyramidal nanosized probe tip (*Thermomicroscopes, Inc.*, Sunnyvale, CA; nominal spring constant, $k = 0.03$ N/m) was functionalized with a carboxyl-terminated SAM (COOH-SAM) by immersing in a 2 mM ethanol solution of a 11-mercaptopundecanoic acid ($\text{HS}(\text{CH}_2)_{10}\text{COOH}$, Sigma-Aldrich) for 24h and was used as a force transducer to record normal force, F (nN), vs probe tip-sample separation distance, D (nm) on loading ("approach" or probe tip advancing toward surface) and unloading ("retract" or probe tip moving away from surface). The probe tip end radius, R_{tip} , was measured after nanomechanical testing, via scanning electron microscopy (SEM, JEOL JSM 6060) and found to be ~ 50 nm. A 1-Dimensional Molecular Force Probe (MFP) (*Asylum Research*, Santa Barbara, CA.) on a *Halcyonics* MOD-1 active vibration isolation system was employed for the experiments. A full description of this instrument, its limits of force and displacement detection in fluids, procedures for cantilever spring constant calibration and conversion of raw data, details of measurement errors, and description of F-D curves including the mechanical instabilities of the cantilever were described previously.[69] F-D curves between COOH-SAM probe tips and the chemically end-grafted poly(MAA-g-EG) monolayers were carried out in buffer solutions of varying pH with a constant ionic strength of 0.005M at room temperature. pH4, pH5 and pH6 buffer solutions were formate, acetate, and MES, respectively, while pH7.1, pH8 and pH9 were Tris. All buffer

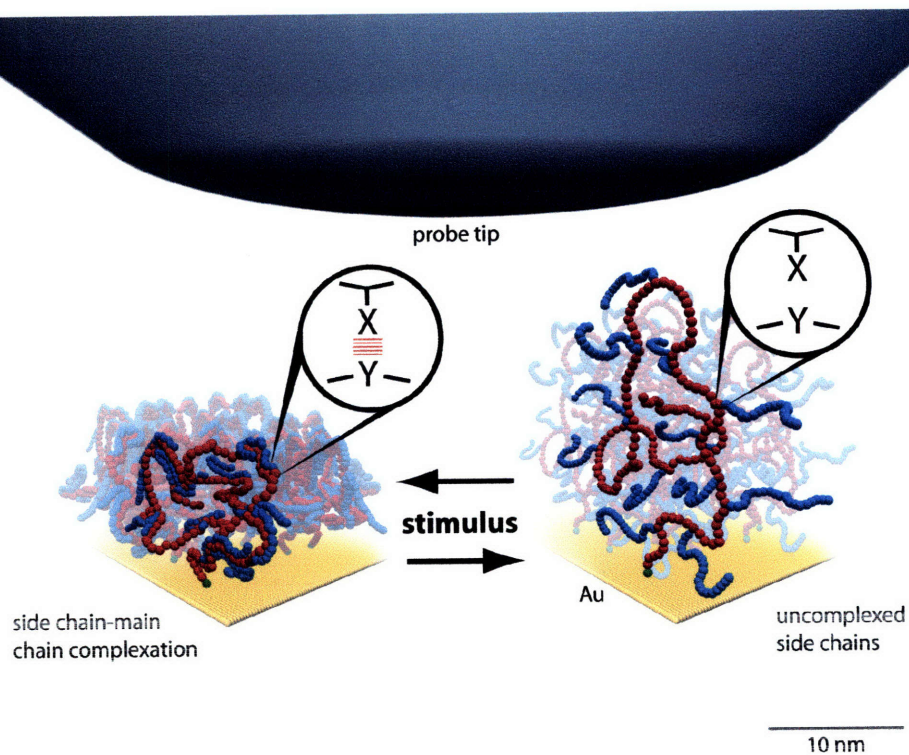


Figure 4.1 Schematic illustration of the pH-stimulated conformational change of poly(methacrylic acid-g-ethylene glycol) or poly(MAA-g-EG) polymer via high resolution force spectroscopy measurement on the polymer layer chemically end-attached to Au by probe tip. The scale is based on the data of the 15K polymer and the probe tip radius is set as 50 nm. X stands for -COOH groups. Y stands for O atoms.

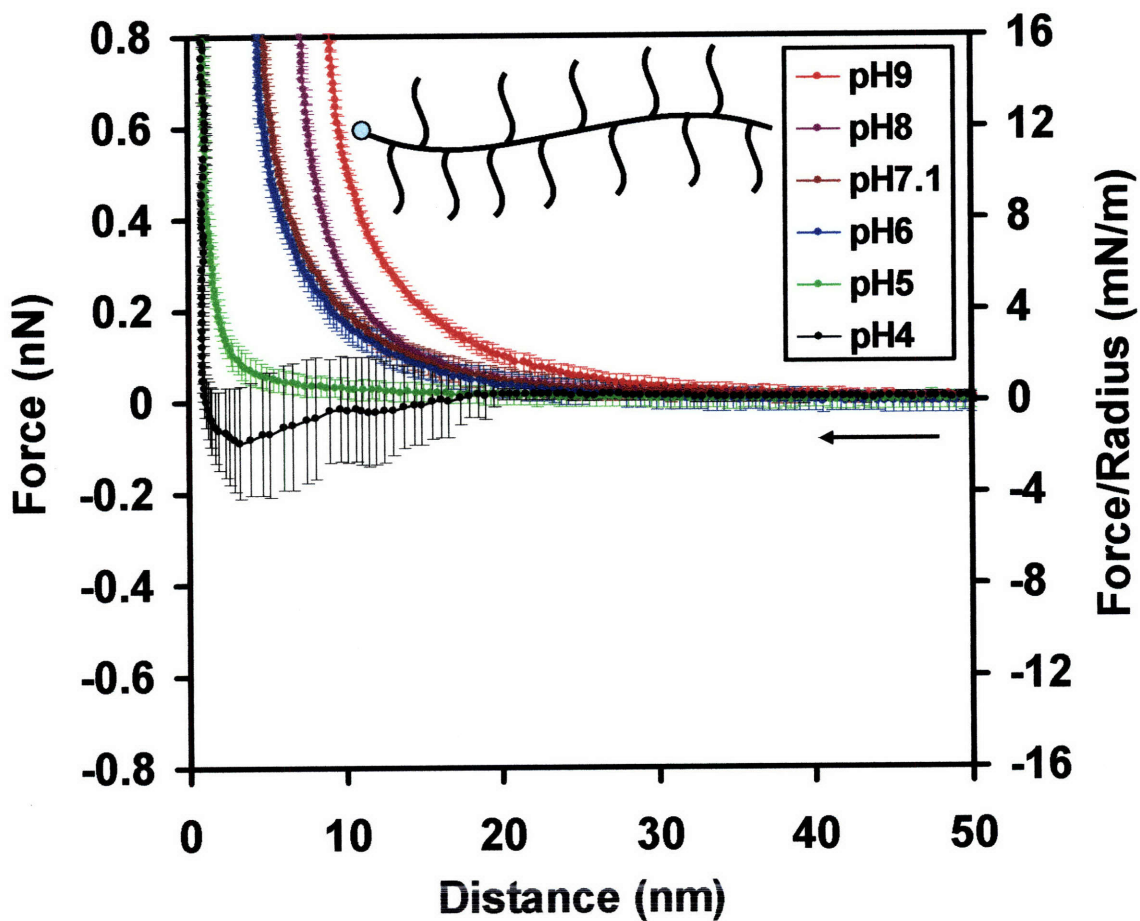
solutions used sodium chloride to adjust the ionic strength to 0.005M. The experimental conditions used a z-piezo velocity of 1 $\mu\text{m/s}$ (where z is the direction normal to the sample plane), a z-range of 1 μm , a z-scan rate=1.0 Hz, and a rate of data acquisition = 5000 points/s. ~ 60 F-D experiments were carried out at six different sites on the sample surface. The vertical constant compliance contact regime of the F-D curves was shifted along the x-axis by the compressed height of the layer at ~1 nN in the experiments, which was measured from height vs. force data obtained by contact mode AFM imaging of microcontact printed samples.[46] The adhesion force / radius for each curve was measured as the maximum force on retract. The maximum adhesion forces of ~60 individual retract F-D curves were averaged to yield the averaged maximum adhesion force (Fig. S1). The series of experiments reported here were reproduced with different probe tips multiple times. Control experiments were run on a COOH-SAM planar substrate at pH9 before and after testing the polymer monolayers to confirm the correct intersurface interaction profile and that the tip chemistry and geometry remained constant throughout the course of the experiments. A single probe tip was used for all nanomechanical experiments to avoid possible variations in the data due to probe tip geometry. The maximum number of chains on the substrate interacting with the probe tip can be approximated from the tip (A_{tip}) and substrate ($A_{\text{substrate}}$) maximum surface interaction areas based on the known tip end radius, R_{tip} , and maximum interaction distance range in a high resolution force spectroscopy experiment, D_I , assuming hemispherical geometry for the probe tip as follows; $A_{\text{tip}}=\pi R_{\text{tip}}D_I$ and $A_{\text{substrate}}=\pi(R_{\text{tip}}^2 - (R_{\text{tip}}-D_I)^2)$, also taking into account the known polymer surface packing density, Γ (chains/ nm^2). The estimated maximum number of polymer chains interacting with the probe tip at contact ($D=0$) was a few hundred.

4.3 Results and Discussion

4.3.1 HRFS on Approach

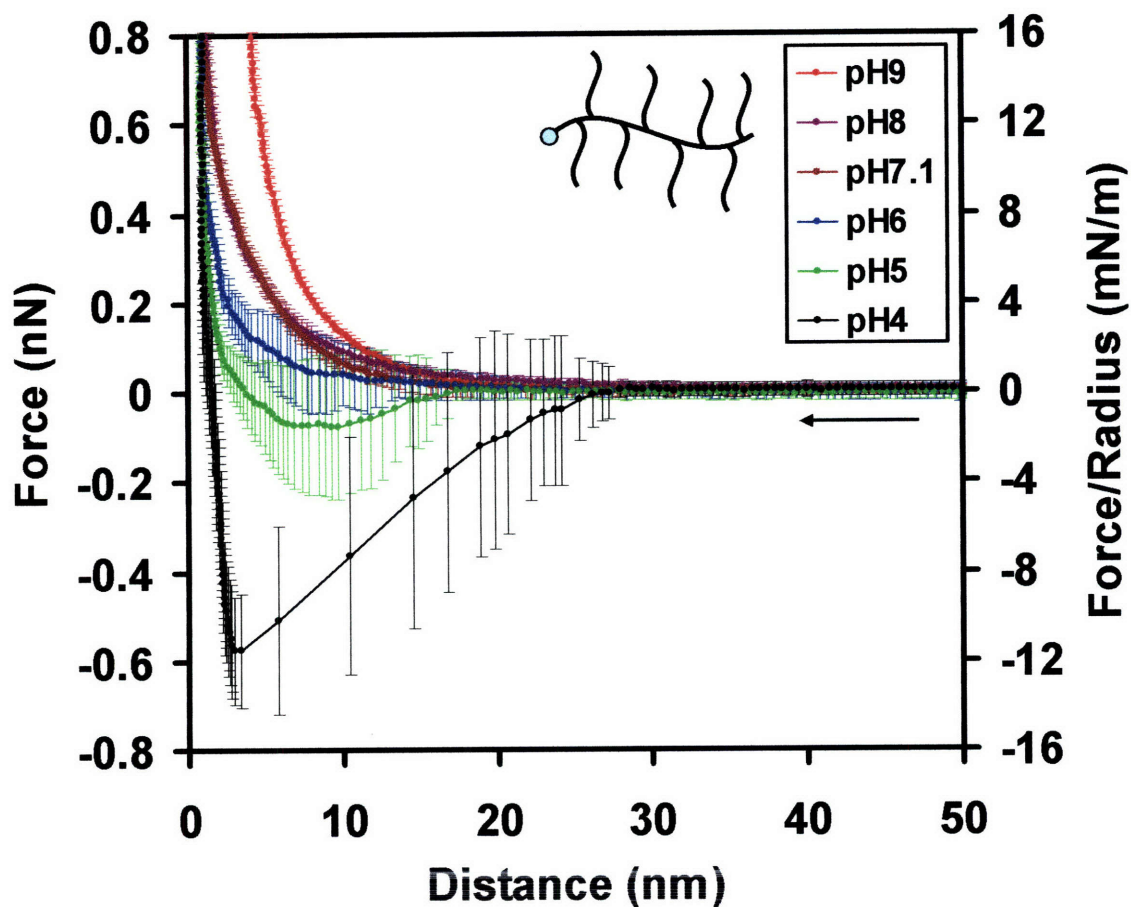
Chemically specific high resolution force spectroscopy using a nanosized probe tip (end radius, $R_{\text{tip}} \sim 50$ nm) was employed to measure the normal intersurface force (F) versus probe-tip sample separation distance (D) in aqueous electrolyte solution as a function of pH at constant ionic strength ($IS = 0.005M$) on "approach" (probe tip advancing towards surface) and "retract" (probe tip retracting away from surface) for the chemically end-grafted poly(MAA-*g*-EG) layers. The estimated maximum number of polymer chains interacting with the probe tip at contact ($D=0$) was \sim a few hundred (see Methods 4.2.2). The probe tip was functionalized with a carboxyl-terminated self-assembling monolayer (COOH-SAM) in order to amplify the magnitude of the forces measured since the COOH-SAM has a $pK_a \sim 5.5$ [100] which is similar to the pH value of the stimulus responsive transition for the poly(MAA-*g*-EG) layer. Nanomechanical switching on approach was observed for the 27K polymer (longer main chain, higher density of side chains) between pH 4 and 5 (**Figure 4.2a**) and for the 15K polymer (shorter main chain, higher density of side chains) between pH5 and 6 (**Figure 4.2b**), but not for the 17K polymer (longer main chain, lower density of side chains) which remained net repulsive throughout the pH range tested (**Figure 4.2c**).

For the 27K polymer at high pH 6-9, a net nonlinear repulsive, interaction was observed, the range of which decreased from ~ 42 nm at pH9 to ~ 30 nm at pH6. At lower pH5 the repulsive range decreased to ~ 15 nm and at pH4, the net intersurface interaction reversed in sign becoming purely attractive and nonlinear with decreasing D . The range of the interaction at pH4 was ~ 20 nm and the magnitude of the average maximum attractive force was ~ 0.08 nN. This "nanomechanical switching" or conversion from a net repulsive intersurface interaction to a net attractive intersurface interaction as a function of a given stimulus was observed to be reversible - systems with this property are particularly interesting due to the expected dramatic change in surface properties that likely accompany this transition. The increase in standard deviation of the data observed with decreasing pH also indicates the change in molecular mechanism of interaction. The 15K polymer also exhibited a repulsive to attractive transition (**Figure 2b**), except the pH at



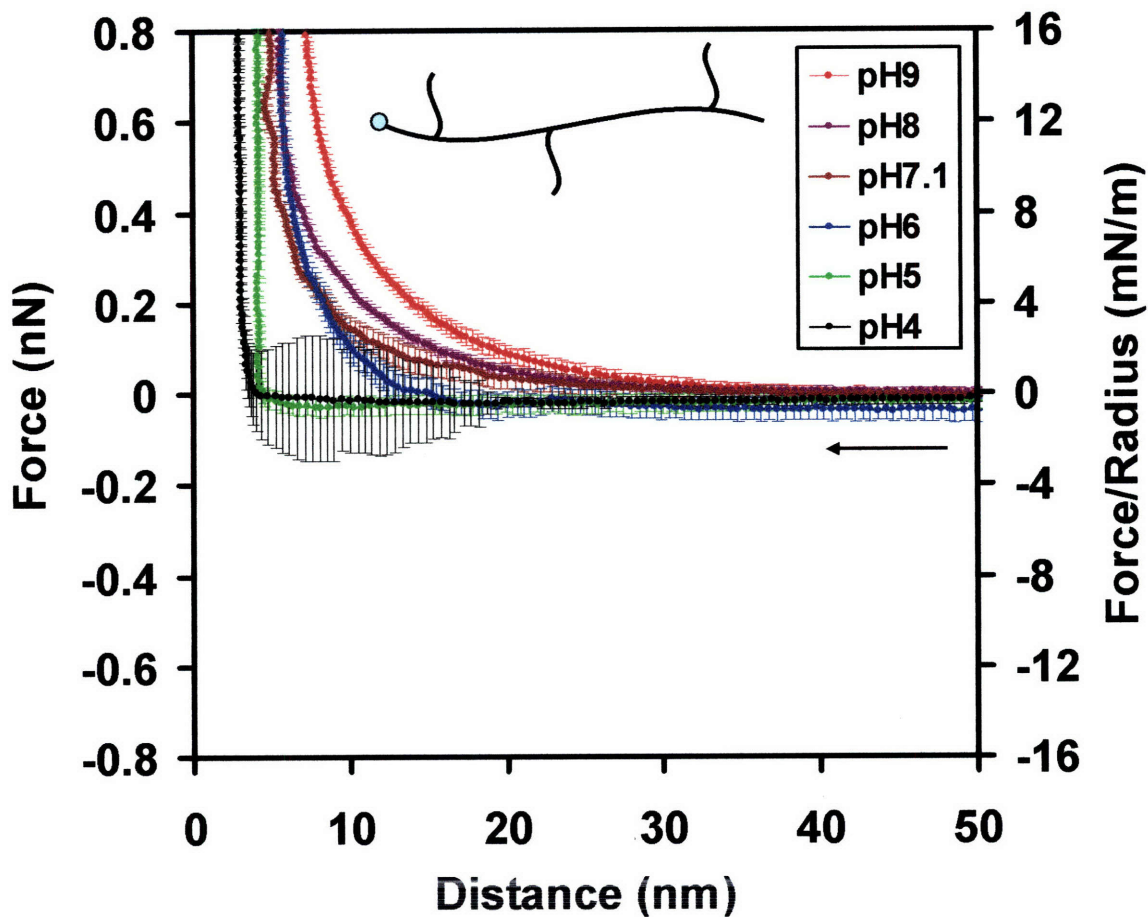
(a)

Figure 4.2(a) Averaged nanomechanical data measured on approach between a probe tip functionalized with a carboxy-terminated self-assembling monolayer or COOH-SAM ($\text{HS}-(\text{CH}_2)_{10}\text{COOH}$) (probe tip end radius, $R_{tip} \sim 50$ nm) and chemically end-grafted poly(methacrylic acid-g-ethylene glycol) or poly(MAA-g-EG) layers as a function of pH at a constant ionic strength of 0.005M. Hi-lo bars represent one standard deviation for $n=60$ experiments; (a) 27K, (b) 15K, and (c) 17K. The inset schematic does not represent the actual conformation of the polymer (as this is changing with pH).



(b)

Figure 4.2(b) Averaged nanomechanical data measured on approach between a probe tip functionalized with a carboxy-terminated self-assembling monolayer or COOH-SAM ($\text{HS}-(\text{CH}_2)_{10}\text{COOH}$) (probe tip end radius, $R_{\text{tip}} \sim 50$ nm) and chemically end-grafted poly(methacrylic acid-*g*-ethylene glycol) or poly(MAA-*g*-EG) layers as a function of pH at a constant ionic strength of 0.005M. Hi-lo bars represent one standard deviation for $n=60$ experiments; (a) 27K, (b) 15K, and (c) 17K. The inset schematic does not represent the actual conformation of the polymer (as this is changing with pH).



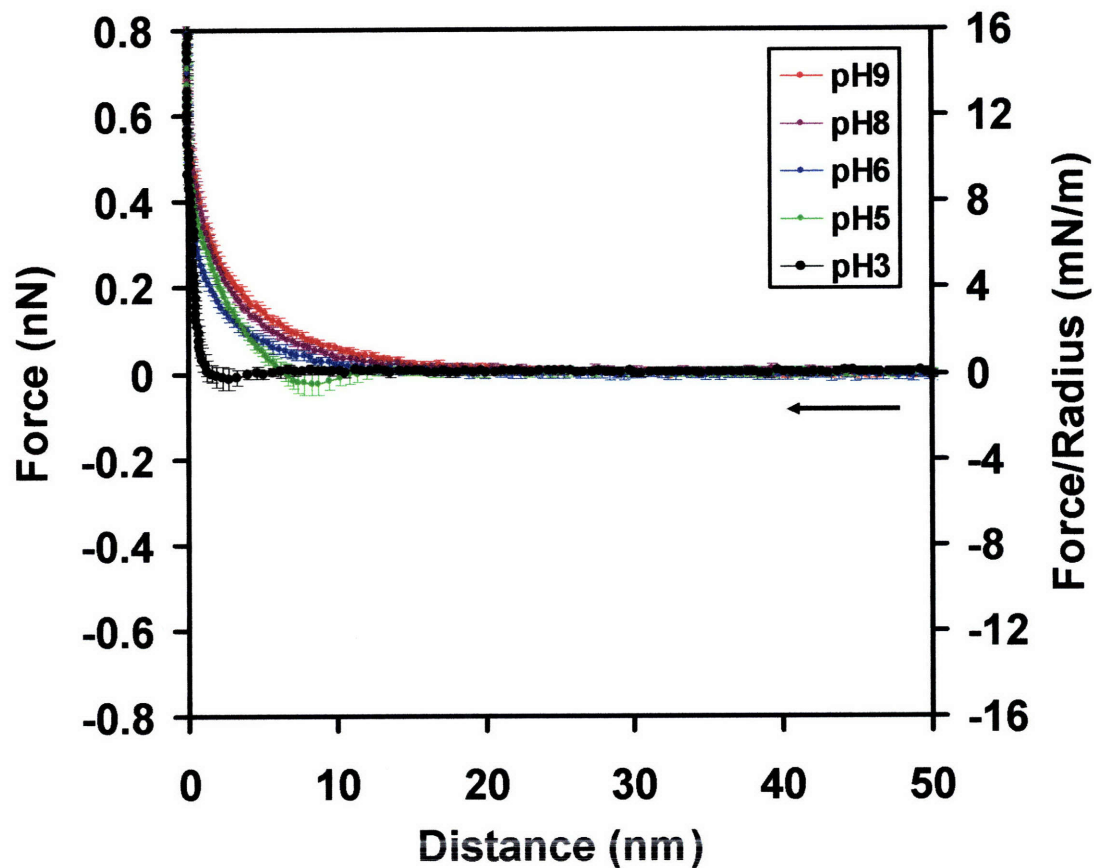
(c)

Figure 4.2(c) Averaged nanomechanical data measured on approach between a probe tip functionalized with a carboxy-terminated self-assembling monolayer or COOH-SAM ($\text{HS}-(\text{CH}_2)_{10}\text{COOH}$, probe tip end radius, $R_{tip} \sim 50$ nm) and chemically end-grafted poly(methacrylic acid-*g*-ethylene glycol) or poly(MAA-*g*-EG) layers as a function of pH at a constant ionic strength of 0.005M. Hi-lo bars represent one standard deviation for $n=60$ experiments; (a) 27K, (b) 15K, and (c) 17K. The inset schematic does not represent the actual conformation of the polymer (as this is changing with pH).

which this occurs was shifted compared to the 27K, with both the pH4 and pH5 being net attractive. The average maximum attractive force increased from $\sim 0.07\text{nN}$ at pH5 to $\sim 0.58\text{nN}$ at pH4, which is much greater than that for the 27K polymer. It is probably caused by the interaction between the probe tip and a portion of the gold substrate not covered by the 15K polymer layers, instead of indicative of the characteristics of the polymer layers, since the 15K polymer has the shortest backbone length among the three polymers and may not be able to fully cover the substrate area at a collapsed state. The 17K polymer did not exhibit any net attractive profiles and instead was repulsive for the entire pH range, with the maximum distance of repulsion decreasing with decreasing pH from $\sim 39\text{nm}$ at pH9 to $\sim 5\text{nm}$ at pH4.

At high pH and at longer distance ranges, electrostatic double layer repulsion between ionized COO^- groups on the probe tip SAM and the PMAA main chain of the graft copolymer are expected to dominate the net repulsive interaction profile since both the polymer and probe tip will be negatively charged (the pK_a of PMAA is $\sim 5-6.5$ [101]). The reduction in the range of the repulsive interactions with decreasing pH in the high pH regime can be attributed to titration of the carboxylic acid groups on the PMAA main chain of the copolymer on the surface (reducing both the surface charge density and polymer layer height), as well as on the probe tip. At low pH the attractive interaction is likely a combination of the more hydrophobic nature of the side-chain main-chain complex, as well as H-bonding between uncomplexed protonated COOH groups on the PMAA main chain and probe tip. The increase in the standard deviation of the data observed with decreasing pH indicates the change in molecular mechanism of interaction. At high pH, the electrostatic double layer dominated profiles have relatively small standard deviations indicating homogeneity of the interaction, while the lower pH attractive profiles exhibits a broader more heterogeneous distribution in the interaction profiles which is expected due to the collapse of the polymer chains in conjunction with the small nanoscale dimensions of the probe tip.

The 15K polymer had a similar side chain grafting density as the 27K but the contour length was approximately 0.5 that of the 27K polymer, which changed the nanomechanical interaction profiles in a number of ways. The range of the interaction decreased accordingly by ~ 0.5 ; the pH of nanomechanical reversal shifted up to pH 5-6;



(c)

Figure 4.3 Averaged nanomechanical data measured on approach between a probe tip functionalized with a carboxy-terminated self-assembling monolayer or COOH-SAM ($\text{HS}-(\text{CH}_2)_{10}\text{COOH}$, probe tip end radius, $R_{tip} \sim 50$ nm) and chemically end-grafted COOH-SAM ($\text{HS}-(\text{CH}_2)_{10}\text{COOH}$) as a function of pH at a constant ionic strength of 0.005M. Hi-lo bars represent one standard deviation for $n=60$ experiments.

the average maximum attractive force increased to ~0.58 nN at pH4 (~7× times larger than the 27K at this pH). The 17K polymer had a similar contour length as the 27K polymer but a grafting density 4.4× smaller and only exhibited a net repulsive interaction throughout the entire pH range studied, suggesting that this polymer remains much less hydrophobic at low pH due to the smaller PEG side chain grafting density. The effect of macromolecular architecture on the nanomechanical switching properties of end-grafted polymer layers was also supported by the high resolution force spectroscopy on approach of end-grafted COOH-SAM using COOH-SAM functionalized probe tip **Figure 4.3**. Without intramolecular complexation occurring via hydrogen bonding, the end-grafted COOH-SAM was much less hydrophobic and more hydrophilic at low pH 3 - 5, resulting in a very weak nanomechanical switching as pH decreased.

The compressive stress versus strain data between a -COOH SAM tip and the polymer layer surface were calculated based on the averaged F-D curves on approach at pH9 and are plotted in **Figure 4.4**. The full polymer layer thickness, h , was calculated from the electrostatic interaction distance minus five times of the Debye length[102] (~4.3 nm when IS=0.005M). When the separation distance, D , is less than h , the tip will touch the polymer layer and compress it. The strain is given by $1-D/h$. While the stress was calculated using the approximation that the modulus of the polymer layer doesn't change when the tip compresses the polymer layer by a very small distance dX and the effective tip area (area that the interaction force, F , applied to) increases by $\Delta = 2\pi * R_{tip} * dX$, where R_{tip} is the radius of the curvature of the probe tip. When the force increases from F_1 to F_2 as the tip compress the polymer layer by dX , the effective tip area increases from A to $A+\Delta$. The compressive stress P at distance $X-dX$ is given by the following equation:

$$\frac{A + \Delta}{A} = \frac{F_2}{F_1} \Rightarrow P = \frac{F_2}{A + \Delta} = \frac{F_2}{\Delta} - \frac{F_1}{\Delta}$$

The force, F , and the separation distance, D , were fitted to get the appropriate dX value and the compressive stress P was obtained from the analytical solution. As shown in **Figure 4.4**, all three polymers exhibit a nonlinear increase in stress as strain increases. No significant difference was observed between the three datasets indicating neither the

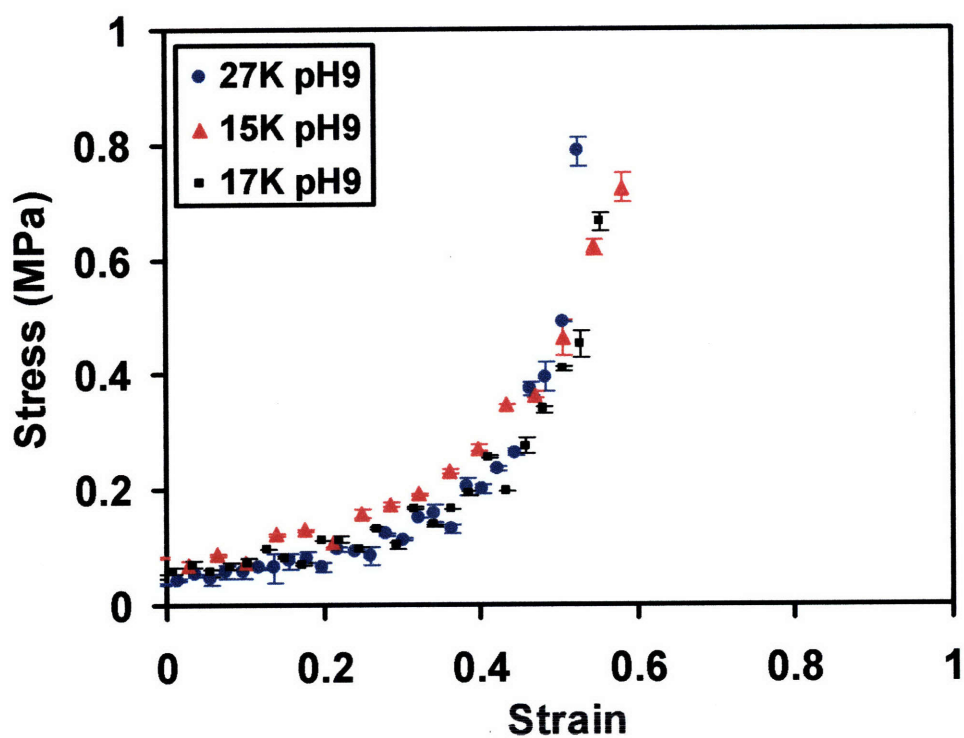


Figure 4.4 Nanoscale compressive stress vs. strain plot calculated from nanomechanical data measured on approach between a probe tip functionalized with a carboxyl-terminated self-assembling monolayer and chemically end-grafted poly(methacrylic acid-*g*-ethylene glycol) or poly(MAA-*g*-EG) layers at pH9 and a constant ionic strength of 0.005M. Hi-lo bars represent one standard deviation.

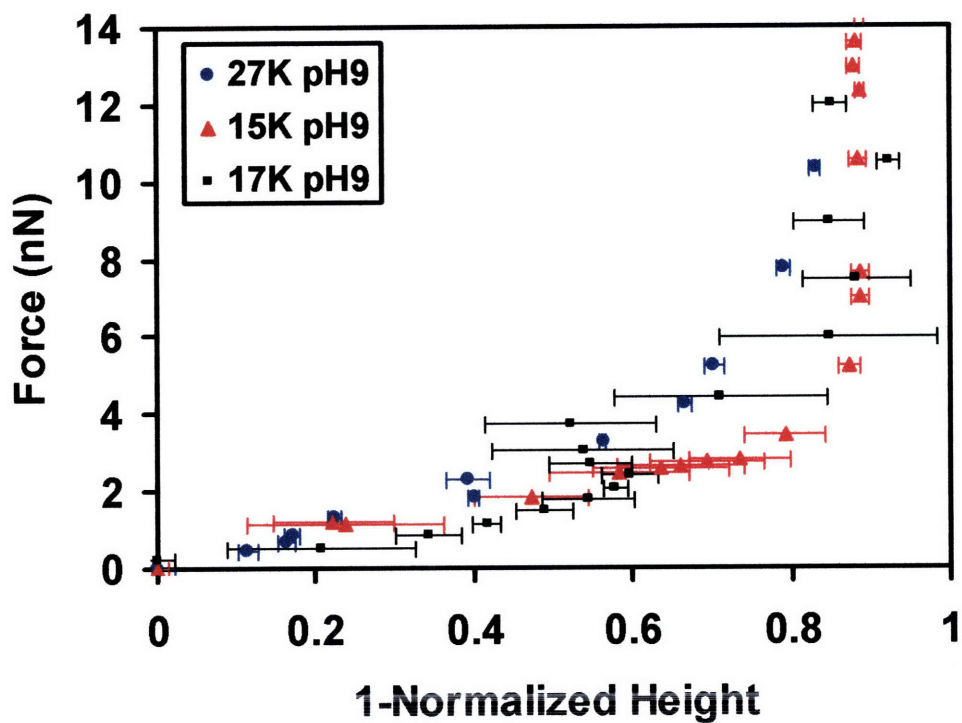


Figure 4.5 Force versus [1-Normalized Height] derived from Height versus Force measurement via contact mode AFM, where left- and right- error bars represent the standard deviation of eight scan lines in height measurement. The probe tip was functionalized with a hydroxyl-terminated self-assembling monolayer. The AFM imaging was conducted at pH9 and a constant ionic strength of 0.005M.

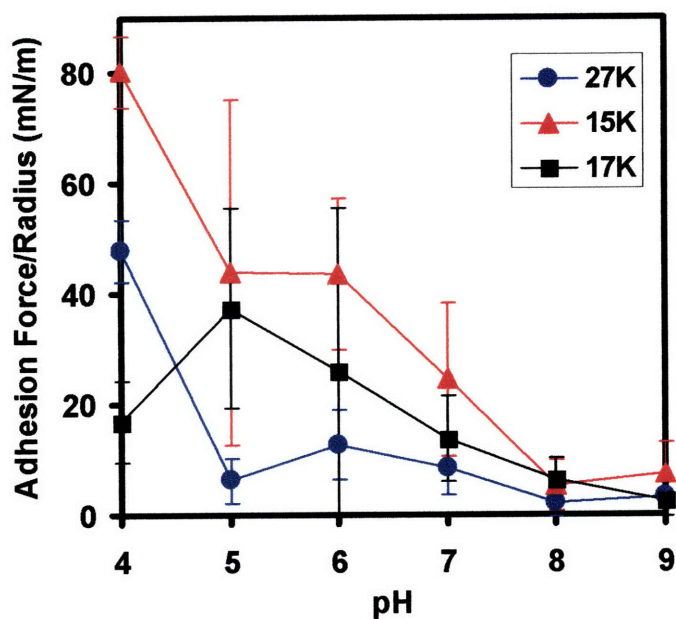
grafted PEG side chains nor the molecular weight of PMAA backbone influence the compressive modulus of the three polymer layers in a fully charged, uncomplexed and hydrophilic conformation.

For comparison, the force versus 1-normalized height calculated from measuring the height of end-grafted polymer layer with varying normal load via contact mode AFM (chapter 3.3 (D)) is plotted in **Figure 4.5**, where 1-normalized height = $1 - d/h$ (d is the measured height of end-grafted polymer layer. The full polymer layer thickness, h , was calculated from the electrostatic interaction distance from HRFS approach curves minus five times of the Debye length ~ 4.3 nm when $IS=0.005M$). The difference in the compression resistance of all three polymer monolayers in aqueous solution at pH9 is not significant, which is consistent with **Figure 4.4**.

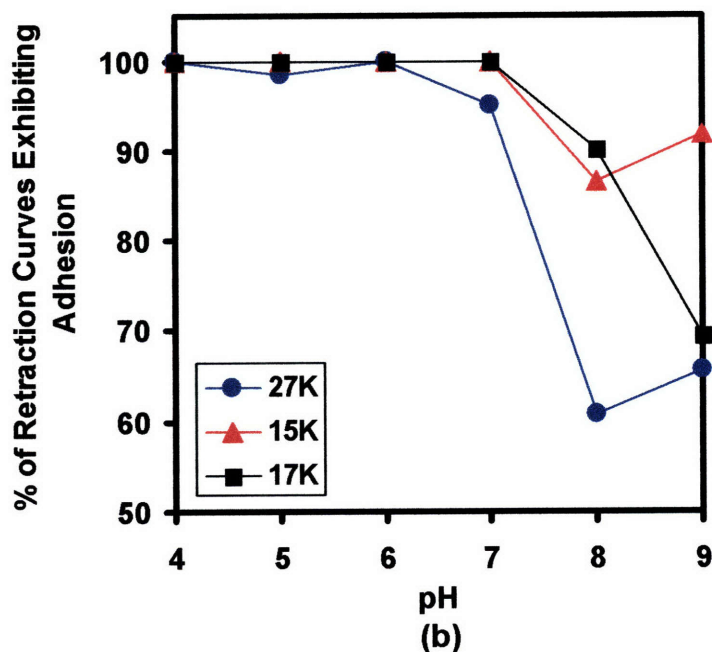
4.3.2 HRFS on Retract

Nanomechanical switching was also observed for all of the polymer layers on retract where a gradual reduction in adhesion (maximum force on retract) takes place from pH 4 (20-80 mN/m) to pH 9 (essentially zero). At low pH4, the 15K polymers exhibited the greatest adhesion (higher side chain grafting density, shorter length of backbone), followed by the 27K (higher side chain graft density, longer length of backbone), followed by the 17K (longer length of backbone, lower side chain grafting density), a trend consistent with the approach interaction profiles which again highlight the effect of macromolecular architecture and the ability to tune nanomechanical properties. The percentage of nanomechanical experiments exhibiting adhesion was also modulated by pH with all polymers exhibiting adhesion 100% of the time at low pH and decreasing above pH6-7.

For the 27K polymer layer, the average maximum adhesion force jumped from $\sim 0.31nN$ ($\sim 6.25mN/m$) at pH5 to $\sim 2.4nN$ ($\sim 47.8mN/m$) at pH4 (**Figure 4.5a**). The 15K and 17K polymer layers exhibited similar trend that the average maximum adhesion force generally increases as pH decreases. The typical nanomechanical adhesion F-D curves at pH4 shows the magnitude of the adhesion force is in the order of $15K > 27K > 17K$ (**Figure 4.7**), which is consistent with the comparison of the nanomechanical data on approach at pH4.



(a)



(b)

Figure 4.6 Nanomechanical data measured on retract between a probe tip functionalized with a carboxyl-terminated self-assembling monolayer ($\text{HS}-(\text{CH}_2)_{10}\text{COOH}$, probe tip end radius, $R_{\text{tip}} \sim 50$ nm) and chemically end-grafted poly(methacrylic acid-*g*-ethylene glycol) or poly(MAA-*g*-EG) layers as a function of pH at a constant ionic strength of 0.005M. (a) Nanoscale adhesion force (maximum force exhibited on retraction) normalized by the probe tip end-radius where the hi-low bars represent one standard deviation and (b) Percentage of retraction curves exhibiting adhesion ($n=60$ experiments).

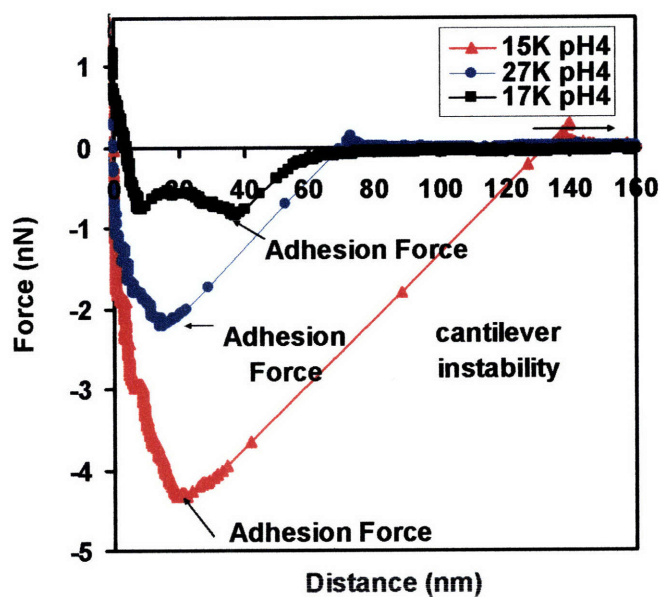


Figure 4.7 Nanomechanical data measured on retract between a probe tip functionalized with a carboxyl-terminated self-assembling monolayer and a chemically end-grafted poly(methacrylic acid-*g*-ethylene glycol) or poly(MAA-*g*-EG) layers at pH4 and a constant ionic strength of 0.005M (probe tip end radius, $R_{tip} \sim 50$ nm). Typical individual curves are shown.

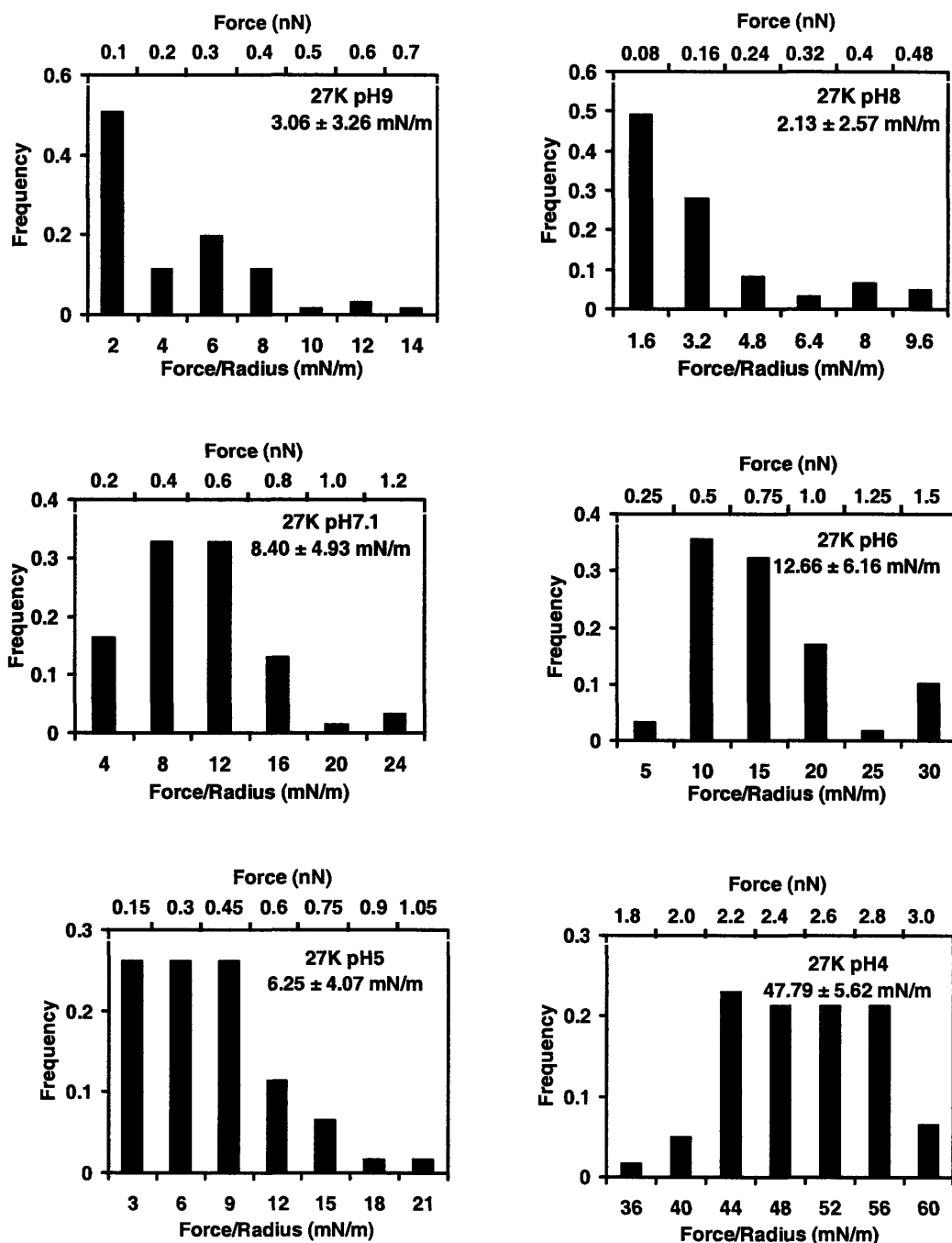


Figure 4.8(a) Probability histograms for nanoscale adhesion between a probe tip functionalized with a carboxyl-terminated self-assembling monolayer and a chemically end-grafted poly(methacrylic acid-*g*-ethylene glycol) or poly(MAA-*g*-EG)_{27K} layer as a function of pH and a constant ionic strength of 0.005M. Hi-lo bars represent one standard deviation for $n=60$ experiments.

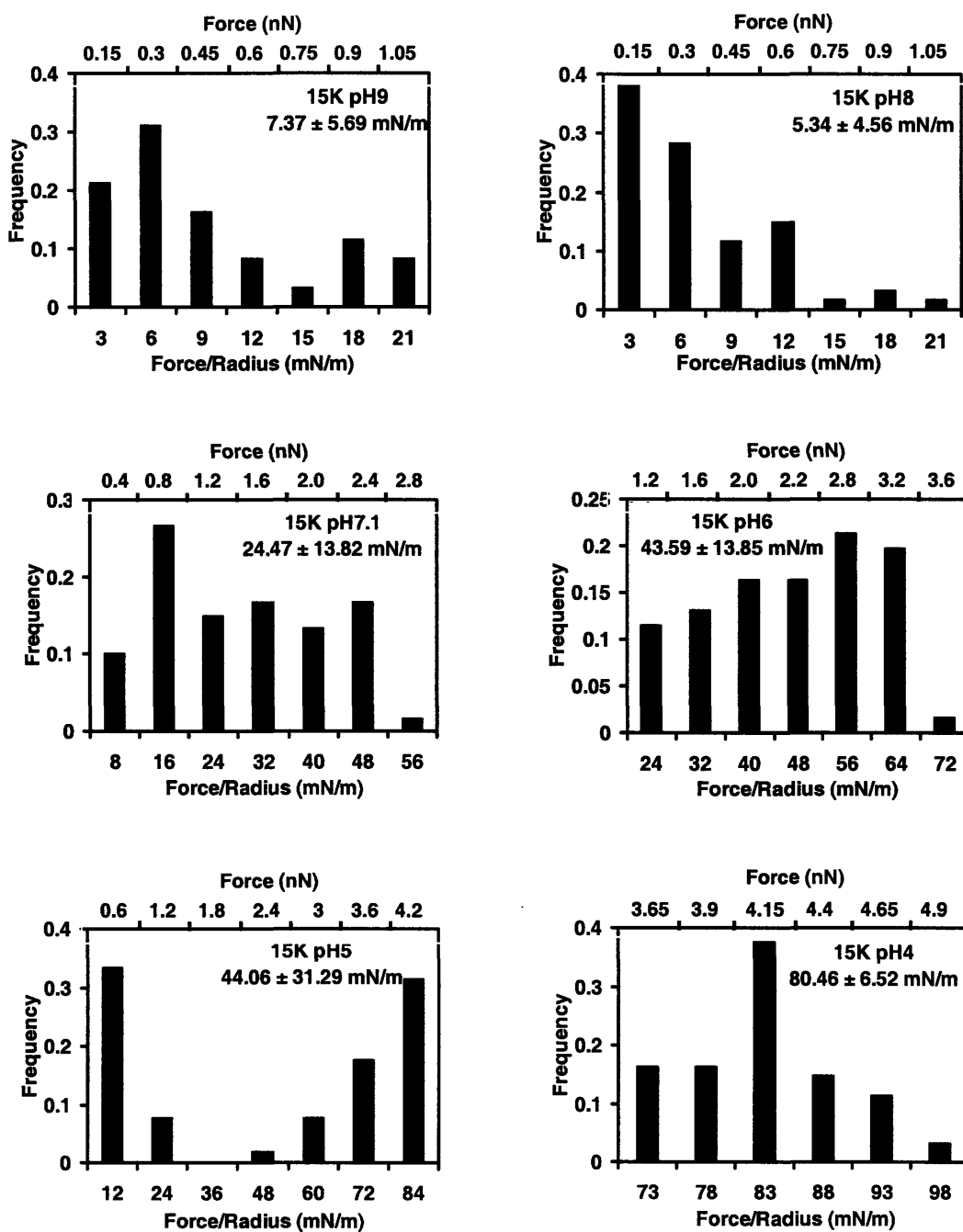


Figure 4.8(b) Probability histograms for nanoscale adhesion between a probe tip functionalized with a carboxyl-terminated self-assembling monolayer and a chemically end-grafted poly(methacrylic acid-*g*-ethylene glycol) or poly(MAA-*g*-EG)_{15K} layer as a function of pH and a constant ionic strength of 0.005M. Hi-lo bars represent one standard deviation for $n=60$ experiments.

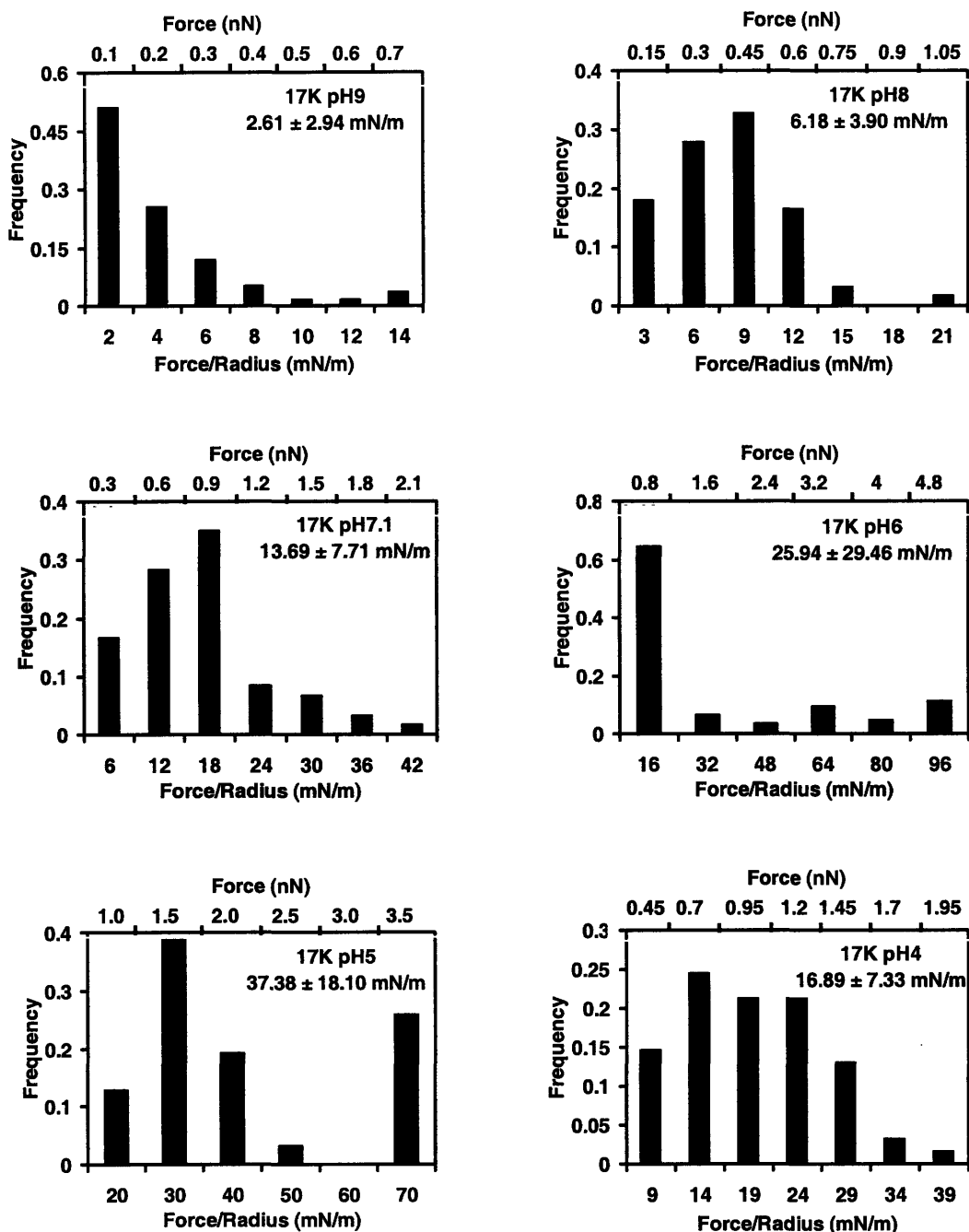


Figure 4.8(c) Probability histograms for nanoscale adhesion between a probe tip functionalized with a carboxyl-terminated self-assembling monolayer and a chemically end-grafted poly(methacrylic acid-g-ethylene glycol) or poly(MAA-g-EG)_{17K} layer as a function of pH and a constant ionic strength of 0.005M. At pH 9 and pH8, adhesion was not observed for all the experiments. Hi-lo bars represent one standard deviation for $n=60$ experiments.

Statistically, ~ 65-70% of the retract force curves exhibited adhesion at pH8, while almost 100% of the retract force curves showed adhesion force at pH<7 for the 27K and the 17K polymers. The percentages of the adhesion retract force curves are ~ 85-90% at pH>8 and 100% at pH<7 for the 15K polymer (**Figure 4.6b**). The detailed statistical analysis of adhesion forces on retracts for all three polymer layers is summarized in **Figure 4.8**.

4.3.3 Comparison between HRFS on Approach and Predictions of a Poisson-Boltzmann Based Theoretical Model for Electrostatic Forces

Nanomechanical data for the 27K polymer at high pH were compared to the predictions of two types of Poisson-Boltzmann based theoretical models for the electrostatic double layer component of the interaction where all of the parameters were fixed to known values; a "surface charge" model which approximates the macromolecular layer as a uniform, flat surface charge density[103] and a "volume charge" model which assumes the charge is homogeneously distributed throughout a volume of the polymer layer (**Figure 4.9**).[104] The polymer layer heights can be estimated from the nanomechanical data as the range of the interaction (maximum distance of first detectable force above the noise level, D_{max}) minus $5\kappa^{-1}$ (where κ^{-1} is the electrical interaction (Debye) length ~ 4.3 nm for IS = 0.005M). For example, in **Figure 4.9a** the polymer layer height would be equivalent to ~ 30 nm and hence, for $D < 30$ nm additional repulsive contributions such as steric interactions may take place. As shown in **Figure 4.9a**, the surface charge model significantly underestimates the interaction force at pH9, which is as expected because the polymer layers are charged and extended away from the surface at high pH (as quantified by the height values of $0.2-0.4L_{contour}$) and in the surface charge model both long range electrostatics and sterics due to the volume of the polymer layer are not taken into account. Given that the Debye length $\kappa^{-1} = \sim 4.3$ nm (at IS=0.005M) is comparable to the separation distance of end-grafted polymer molecules (~3-4 nm), we expect that the charge distribution inside the polymer layers can be approximated as a uniform volume charge density. But as indicated by **Figure 4.9a**, the volume charge model prediction overestimates the interaction force throughout the entire

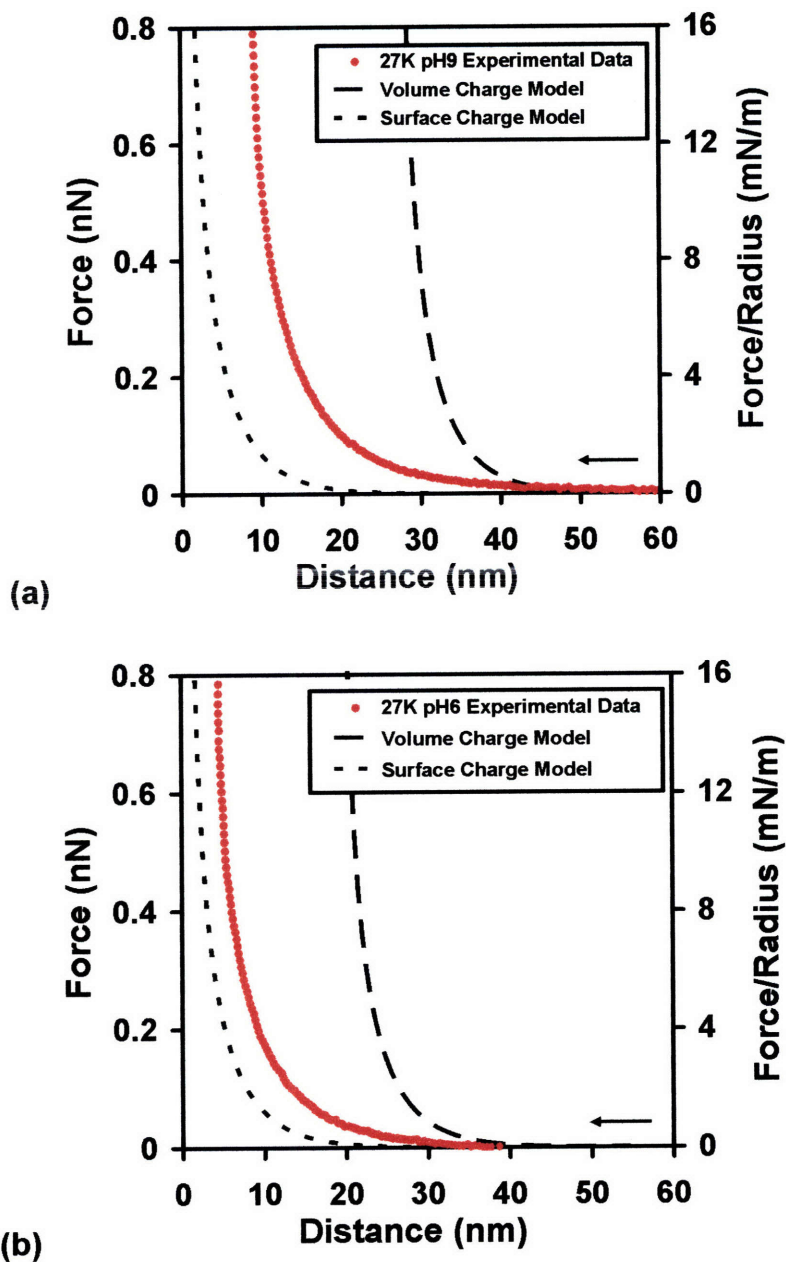
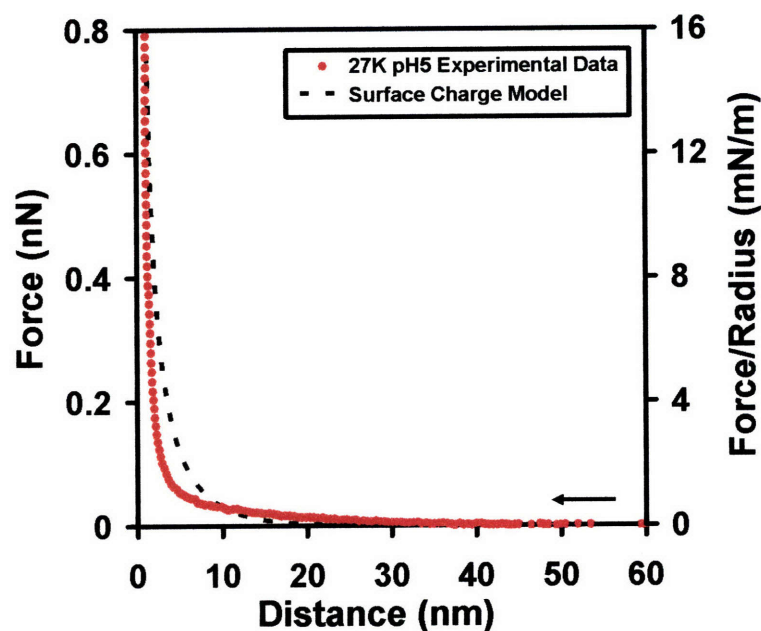


Figure 4.9a,b Comparison of the theoretical predictions of Poisson-Boltzmann based electrostatic double layer surface and volume charge models with nanomechanical data on approach of a probe tip functionalized with a carboxyl-terminated self-assembling monolayer (HS-(CH₂)₁₀COOH, probe tip end radius, $R_{tip} \sim 50$ nm) and chemically end-grafted poly(methacrylic acid-*g*-ethylene glycol)_{27K} layers at (a) pH9 (model parameters were estimated as detailed in the Supplementary Materials section and fixed to $\sigma_{tip} = \sigma_{COO^-}$ (C/m²) = -0.021, $\sigma_{sub} = \sigma_{polymer}$ (C/m²) = -1.2992, $\rho_{sub} = \rho_{polymer}$ (C/m³) = -4.64×10^7) (b) pH6 ($\sigma_{tip} = \sigma_{COO^-}$ (C/m²) = -0.01596, $\sigma_{sub} = \sigma_{polymer}$ (C/m²) = -0.98738, $\rho_{sub} = \rho_{polymer}$ (C/m³) = -4.91×10^7), (c) pH5 ($\sigma_{tip} = \sigma_{COO^-}$ (C/m²) = -0.00504, $\sigma_{sub} = \sigma_{polymer}$ (C/m²) = -0.31224) and a constant ionic strength of 0.005M (see Supplementary Material for details of calculations). Experimental data represents averages of $n=60$ experiments.



(c)

Figure 4.9c. Comparison of the theoretical predictions of Poisson-Boltzmann based electrostatic double layer surface and volume charge models with nanomechanical data on approach of a probe tip functionalized with a carboxyl-terminated self-assembling monolayer (HS-(CH₂)₁₀COOH, probe tip end radius, $R_{tip} \sim 50$ nm) and chemically end-grafted poly(methacrylic acid-*g*-ethylene glycol)_{27K} layers at (a) pH9 (model parameters were estimated as detailed in the Supplementary Materials section and fixed to $\sigma_{tip} = \sigma_{COO^-}$ (C/m²) = -0.021, $\sigma_{sub} = \sigma_{polymer}$ (C/m²) = -1.2992, $\rho_{sub} = \rho_{polymer}$ (C/m³) = -4.64×10^7) (b) pH6 ($\sigma_{tip} = \sigma_{COO^-}$ (C/m²) = -0.01596, $\sigma_{sub} = \sigma_{polymer}$ (C/m²) = -0.98738, $\rho_{sub} = \rho_{polymer}$ (C/m³) = -4.91×10^7), (c) pH5 ($\sigma_{tip} = \sigma_{COO^-}$ (C/m²) = -0.00504, $\sigma_{sub} = \sigma_{polymer}$ (C/m²) = -0.31224) and a constant ionic strength of 0.005M (see Supplementary Material for details of calculations). Experimental data represents averages of $n=60$ experiments.

range of the interaction. According to the Manning criterion,[105] if the equivalent line charge density of a polyelectrolyte, $\xi=\lambda_B/d$, is greater than unity, where d is the intercharge spacing and $\lambda_B=e^2/\epsilon k_B T$ is the Bjerrum length, defined to be the distance at which the Coulombic interaction energy between two monovalent charges embedded in a uniform dielectric medium is equal to $k_B T$ ($\lambda_B=0.714$ nm in water at 298K), monovalent counterions will condense on the polyelectrolyte until its effective charge density is reduced to unity. For poly(MAA-g-EG), the theoretical equivalent line charge density is 0.97 (assuming a trans conformation, bond angle of 109.5°, C-O bond length of 0.142nm, C-C bond length of 0.154 nm and a Bjerrum length of 0.714 nm). When the polymer layer is compressed, it is very likely that the equivalent line charge density becomes greater than unity and then the lack of inclusion of counterion condensation would make the charge density and hence, repulsive force overestimated at pH9. At pH 6, a similar trend is observed for the predictions of the surface charge model and the volume charge model except the theoretical curves are somewhat closer to the experimental data (**Figure 4.9b**). At pH5 the polymer height drops dramatically due to the conformational transition and hence, the surface charge model fits the data fairly well (**Figure 4.9c**), slightly overestimating the data likely due to additional hydrophobicity.

Poisson-Boltzmann-based electrostatic double layer models

The averaged nanomechanical data on approach were compared to the predictions of two Poisson-Boltzmann-based theoretical models for the electrostatic double layer component of the net intersurface interaction; a planar constant surface charge density.[103] and a homogeneous volume charge density.[106] The PB equation was solved numerically in a plane parallel geometry to obtain the electrical potential, Φ , in all space using a Newton method on finite difference grid.[102] Φ was then used to calculate the electrostatic free energy, and the force was calculated as the derivative of the free energy with respect to distance perpendicular to the sample plane. The probe tip geometry was approximated as a hemisphere with an end-radius ~ 50 nm by using the calculated force between the planar surfaces and summing up the force on appropriately sized concentric cylinders. The control data for the COOH-SAM probe tip versus the

COOH-SAM substrate at pH 9 was fit to the surface charge model assuming the surface charge density on the tip, σ_{tip} , was equal to the surface charge density on the substrate, σ_{sub} , resulting in $\sigma_{COO^-} = -0.021 \text{ C/m}^2$. All of the parameters used in the simulations were calculated and fixed to their measured values as follows (**Table 4.2**).

At pH = 9, $\sigma_{tip} = \sigma_{COO^-} = -0.021 \text{ C/m}^2$. At pH = 6 and 5, σ_{tip} was determined by the following formula :

$$\sigma_{tip} = \sigma_{COO^-} = -0.021 \times \frac{10^{-5.5}}{10^{-pH} + 10^{-5.5}} \quad (a)$$

$\sigma_{polymer}$ is the surface charge density on the substrate due to the polymer in the surface charge density model determined by:

$$\sigma_{sub} = \sigma_{polymer} = \frac{\# \text{ MAA} \times 1.602 \times 10^{-19}}{s^2} \times \frac{10^{-5.5}}{10^{-pH} + 10^{-5.5}} \quad (b)$$

$\rho_{polymer}$ is the volume charge density on the substrate due to the polymer in the volume charge density model. Similarly :

$$\rho_{sub} = \rho_{polymer} = \frac{\# \text{ MAA} \times 1.602 \times 10^{-19}}{\text{height} \times s^2} \times \frac{10^{-5.5}}{10^{-pH} + 10^{-5.5}} \quad (c)$$

MAA is the number of carboxylic groups on the backbone per polymer chain. The height of the polymer layer was estimated from the nanomechanical data on approach as the range of the interaction (maximum distance at which force is first detected) minus $5 \times 4.3 \text{ nm}$ (the Debye length at IS=0.005M).

Polymer	pH 9			pH 6			pH 5	
		Surface Charge Model	Volume Charge Model		Surface Charge Model	Volume Charge Model	Surface Charge Model	
	$\sigma_{tip}=\sigma_{COO^-}$ (C/m ²)	$\sigma_{sub}=\sigma_{polymer}$ (C/m ²)	$\rho_{sub}=\rho_{polymer}$ (C/m ³)	$\sigma_{tip}=\sigma_{COO^-}$ (C/m ²)	$\sigma_{sub}=\sigma_{polymer}$ (C/m ²)	$\rho_{sub}=\rho_{polymer}$ (C/m ³)	$\sigma_{tip}=\sigma_{COO^-}$ (C/m ²)	$\sigma_{sub}=\sigma_{polymer}$ (C/m ²)
HS-poly(MAA-g-EG) _{27K}	-0.021	-1.2992	-4.64×10 ⁷	-0.01596	-0.98738	-4.91×10 ⁷	-0.00504	-0.31224

Table 4.2 Fixed parameters in the surface charge and volume charge models used to predict the interaction force versus distance when a probe tip ($R_{tip} \sim 50\text{nm}$) functionalized with a carboxyl-terminated self-assembling monolayer approaches a chemically end-grafted poly(methacrylic acid-g-ethylene glycol) or poly(MAA-g-EG) layer at pH9, pH6, and pH5 and a constant ionic strength of 0.005M. $\sigma_{tip} = \sigma_{COO^-}$ is the tip surface charge density due to the COO^- -SAM determined by equation (a), $\sigma_{sub} = \sigma_{polymer}$ (C/m²) is the substrate surface charge density due to the polymer layer (C/m²) determined by equation (b) in the surface charge model, and $\rho_{sub} = \rho_{polymer}$ is the volume charge density (C/m³) in the volume charge model which is determined by equation (c) above.

Surface charge model and volume charge model are based on Poisson-Boltzmann (PB) equation. The PB equation relates the spatial distribution of the electrical potential, Φ , in an electrolyte solution to the concentration of fixed and mobile charges within the electrolyte and at the boundaries of the solution phase.[103] Then the electrostatic free energy can be calculated from the spatial distribution of the electrical potential, Φ :[107, 108]

$$W_e(z, q) = \int_{surface} \sigma \Phi dS + \int_{volume} \rho_{fix} \Phi dV - \int_{volume} \left(2RTC_0 \left(\cosh\left(\frac{F\Phi}{RT}\right) - 1 \right) + \frac{\epsilon_w}{2} (\nabla\Phi)^2 \right) dV \quad (1)$$

where σ is the surface charge density due to fixed charge groups, ρ_{fix} is the volume charge density due to fixed charge groups, R is the universal gas constant(=8.314 J/mol•K), T is the absolute temperature(=298K), C_0 is the bath concentration of a containing monovalent salt, F is the Faraday constant(=96,5000 C/mol) and ϵ_w is the dielectric permittivity of water(=6.92 × 10⁻¹⁰ C/N•m²). Also the length scale over which the electrostatic potential decays is known as the Debye length, κ^{-1} .[103]

$$\kappa^{-1} = \sqrt{\frac{\epsilon_w RT}{2F^2 C_0}} \quad (2)$$

The electrostatic force acting on the brush layer is equal to the z-derivative of the free energy while keeping the charge constant:

$$F_z = \left(-\frac{\partial}{\partial z}(W_e) \right) \Big|_{q_{constant}} \quad (3)$$

The surface charge model approximates the polyelectrolyte brush as a uniform, flat constant surface charge density. The total interaction force is a linear sum of attractive van der Waals, repulsive electrostatic double layer, and hydrophilic “hydration” forces.[109] At high pH (pH8-9), the surface charge model significantly underestimated the force over the fitting range of 10-30 nm. It is because at those pHs the polymers should be mostly fully charged and would be standing up away from the surface, which is more like the volume charge model instead of surface charge model.

Volume Charge Model.[106] The volume charge model approximates the polyelectrolyte brush as a uniform volume charge density. The total interaction force is:

$$F_{total}(D) = F_{VDW}(D) + F_{electrostatic}(D) + F_{hydration}(D) + F_{steric}(D) \quad (4)$$

where the hydrophilic “hydration” force, $F_{hydration}(D)$, is a very short range (< 4 nm) repulsive force.[110] $F_{VDW}(D)$, van der Waals force, is derived by:[111]

$$F_{VDW}(D) = \frac{d \left[-\left(\frac{A}{6}\right) \left[\frac{R}{D} + \frac{R}{D+2R} + \text{LN}\left(\frac{D}{D+2R}\right) \right] \right]}{dD} \quad (5)$$

where R is the probe tip radius, D is the separation distance between the probe tip and a planar surface and A is the Hamaker constant. $F_{steric}(D)$ is the repulsion due to the deformation of polymer brush under compression.[112] In our fitting, $F_{VDW}(D)$, $F_{hydration}(D)$ and $F_{steric}(D)$ are not taken into account.

In the electrolyte region above the fixed volume charge, $F_{electrostatic}(D)$ can be calculated from eq (3), while Φ can be expressed as the PB equation:[102]

$$\nabla^2\Phi = \frac{2FC_0}{\epsilon_w} \sinh\left(\frac{F\Phi}{RT}\right) \quad (6)$$

In region inside the fixed volume charge, the PB equation is expressed as:[102]

$$\nabla^2\Phi = \frac{2FC_0}{\epsilon_w} \sinh\left(\frac{F\Phi}{RT}\right) - \frac{\rho_{volume}}{\epsilon_w} \quad (7)$$

where ρ_{volume} is the polyelectrolyte brush fixed volume charge density.

4.4 Conclusions

Macromolecular stimulus-responsive surfaces that undergo "nanomechanical switching" based on synthesized monothiol-functionalized poly(MAA-g-EG) system were prepared and tested via chemically specific high resolution force spectroscopy. It was observed the normal intersurface interaction generally changes from net repulsive (loading) and nonadhesive (unloading) to net attractive (loading) and adhesive (unloading) with decreasing pH. Comparison on the picoNewton-resolution experimental data and theoretical nanomechanical predictions of three different branched macromolecular architectures ($M_n=27K$, $L_{contour}=41nm$ and $PEG\%=7.7\%$; $M_n=15K$, $L_{contour}=22nm$ and $PEG\%=8.8\%$; $M_n=17K$, $L_{contour}=40nm$ and $PEG\%=1.9\%$) shows the molecular-level parameters such as polymer chain length and side chain grafting density affect the stimulus-responsive transition as well as the surface nanomechanical properties of the polymer layers.

At high pH, all three polymer layers are expanded, charged and hydrophilic exhibiting net repulsive interactions (loading) with the ionized -COOH SAM functionalized tip. At low pH, the polymer layers with relatively higher PEG side chain grafting density (27K, 15K) shows the typical net attractive interaction (loading) with the neutral and hydrophilic tip while the polymer layer with relatively lower PEG side chain grafting density (17K) still demonstrates repulsive interaction with the hydrophilic tip due to its more hydrophilic nature even in the collapsed and complexed state. On "retraction" (i.e. unloading, probe tip moving away from the surface), at pH 9.0 minimal hysteresis was observed and as the pH was decreased, the amount of hysteresis increased and the

curves exhibited surface adhesion. For $\text{pH} \geq 7.0$, the maximum average maximum adhesion force and distance was $0.45 \pm 0.22 \text{ nN}$ and $24.1 \pm 13.8 \text{ nm}$ (27K polymer) and $0.15 \pm 0.13 \text{ nN}$ and $14.9 \pm 4.7 \text{ nm}$ (15K polymer), respectively. For $\text{pH} \leq 6.0$, the average adhesion force and distance was $0.76 \pm 0.44 \text{ nN}$ and $20.0 \pm 11.8 \text{ nm}$ (27K polymer) and $1.80 \pm 0.62 \text{ nN}$ and $14.9 \pm 5.9 \text{ nm}$ (15K polymer).

Chapter 5

Nanomechanical Switching in Lateral Intersurface Interactions of End-Grafted Poly(methacrylic acid-g-ethylene glycol) Polymer Layer on Planar Substrate

5.1 Introduction

The friction/lubrication behavior of polymer brushes in solution has been studied in many respects in the past two decades, e.g. brush-brush sliding,[113, 114] brush-solid surface sliding[113], sliding of homopolymer brushes[115], block copolymer brushes[116], friction of neutral polymer brushes[115], charged polymer brushes[117, 118], responsive polymer brushes that are sensitive to stimulus like solvents[119] and friction of pure and mixed polymer brushes.[120] It was reported the friction coefficient between brushes of poly(methyl methacrylate)-block-poly(sodium sulphonated glycidyl methacrylate) copolymer (PMMA-b-PSGMA) could reach as low as 0.0006 – 0.001 in water[117]. In the case of stimulus responsive polymer brushes, the friction and wear properties of varied dramatically when brushes of Y-shaped polymers with one polystyrene arm and one poly(acrylic acid) arm exposed to different solvents.[119]

In this chapter, the lateral intersurface "nanomechanical switching" where the lateral intersurface force coefficient changed as macromolecules on the surface changed from

extended, negatively charged and hydrophilic conformation to collapsed, neutral and hydrophobic state with decreasing pH was studied via picoNewton-resolution experimental nanomechanical methodology. The correlations of this nanomechanical switching to the macromolecular architectures of the end-grafted polymer layers are also discussed.

5.2 Methods

5.2.1 Sample Preparation

The lateral intersurface nanomechanical properties of end-grafted polymer layers were measured on micro-contact printed samples in 0.005M ionic strength (IS) buffered aqueous solution as a function of pH using contact mode AFM.

The patterned samples were prepared with micrometer-sized areas of the end-grafted poly(MAA-g-EG) surrounded by areas of a neutral hydroxyl-terminated self-assembled monolayer (OH-SAM). A polydimethylsiloxane stamp with a hexagonal pattern with 15 μm side lengths was compressed onto piranha (98% H_2SO_4 /30% H_2O_2 , volume ratio 3:1)-cleaned Au substrates using 2mM ethanol solution of 11-mercaptoundecanol, $\text{HS}(\text{CH}_2)_{11}\text{OH}$ (Sigma-Aldrich), to fill the areas outside of the lines. Then the patterned substrate was immersed into a DTT-treated poly(MAA-g-EG) solution of 0.4 mg/mL for 72 h to allow the polymer to chemisorb to the inner areas of the hexagons. The samples were rinsed thoroughly with methanol, ethanol, and DI water prior to experimentation. Height images were taken as a function of pH using these samples by contact mode atomic force microscopy (AFM) imaging in 0.005M ionic strength (IS) buffered aqueous solution as a function of pH. pH 4, pH5 and pH6 buffer solutions were formate, acetate, and MES, respectively, while pH7.1, pH8 and pH9 were Tris. All buffer solutions used sodium chloride to adjust the ionic strength to 0.005M.

5.2.1 Lateral Force Spectroscopy

A Au-coated Si_3N_4 V-shaped cantilevers with square-pyramidal nanosized probe tips (Veeco, Santa Barbara, CA; nominal spring constant, $k = 0.06 \text{ N/m}$) were functionalized

with a hydroxyl-terminated SAM (OH-SAM) by immersing in a 2 mM ethanol solution of a HS(CH₂)₁₁OH (Sigma-Aldrich) for 24h and were used as a force transducer to record lateral force, F_{lateral} (nN), versus normal force, F_{normal} (nN). The scanning parameters were: normal force ~1-20 nN, scan rate=1 Hz, tip velocity=80 $\mu\text{m/s}$, scan size=40 μm . During lateral force microscopy scans, polymer layer heights as well as friction signal on trace and retrace were recorded simultaneously. As the probe tip scans across the surface under a constant normal force, the cantilever twists in the scanning (lateral) direction resulting in a horizontal deflection of the laser spot on a 4-quadrant position sensitive photodiode (PSPD), giving a voltage output proportional to lateral deflection. Individual 30 μm lateral signal "loops" comprised of a forward line scan (trace) and reverse (retrace) were recorded during imaging. The magnitude of the lateral force during the scan line was calculated as the product of the average lateral deflection signal (one half the trace minus retrace signal) and the lateral sensitivity of the cantilever (nN/V) derived from separate calibration. For each individual scan line, 256 data points were recorded on each trace and retrace line. Ten data points at the beginning and end of the loop (the tip reversal region), and ten data points corresponding to each pattern edge were excluded. Lateral force microscopy images of individual polymer patterned hexagons, demonstrating the lateral cantilever deflection signal at each scan location (in the unit of volt, proportional to the absolute value of lateral force), were also created to directly visualize the lateral force contrast between the inside and outside of the hexagonal patterned areas of the micro-contact printed surfaces. The lateral force was derived from the average of 16 scan lines.

The calibration of the nanosized tip for lateral force microscopy was conducted on a TGF11 silicon calibration grating follow the protocol described in literatures.[121, 122] A series of the half-width of the lateral signal loop, W , and the offsets of the loop, Δ , were obtained from raw AFM data with varying normal load. The two slopes of W versus normal load and Δ versus normal load were fitted and used to calculate the friction constant μ . The cantilever lateral sensitivity α (nN/V) was then calculated based on the known friction constant μ , the geometry of the calibration grating and the previously obtained slope of W versus normal load or Δ versus normal load.

Wedge method for calibration of nanosized probe tips [122]

The details of calibrating nanosized probe tips for lateral force spectroscopy have been reported by Han and Grodzinsky.[122] When a nanosized probe tip was scanned on a tilted surface, the normal deflection profiles detected by AFM during the uphill motion (trace) and down hill motion (retrace), L_u and L_d , were different. The deflection signals recorded were used to calculate the normal forces exerted from the cantilever,

$$L = (d + s - b_v) \times \beta \quad (1)$$

where d is the vertical deflection signal, s the setpoint, b_v the vertical baseline (corresponding to the vertical signal in the unengaged state), and β (nN/V) the cantilever's normal deflection sensitivity, which is the product of its normal spring constant k (nN/nm) and inverse optical lever sensitivity (nm/V). For a given tilted angle θ and tip scanning rate, d was observed to be independent of s and remained constant during scanning under a series of vertical setpoints. In addition, it was found that for uphill and downhill motion,

$$d_u = -d_d \quad (2)$$

The applied normal force can be rewritten as

$$L_u = L_0 + \delta \quad (3)$$

$$L_d = L_0 - \delta \quad (4)$$

where $L_0 = (s - b_v) \times \beta$ is the normal force on the horizontal surface (the subscript 0 indicates the force on the horizontal region), and $\delta = d_u \beta$ is the additional normal force that resulted from scanning on a tilted surface. The value δ was observed to remain constant for the series of applied normal forces L_0 at a given tilted angle and tip displacement rate. Hence,

$$W_0 \alpha = \frac{\mu L_0 + (1 + \mu^2) \delta \sin \theta \cos \theta}{\cos^2 \theta - \mu^2 \sin^2 \theta} \quad (5)$$

$$\Delta_0(\theta - 0) \alpha = \frac{\mu \delta + (1 + \mu^2) L_0 \sin \theta \cos \theta}{\cos^2 \theta - \mu^2 \sin^2 \theta} \quad (6)$$

$W_0(0)$, $W_0(\theta)$ and $\Delta_0(\theta - 0)$ were plotted as a function of applied normal force L_0 , where the slopes $W_0' \equiv dW_0/dL_0$ and $\Delta_0'(\theta - 0) \equiv d\Delta_0(\theta - 0)/dL_0$ could be derived. Due to the

observed independence of δ on L_θ , the lateral proportionality coefficient μ between the tip and substrate in the tilted region was calculated following

$$\mu + \frac{1}{\mu} = \frac{2\Delta'_0(\theta-0)}{W'_0(\theta)\sin 2\theta} \quad (7)$$

The lateral sensitivity α was calculated as

$$\alpha = \frac{1}{W'_0(\theta)} \frac{\mu}{\cos^2 \theta - \mu^2 \sin^2 \theta} \quad (8)$$

And the lateral proportionality coefficient on the horizontal surface was then calculated as

$$\mu_0 = \alpha W'_0(\theta) \quad (9)$$

The true physical value of μ and μ_0 may not be equal but should be close to each other. Hence the physical solution from the two possible roots derived from equations (7) to (9), (μ_1, α_1) and (μ_2, α_2) was determined by comparing the values of $|\mu - \mu_0|$; the solution corresponding to the smaller $|\mu - \mu_0|$ is the real solution.

5.3 Results and Discussion

Lateral Intersurface Interactions Using a Nanosized Probe Tip

The lateral nanomechanical properties of the end-grafted 17K and 27K polymer layers was measured in 0.005M ionic strength (IS) buffered aqueous solution at pH9 - pH4 via contact angle AFM on micro-contact printed samples with a nanosized probe tip functionalized with a OH-terminated SAM at a scan angle of 90°. **Figure 5.1** shows the AFM images of the 17K polymer layers at pH9 - 4 under a normal load ~4 nN. The hexagonal pattern on trace (forward line scan) and its counterpart on retrace (reversed line scan) forms a lateral force signal “loop”. 256 data points were recorded on each trace and retrace line. The images of individual polymer patterned hexagons, demonstrating the lateral cantilever deflection signal at each scan location (in the unit of volt, proportional to the absolute value of lateral force), directly visualizing the lateral

10 μm

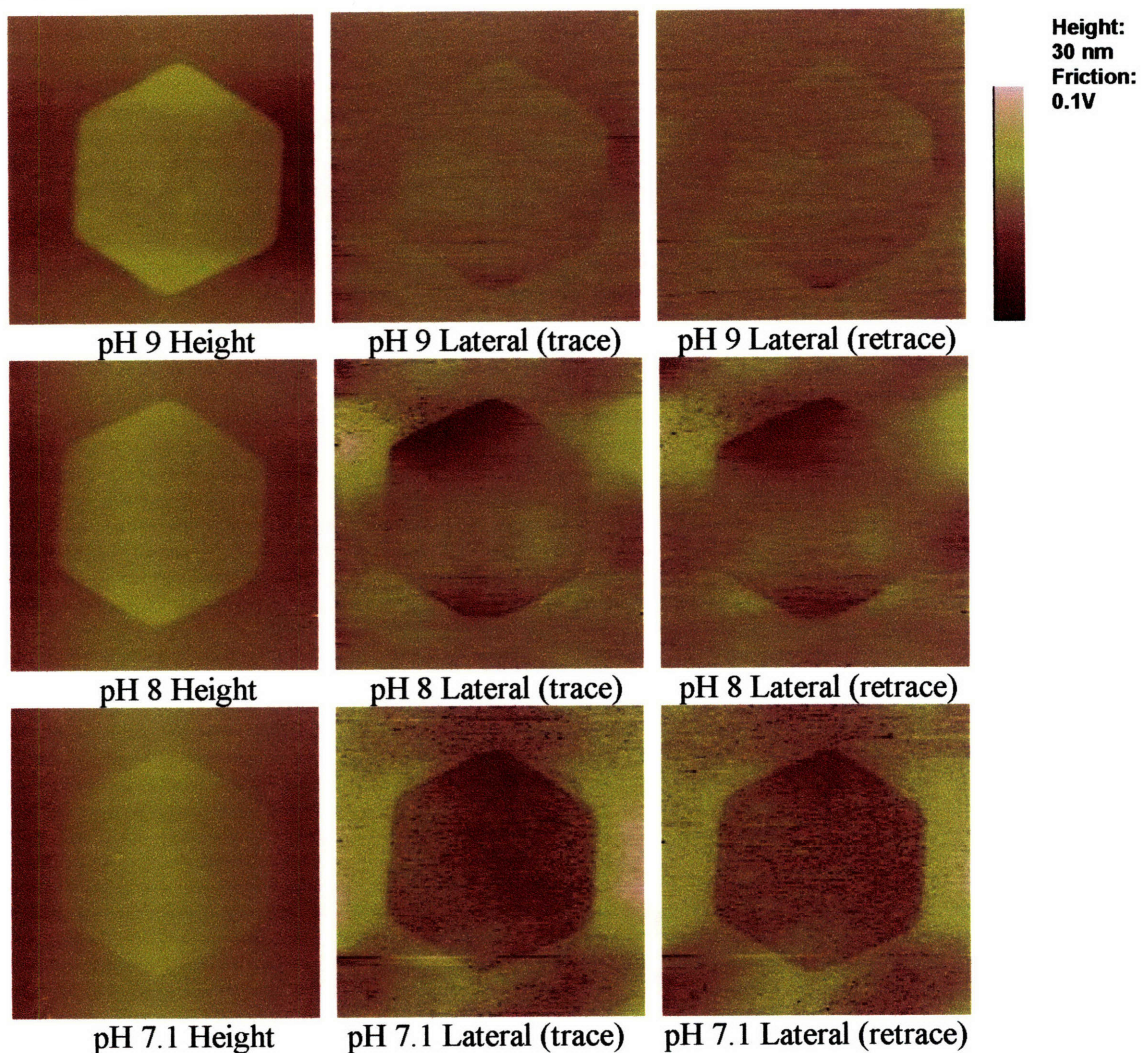


Figure 5.1a Lateral Force Microscopy images of chemically end-grafted 17K poly(MAA-g-EG) layers obtained via contact mode AFM on micro-contact printed samples at scan angle = 90° under normal force ~ 4 nN in aqueous buffer solutions of pH 9 - pH 7.1 and IS=0.005M. The probe tip was -OH functionalized.

10 μm

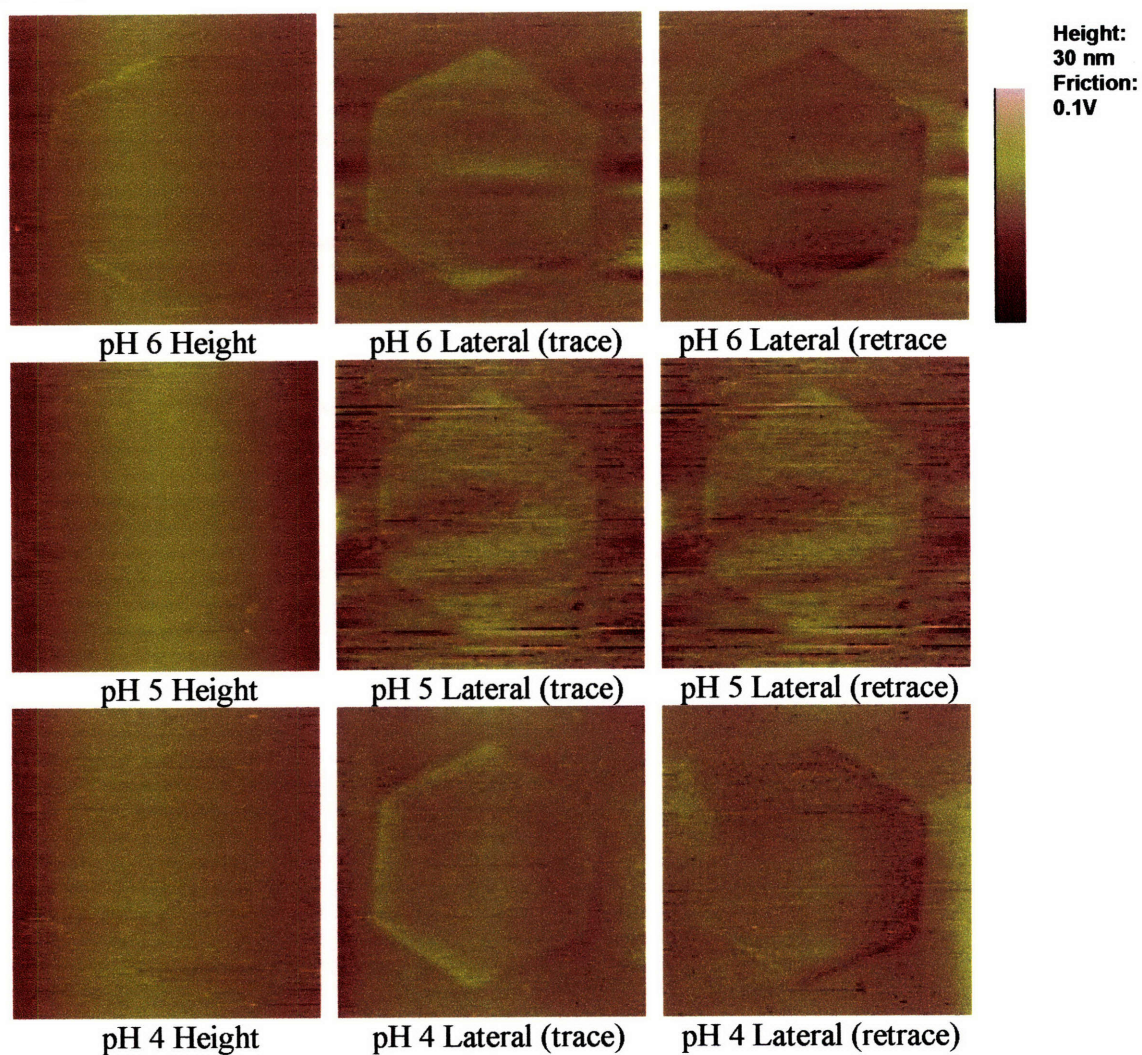


Figure 5.1b Lateral Force Microscopy images of chemically end-grafted 17K poly(MAA-g-EG) layers obtained via contact mode AFM on micro-contact printed samples at scan angle = 90° under normal force ~ 4 nN in aqueous buffer solutions of pH 6 - pH 4 and IS=0.005M. The probe tip was -OH functionalized.

force contrast between the inside and outside of the hexagonal patterned areas of the microcontact printed polymer surfaces. The height image shows that the polymer brush height gradually decreases under the same magnitude of normal load as decreasing pH. To convert the lateral cantilever signal (volt) into later force (nN), the cantilever lateral sensitivity α (nN/V) was calculated using an extension of the “wedge method” and was found to be 124.2 nN/V during the imaging. The normal deflection sensitivity β (nN/V) was determined by calibrating the normal cantilever spring constant via the thermal oscillation method.[123] Based on these methods, lateral force was measured as a function of the applied normal force. On the lateral force scan lines, ten data points at the beginning and end of the loop (the tip reversal region), and ten data points corresponding to each pattern edge were excluded.

Figure 5.2 shows the lateral force versus normal force of the chemically end-grafted 17K and 27K poly(MAA-g-EG) layers in aqueous buffer solutions of pH9 - pH4 and IS = 0.005M. At pH 4-5, the lateral force increases almost linearly as the normal force for both 17K and 27K polymer layers. At pH 7.1-9, there are two observations: first, the proportionality coefficient between lateral and normal forces is significantly smaller than the values at pH 4-5; second, there are two regimes for the correlation between lateral force and normal force. At smaller normal load (~ 6 nN for 17K, ~ 8 nN for 27K), the lateral forces are small, random and not closely correlated to the normal force. When higher normal forces are applied to the probe tip, lateral force increases more linearly as normal load. Similar two-regime observation has also been found in the lateral force microscopy of cartilage aggrecan macromolecules using -OH functionalized nanosized probe tip, which was attributed to the intersurface interaction between probe tip and the substrate when full aggrecan compression and tip penetration occur at high normal force.[124] As described in previous chapters, the 17K and 27K polymers have similar contour length but different side chain grafting density (contour length = 40 nm, 1.9% PEG for 17K polymer and contour length = 41 nm, 7.7% for 27K polymer). At high pH (pH 7.1-9), higher side chain grafting density results in larger intramolecular electrostatic repulsion, therefore the normal force required to enter the regime of considerable probe tip-substrate interaction is larger for the 27K polymers. At low pH (pH4-5), the polymers are fully collapsed and form a hydrophobic surface, the adhesion between the hydrophilic

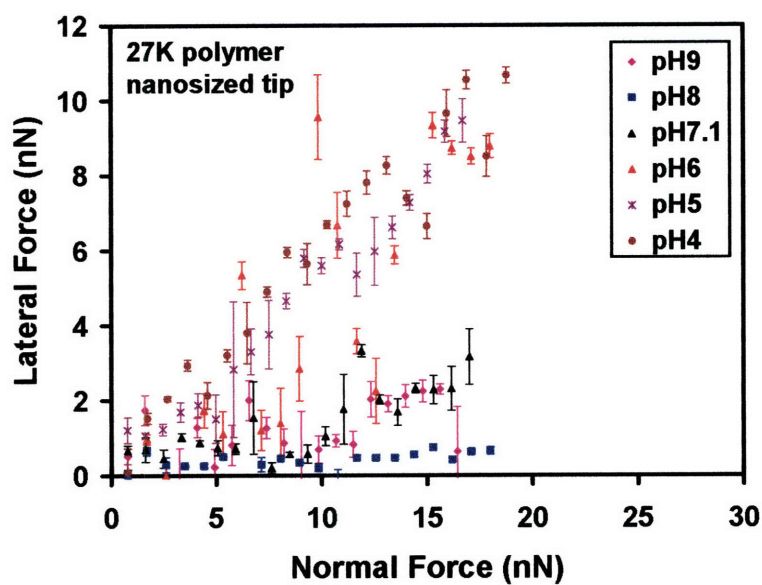
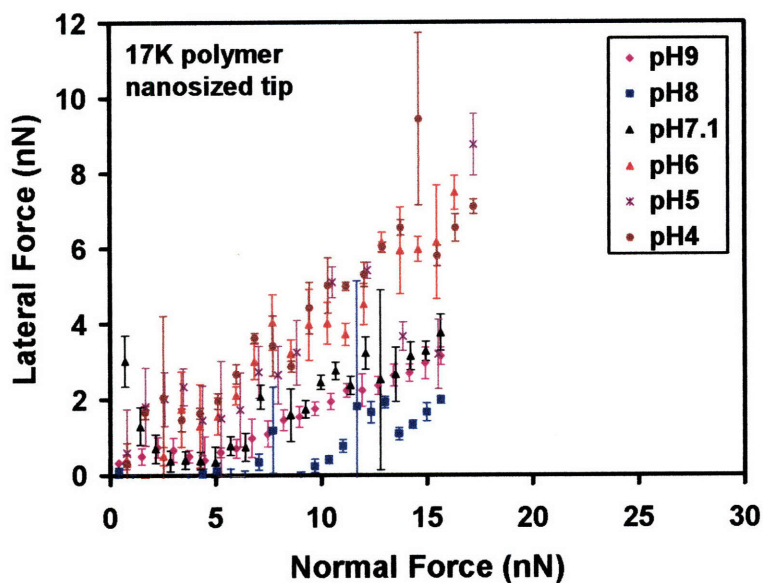


Figure 5.2 Lateral force versus normal force of the chemically end-grafted 17K, 27K poly(MAA-g-EG) layers via contact mode AFM on micro-contact printed samples at scan angle = 90° in aqueous buffer solutions of pH 9-4 (IS=0.005M) using -OH functionalized probe tip. Every data point represents the mean and standard deviation of 16 independent lateral signal loops under a fixed normal load.

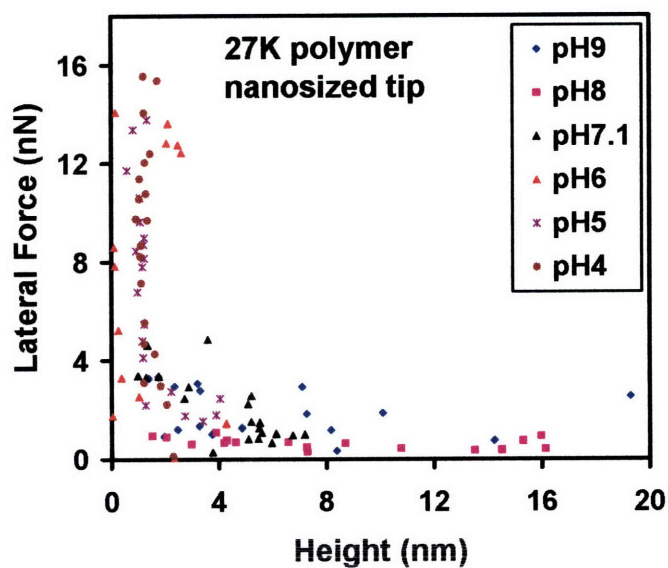
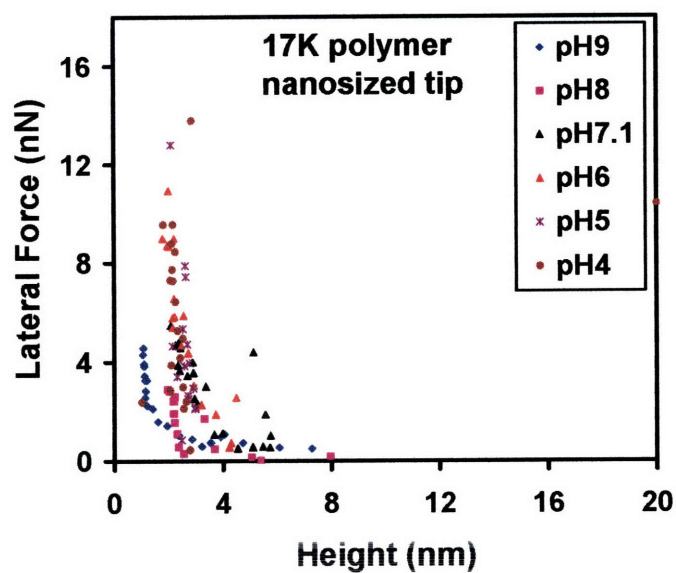


Figure 5.3 Lateral force versus height of the chemically end-grafted 17K, 27K poly(MAA-g-EG) layers via contact mode AFM on micro-contact printed samples at scan angle = 90° in aqueous buffer solutions of pH 9-4 ($IS=0.005M$) using -OH functionalized probe tip. Every data point represents the mean and standard deviation of 16 independent lateral signal loops under a fixed normal load.

-OH functionalized probe tip and the hydrophobic surface in conjunction with the probe tip-substrate interactions make the frictional coefficient much higher than at high pH.

Figure 5.3 shows how lateral forces changed with polymer layer heights for the end-grafted 17K and 27K polymer layers in aqueous buffer solutions of pH9 - pH4 and IS = 0.005M. At higher pH (pH7.1-9), the lateral force remained ~1-2 nN as the polymer layer height decreased from ~8 nm to ~2-3 nm for the 17K polymer and from ~16 nm to ~2nm for the 27K polymer, which indicates the increase in normal force has no influence on the corresponding lateral force while effectively compressing the polymer monolayers at the same time until the normal force elevates beyond a critical value. In this regime, the probe tip slides under the “lubrication” due to the repulsive interaction between the hydrophilic (-OH functionalized) probe tip and the extended, negatively charged polymer layers. At lower pH (pH4-5), the lateral force soared up with small, almost unvaried polymer layer height as normal force increases for both polymers, which is consistent with the observation of high lateral proportionality coefficient when the polymer conformational transition occurs below the critical pH. The fully collapsed polymer layers are “incompressible” even as the normal loads applied keep increasing. The polymer layer heights remained ~ 3 nm for the 17K polymer layer and ~ 2 nm for the 27K polymer as the lateral force increased from ~ 2 nN up to ~ 16 nN.

The linear fit of the experimental data gives an estimate of the lateral proportionality coefficient, as summarized in **Figure 5.4**. It is shown that the proportionality coefficient between lateral and normal forces at pH 4 was 0.63 ± 0.06 for 17K polymer and 0.78 ± 0.05 for 27K polymer, implying a more hydrophobic surface at low pH due to the higher PEG side chain grafting density of the 27K polymer. At pH 6, the 17K polymer brush showed a similar approximately linear increase in lateral force as normal load increases. However, the 27K polymer exhibited a much more scattered pairing between the lateral force and the normal force, indicating a probably very heterogeneous conformational state undergoing constantly dynamic change when external load was applied. The transition effect of pH responsiveness on lateral proportionality coefficient is shown to occur between pH 6 and pH 7.1. The 27K polymer had higher proportionality coefficients at pH < 6 but smaller coefficients at pH > 7.1, indicating that a more dramatic change is

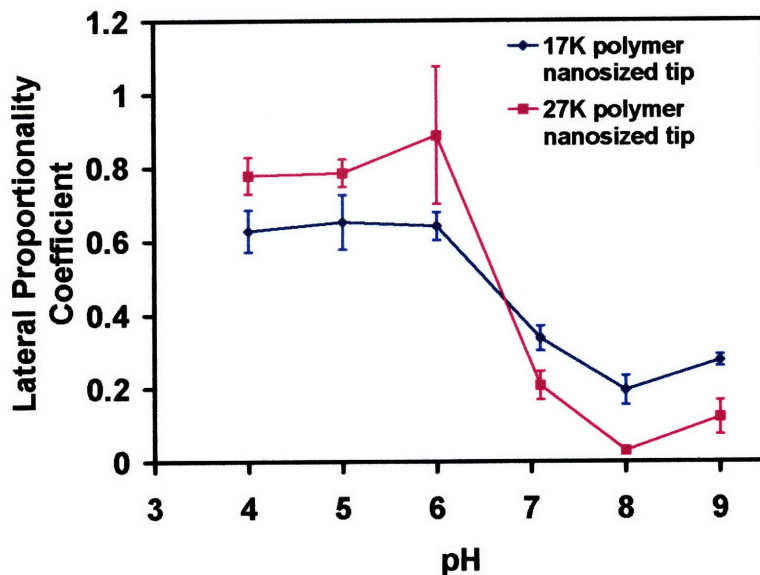


Figure 5.4 Lateral proportionality coefficients of the chemically end-grafted 17K and 27K poly(MAA-g-EG) layers via contact mode AFM on micro-contact printed samples at scan angle = 90° in aqueous buffer solutions of pH 9-4 (IS=0.005M) using -OH functionalized probe tip.

expected for stimulus-responsive graft copolymers with longer backbone and higher side chain grafting density.

5.4 Conclusions

The lateral force interaction between the end-grafted HS-poly(MAA-g-EG) polymer layers and a nanosized probe tip (nominal radius ~ 50 nm) functionalized with a OH-terminated SAM (HS(CH₂)₁₁OH) was studied in buffered aqueous solutions at pH9 - pH4 and an ionic strength of 0.005M via contact angle AFM on micro-contact printed samples at a scan angle of 90°. As pH decreased, both polymer layers exhibit an abrupt change in lateral proportionality coefficient (ratio of lateral force to normal force) between pH7.1 and pH6. At pH 4-5, the lateral force increased almost linearly as the normal force for both the 17K and 27K polymer layers. At pH 7.1-9, there were two regimes for the

correlation between lateral force and normal force. At smaller normal load ($< \sim 6$ nN for 17K, $< \sim 8$ nN for 27K), the lateral force was small (~ 1 nN for 17K and ~ 2 nN for 27K) and independent of the normal force. When higher normal forces were applied ($> \sim 8$ nN) to the probe tip, lateral force increased approximately linearly as normal load. A similar two-regime behaviour has also been found in the lateral force microscopy of cartilage aggrecan macromolecules using an OH-functionalized nanosized probe tip, which was attributed to the intersurface interaction between probe tip and the substrate when full aggrecan compression and tip penetration occur at high normal force. As pH decreases, the conformational transition of the polymer brushes will lead to a collapsed conformation and a hydrophobic surface, the adhesion between the OH-functionalized probe tip and the hydrophobic surface combined with the contribution of probe tip-substrate interactions make μ much higher than at high pH. The 27K polymer had higher μ values at pH < 6 (0.89 ± 0.19) but smaller μ at pH > 7.1 (0.21 ± 0.04), indicating that a more dramatic change in lateral force coefficient is expected for stimulus-responsive graft copolymers with higher side chain grafting density.

Chapter 6

Human Serum Albumin (HSA) Adsorption on End-Grafted Poly(methacrylic acid-*g*-ethylene glycol) Polymer Layer

6.1 Introduction

Surface bound active polymers can dynamically and reversibly capture and release biomacromolecules, such as proteins, through macromolecular conformational transitions that leads to an inversion in the intersurface interaction potential from net repulsive (hindering protein adsorption) to net attractive (promoting protein adsorption), i.e. "nanomechanical switching." The net interaction potentials are a superposition of numerous nonspecific repulsive (e.g. electrostatic counterion double layer, steric, hydration, etc.) and attractive (e.g. van der Waals, hydrophobic, H-bonding, ionic, etc.) components. In addition, secondary stages of protein adsorption depend on, for example, biomolecular adhesive binding processes, the conformation, orientation, and mobility of adsorbed proteins, the time scale of conformational changes, protein exchange and desorption, and interactions of adsorbed proteins with each other.[98, 125]

In this chapter, using human serum albumin (HAS) as a model protein, the adsorption of HSA on the end-grafted poly(MAA-*g*-EG) surface as a function of pH is studied. It is shown that the amount of HSA adsorbed on the macromolecular surface does not follow the same manner as the normal and lateral intersurface "nanomechanical switching" when

pH changes. A maximum response at intermediate pH in which range the macromolecules undergo conformational transition provides novel insight into the correlation between the protein-polymer brush interaction and polymer brush conformation down to a scale of ~ 20-40 nm as well as how molecular-level parameters such as polymer chain length and side chain grafting density affect the nanomechanical transition.

6.2 Methods

6.2.1 Materials and Sample Preparation

Human serum albumin or HSA (fatty acid free, ~97-99% lyophilized, Sigma-Aldrich A9511). The end-grafted poly(MAA-*g*-EG) monolayers were prepared on the sensor chip Au surfaces (SIA Kit Au, Biacore AB, Sweden). Any terminal disulfide bonds formed by the -SH end groups of HS-poly(MAA-*g*-EG) were reduced to a thiol group by diluting polymer to 200 µg/mL of methanol solution in 0.1 mM dithiothreitol (DTT, Sigman Aldrich) and incubating under continuous stirring for 1 h. After removal of the excess reactants using centrifugal filters (Centricon, Millipore, 3000 MW cutoff), the sensor chip Au surfaces were immersed in 0.4 mg/mL of the polymer solution in methanol for 72 h. The end-grafted poly(MAA-*g*-EG) surfaces were rinsed with acetone, methanol, and water thoroughly before experimentation.

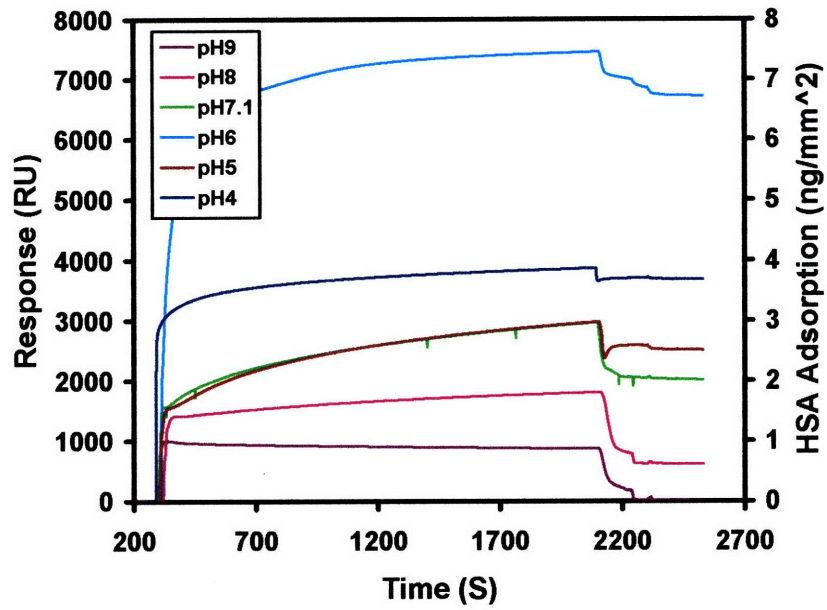
6.2.2 Surface Plasmon Resonance

Surface Plasmon Resonance (SPR) was used to measure the human serum albumin adsorption on the chemically end-grafted poly(MAA-*g*-EG) polymer brushes at different pH in BIACORE 2000 (Biacore AB, Sweden). 1 mg/ml HSA solutions were prepared in the aqueous buffer solutions of varying pH with a constant ionic strength of 0.005M. The measurement used a 2 µl/min of flow rate for HSA solution over 30 minutes. The adsorbed HSA surface concentration was calculated based on the report that 1000 resonance units of SPR response correspond to about 1 ng/mm² of surface concentration in the case of protein adsorption.[126]

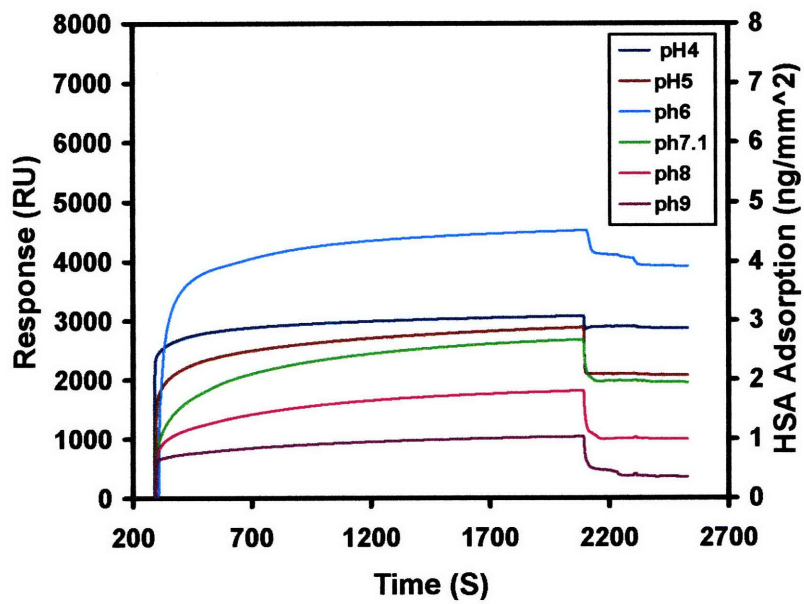
6.3 Results and Discussion

6.3.1 HSA Adsorption Triggered by pH

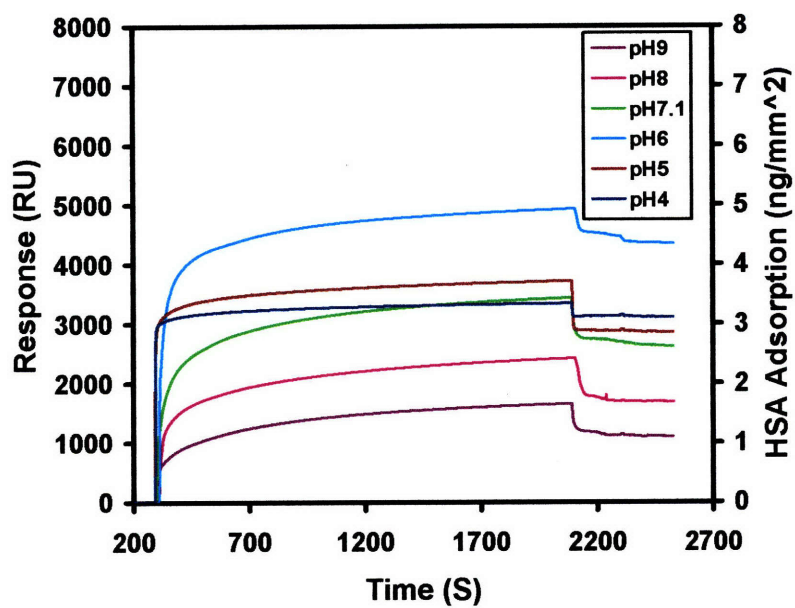
Typical SPR response of Human Serum Albumin (HSA) adsorbed on the chemically end-grafted graft polymer layers at varying pH are shown in **Figure 6.1a-c**. Human Serum Albumin has long been used as a model protein and studied extensively regarding its chemistry and structure.[127] HSA has an isoelectric point of 5.2 with a net negative charge at high pH and a net positive charge at low pH.[128] The popular HSA globule model has been reported as a prolate ellipsoid with the length and width of ~14nm and ~4 nm.[129] It was also reported as an asymmetrical shape, which can be approximated to a solid equilateral triangle with sides of ~8nm and average depth of ~3nm,[127] and an extended ellipsoid less than 11nm of length or a nonsymmetrical oblate ellipsoid with a diameter of 8.5nm, which had a molecular radius of gyration of ~2.7nm in aqueous solution containing 150 mM NaCl studied by small-angle neutron scattering.[130] In the HSA adsorption experiment, all three polymers exhibit a similar trend that the saturated surface concentration of adsorbed HSA generally increased as pH decreased, except at pH6. The adsorption of human serum albumin or HSA (fatty acid free), on the three different poly(MAA-g-EG) layers compared to a COOH-SAM was summarized in **Figure 6.2**. At pH4, all surfaces were found to adsorb proteins, consistent with the observed adhesive nanomechanical profiles, where the 15K and 17K surfaces are comparable to the COOH-SAM ($p > 0.31$) suggesting a significant hydrophobic contribution only for the longer main chain 27K polymer (statistically different from other 3 samples tested, $p < 0.03$). At pH4, the poly(MAA-g-EG) is collapsed down to heights $< \sim 2$ nm and HSA is in the F or fast conformation which is less compact, exhibits a slower rotational relaxation time, and undergoes a decrease in helical content compared to the N or normal conformation which is the most compact at physiological conditions (pH7.4).[129]



(a)



(b)



(c)

Figure 6.1 Typical SPR response of HSA adsorption on the end-grafted poly(MAA-g-EG) surfaces at different pH: (a)27K, (b)15K, (c)17K and average SPR response of HSA adsorption as a function of pH on the 27K, 15K and 17K polymer surfaces (d). Baselines are all zeroed in (a), (b) and (c). Hi-low bars in (d) represent one standard deviation for four different experiments.

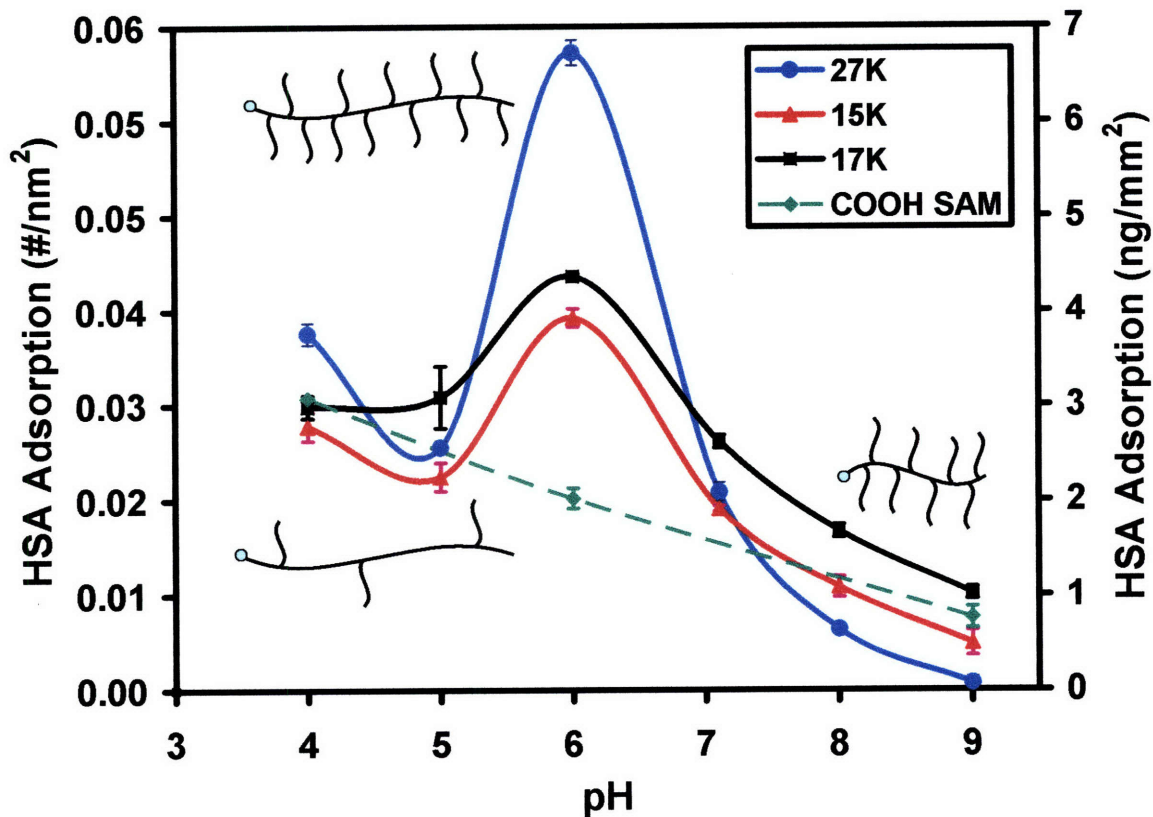


Figure 6.2 Average surface plasmon resonance response for human serum albumin adsorption as a function of pH on the 27K, 15K and 17K end-grafted poly(MAA-g-EG) substrate and COOH-SAM ($\text{HS}(\text{CH}_2)_{10}\text{COOH}$) on Au as a function of pH ($\text{IS} = 0.005 \text{ M}$). Hi-low bars represent one standard deviation for four different experiments.

At high pH9, the protein adsorption decreases dramatically for all polymer surfaces (up to 98× compared to pH6), again consistent with nanomechanical data. The low grafting density 17K polymer actually exhibits greater degree of protein adsorption compared to the COOH-SAM while the 15K is slightly less and the 27K exhibits an undetectable amount of protein adsorption. A comparison of the 17K and 27K shows the critical role of the side chain grafting density in preventing protein adsorption. The low protein adsorption of the 27K polymer at high pH (11× less than the COOH-SAM) can be attributed to a combination of HSA-polymer steric and intermolecular electrostatic double layer repulsion (both are net negatively charged) and poly(MAA-g-EG) intramolecular electrostatic repulsion which causes macromolecular chain extension thereby distributing the water-bound, hydrophilic PEG side chains[64] spatially throughout the volume of the polymer layer. Additionally, the increased apparent "diameter" of the poly(MAA-g-EG) combined with the strong binding to water of the PEG side chains is expected to inhibit short range binding mechanisms such as those suggested above for intermediate pH6. It should be noted that between pH8 and 10, HSA undergoes a conformational transition to the **B** or basic form where breaking of salt bridges in domain I and III cause a loss of rigidity.[129] The magnitude of the protein adsorption for all three polymers at pH9 was found to be statistically different from each other and the COOH-SAM ($p < 0.05$).

6.3.2 HSA Adsorption Amplification at Intermediate pH

For all polymers, as the pH is increased the protein adsorption goes through a maximum at intermediate pH6 (up to 6× greater than that at high pH9) which correlates approximately to the midpoint of the stimulus responsive transition of the poly(MAA-g-EG) and the isoelectric point (pI) of HSA.[131] Interesting, no anomalous deviations in the surface force interaction profile are observed at intermediate pH6 for the COOH-SAM functionalized probe tip (**Figure 6.2**). We hypothesize that this protein adsorption amplification behavior is due to a combination of the unique conditions that exist both for HSA at its pI and poly(MAA-g-EG) at its stimulus responsive transition which can facilitate short range binding leading to increased protein adsorption. In particular, at pH6 the poly(MAA-g-EG) is amphiphilic; partially charged (hydrophilic) and partially

complexed (hydrophobic) leading to a partially extended conformation (as indicated by the polymer layer heights of ~ 16 nm (27K), ~ 4 nm (15K), ~ 7 nm (17K) at pH6 estimated by $D_{max} \cdot 5\kappa^{-1}$ which also correlates with jump-to-contact distances) thereby exposing the complexed hydrophobic side-chain main-chain regions. This partially extended state (due to intramolecular electrostatic repulsion) combined with the low net charge and compact N form of HSA at its pI may facilitate binding to the poly(MAA-g-EG) both geometrically and chemically, possibly penetrating within or around the hydrophobic pockets of HSA[132] (used to carry fatty acids through the blood stream). Since the size of HSA in solution[129] is comparable to the height of the poly(MAA-g-EG) at this pH, diffusion through the polymer layers is not a feasible mechanism. The magnitude of the adsorption at intermediate pH is found to be greater than at low pH4 (up to 1.8 \times) presumably of the collapsed state of the poly(MAA-g-EG) layers and their decreased capability to penetrate and interact hydrophobically with the HSA. The protein adsorption amplification is observed to increase with increasing length of the poly(MAA-g-EG) backbone (**Figure 6.2**, the 27K polymer exhibits the highest peak magnitude followed by the 17K, and then the shorter 15K), consistent with our interpretation above. The higher side chain grafting density (comparing 27K to 17K) appears to facilitate binding due to the larger number of complexed hydrophobic side chains at pH6. The magnitude of the protein adsorption for all three polymers at pH6 was found to be statistically different from each other and the COOH-SAM ($p < 0.02$).

6.4 Conclusions

The end-grafted stimulus-responsive polymer "brush-brushes" from comb-like side-chain graft copolymers show that they can be used as nanomechanically switchable surfaces with tunable protein adsorption properties. The protein adsorption magnitude and form of the profile can be tuned based on the macromolecular architecture and pH range selected, i.e. a surface can be chosen to undergo large changes in protein adsorption properties for a short range of stimulus near the highly nonlinear region of the stimulus responsive transition (to act as an on-off switch, for example) or a high or low pH range can be selected for a gradual change. Based on the experimental trends observed, it is

likely that higher molecular weights and side chain grafting densities would enable even greater protein adsorption amplification at the stimulus responsive transition. Such versatility will be beneficial to the design of well-controlled bioseparation, biosensor, and drug-delivery applications. Such versatility will be beneficial to the design of well-controlled bioseparation and biosensor with programmable pulsatory capture and release of solutes by adjusting the acidity of the solution. It also provides a promising leverage for targeted drug release at specific sites where the deviation of normal physiological pH can trigger the detachment of drug molecules along with its binding proteins.

Appendix

Au Nanoparticles Functionalized with HS-Poly(methacrylic acid-g-ethylene glycol)

To prepare stimulus responsive nanostructures as shown in **Figure 1.3b**, Au nanoparticles were coated with HS-poly(methacrylic acid-g-ethylene glycol) copolymers by chemisorption in methanol/water solution. These types of stimulus-responsive polymer-capped Au nanoparticles can be then embedded into a matrix, for example, hydrogels or composite materials, to achieve tunable environment-sensitive percolation properties.

Materials and Method

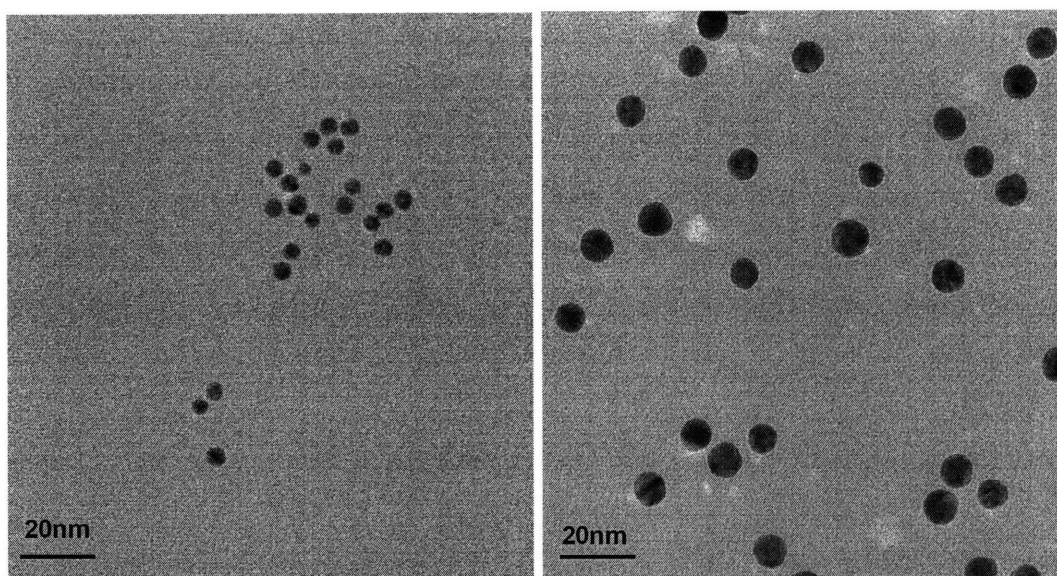
Materials: colloidal gold solutions (0.1%v/v, nominal size 5 nm, G-1402; nominal size 10 nm, G-1527; nominal size 20 nm, G-1652, Sigma-Aldrich) were used as received.

Sample Preparation and Characterization: 1 ml of colloidal gold solution was mixed with 4 ml of HS-poly(methacrylic acid-g-ethylene glycol) of 0.4 mg/ml in methanol under stirring for 72 hours. The polymer-capped gold nanoparticles in the mixture were then precipitated by centrifuging. After removing the solvent, the polymer-capped nanoparticles were dispersed in 2 ml of DI water or aqueous buffer solutions of pH9, pH8, pH7.1, pH6, pH5 and pH4 with ionic strength of 0.005M.

The gold particle size in solution was measured on 90Plus Particle Size Analyzer (Brookhaven Instruments Corporation, Holtsville, NY) at a dynamic scattering angle of 90° . The radius and shape of gold particles were also characterized by using transmission electron microscope (JEOL JEM-200CX) at HV=200 KV.

Results and Discussion

The radius and the shape of gold nanoparticles are shown by the TEM images in **Figure A1**. The gold nanoparticles were analyzed as spheres. The diameters of the two types of gold particles were calculated to be 5.0 ± 0.8 nm for 5 nm gold particles and 9.8 ± 0.7 nm for 10 nm particles respectively.



(a) (b)
Figure A1 TEM images of (a) 5 nm Au nanoparticles and (b) 10 nm Au nanoparticles.

However, the hydrodynamic size measured by dynamic light scattering in DI water turned out to be ~ 42 nm for 5 nm gold particles, ~ 11 - 29 nm for 10 nm gold particles and ~ 58 - 61 nm for 20 nm gold particles, suggesting the aggregating of gold particles in aqueous solution.

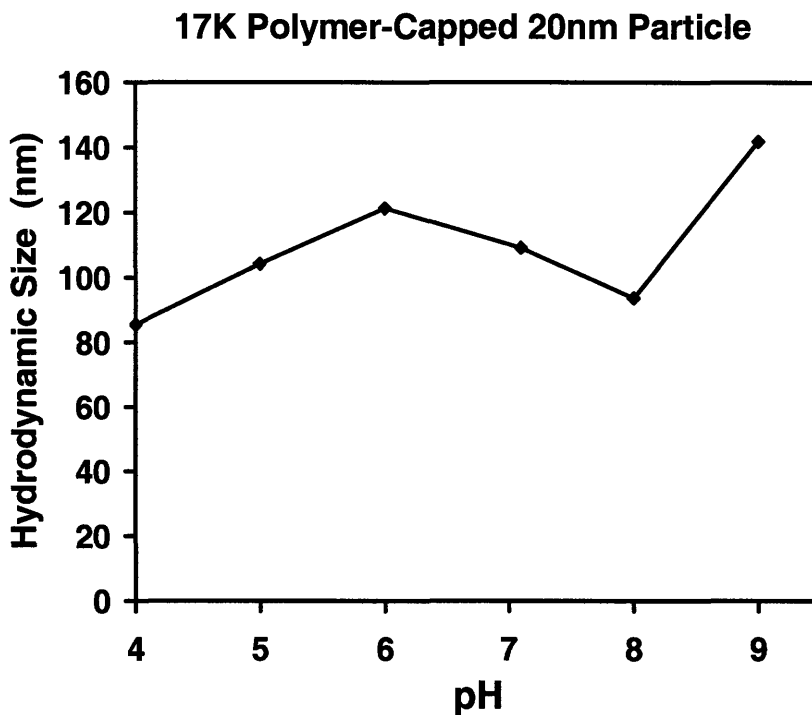
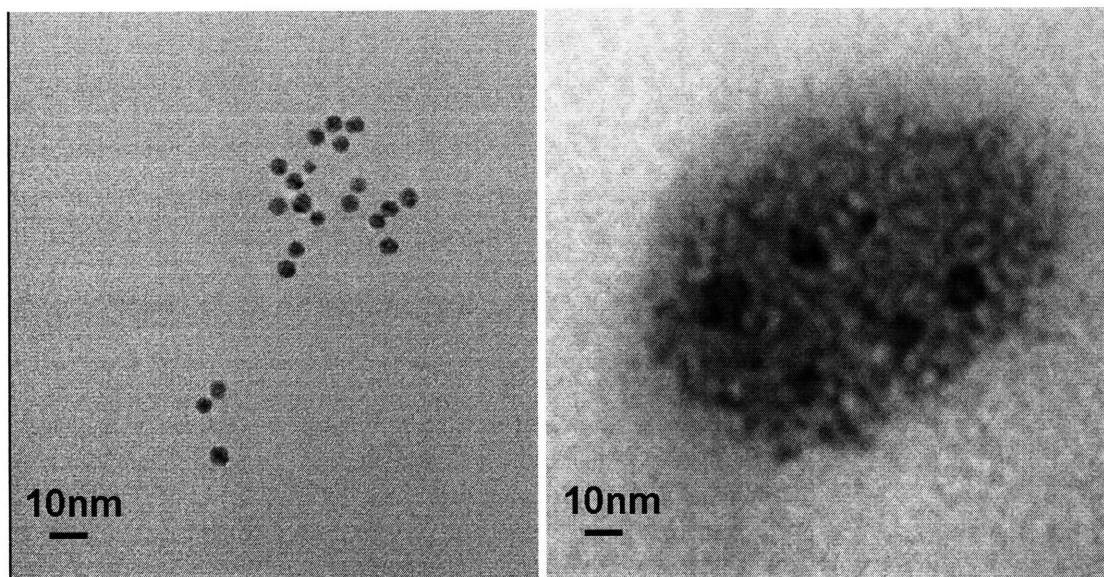


Figure A2 Hydrodynamic size of Au nanoparticles (nominal size 20 nm) capped with 17K poly(methacrylic acid-g-ethylene glycol) copolymer in aqueous buffer solutions of pH9 – pH4 at IS = 0.005M.

The hydrodynamic size of 20 nm gold particle capped with the 17K poly(methacrylic acid-g-ethylene glycol) copolymer was measured and plotted as a function of pH in **Figure A2**. Due to the aggregating behavior of gold nanoparticles, it is difficult to quantify the change in the hydrodynamic size of one single stimulus-responsive polymer capped gold particle as pH varies. However, some information about the effect of polymer conformational transition on the hydrodynamic size of polymer-capped gold particles can be extracted by comparing the hydrodynamic size at pH4 with that at pH9. At pH4, poly(methacrylic acid-g-ethylene glycol) assumes a much more hydrophobic conformation which favors the aggregation of polymer-capped gold particles. At pH9, polymers on the gold particle surface are in negatively charged, extended state with electrostatic intra- and inter-molecular repulsion and therefore the degree of aggregation should be lower than pH4. The hydrodynamic size was ~ 85 nm at pH4 and ~ 142 nm at

pH, indicating the hydrodynamic size of one single poly(MAA-g-EG)_{17K} capped 20 nm gold particles increased at least by $\sim 1.7 \times$.

TEM images of 15K polymer-capped 5 nm Au nanoparticles showed that the polymer-capped Au nanoparticles exist in aggregates of ~ 3 -6 nanoparticles (**Figure A3**).



(a) (b)
Figure A3 TEM images of (a) 5 nm Au nanoparticles and (b) 15K polymer-capped nm Au nanoparticles.

References:

- [1] Russell, T. P. Surface-responsive materials. *Science*, 297: 964-967 (2002).
- [2] Mendez, S., Ista, L. K. & Lopez, G. P. Use of stimuli responsive polymers grafted on mixed self-assembled monolayers to tune transitions in surface energy. *Langmuir*, 19: 8115 (2003).
- [3] Lahann, J. et al. A Reversibly Switching Surface. *Science*, 299: 371 (2003).
- [4] Mendez, S., Subramanian, B., Balamurugan, S. S., O'Brien II, M. J. & Lopez, G. P. LCST phase behavior of end-grafted poly(N-isopropylacrylamide). *The American Chemical Society National Meeting, Division of Polymer Chemistry, New Orleans, LA, 2003*.
- [5] Wilson, M. D. & Whitesides, G. M. The anthranilate amide of "polyethylene carboxylic acid" shows an exceptionally large change with pH in its wettability by water. *J. Am. Chem. Soc.*, 110: 8718-8719 (1988).
- [6] Bekturov, E. & Bimendina, L. A. Interpolymer Complexes. *Adv. Polym. Sci.*, 41: 99 (1981).
- [7] Tsuchida, E. & Abe, K. Interactions between Macromolecules in Solution and Intermacromolecular Complexes. *Adv. Polym. Sci.*, 45: 1-119 (1982).
- [8] Mathur, A. M., Drescher, B., Scranton, A. B. & Klier, J. Polymeric emulsifiers based on reversible formation of hydrophobic units. *Nature*, 392: 367-370 (1998).
- [9] Khokhlov, A. R., Makhaeva, E. E., Philippova, O. E. & Starodubtzev, S. G. Supramolecular Structures and Conformational Transitions in Polyelectrolyte Gels. *Makromol. Chem., Macromol.Symp.*, 87: 69 (1994).
- [10] Iliopoulos, I. & Audebert, R. Polymer Complexes Stabilized through Hydrogen Bonds: A Semiquantitative Theoretical Model. *J. Polymer Sci.: Part B: Polymer Physics*, 26: 2093 (1988).
- [11] Iliopoulos, I. & Audebert, R. Polymer Complexes Stabilized through Hydrogen Bonds. Influence of "Structure Defects" on Complex Formation: Potentiometric Study. *Eur. Polym. J.*, 24: 171 (1988).

- [12] Adachi, H., Nishi, S. & Kotaka, T. Structure and Mechanical Properties of Sequential Interpenetrating Polymer Networks II. Complex-Forming Polyoxyethylene: Poly(acrylic acid) Systems. *Polym. J.*, 14: 985 (1982).
- [13] Nishi, S. & Kotaka, T. Complex-Forming Poly(oxyethylene):Poly(acrylic acid) Interpenetrating Polymer Networks. I. Preparation, Structure, and Viscoelastic Properties. *Macromolecules*, 18: 1519-1525 (1985).
- [14] Lu, X. & Weiss, R. A. Phase Behavior of Blends of Poly(ethylene glycol) and Partially Neutralized Poly(acrylic acid). *Macromolecules*, 28: 3022 (1995).
- [15] Chen, H. L. & Morawetz, H. Fluorometric Study of the Equilibrium and Kinetics of Poly(acrylic acid) Association with Poxoxyethylene or Poly(vinyl pyrrolidone). *Eur. Polym. J.*, 19: 923-928 (1983).
- [16] Cleveland, C. S., Guigley, K. S., Painter, P. C. & Coleman, M. M. Infrared Spectroscopic Studies of Poly(styrene-co-methacrylic acid) Blends with Polytetrahydrofuran. *Macromolecules*, 33: 4278 (2000).
- [17] Drummond, R. K., Klier, J., Alameda, J. A. & Peppas, N. A. Preparation of poly(methacrylic acid-g-ethylene oxide) microspheres. *Macromolecules*, 22: 3816 (1989).
- [18] Georgiades, S. N., Vamvakaki, M. & Patrickios, C. S. Synthesis and Characterization of Double-Hydrophilic Model Networks Based on Cross-linked Star Polymers of Poly(ethylene glycol) Methacrylate and Methacrylic Acid. *Macromolecules*, 35: 4903 (2002).
- [19] Hassan, C. M., Doyle III, F. J. & Peppas, N. A. Dynamic Behavior of Glucose-responsive poly(methacrylic acid-g-ethylene glycol) hydrogels. *Macromolecules*, 30: 6166 (1997).
- [20] Hilt, J. Z., Gupta, A. K., Bashir, R. & Peppas, N. A. Ultrasensitive Biomems Sensors Based on Microcantilevers with environmentally responsive hydrogels. *Biomedical Microdevices*, 5: 177 (2003).
- [21] Kim, B. & Peppas, N. A. Complexation Phenomena in pH-Responsive Copolymer Networks with Pendent Saccharides. *Macromolecules*, 35: 9545 (2002).

- [22] Kim, B. & Peppas, N. A. Analysis of molecular interactions in poly(methacrylic acid-g-ethylene glycol) hydrogels. *Polymer*, 44: 3701 (2003).
- [23] Klier, J., Scranton, A. B. & Peppas, N. A. Self-associating networks of poly(methacrylic acid-g-ethylene glycol). *Macromolecules*, 23: 4944-4949 (1990).
- [24] Madsen, F. & Peppas, N. A. Complexation graft copolymer networks: swelling properties, calcium binding, and proteolytic enzyme inhibition. *Biomaterials*, 20: 1701 (1999).
- [25] Peppas, N. A., Huang, Y., Torres-Lugo, M., Ward, J. H. & Zhang, J. Physiochemical Foundations and structural design of hydrogels in medicine and biology. *Annu. Rev. Biomed. Eng.*, 2: 9-29 (2000).
- [26] Philippova, O. E., Karibyants, N. S. & Starodubtzev, S. G. Conformational Changes of Hydrogels of Poly(methacrylic acid) Induced by Interaction with Poly(ethylene glycol). *Macromolecules*, 27: 2398-2401 (1994).
- [27] Skirda, V. D., Aslanyan, I. Y., Philippova, O. E., Karybiants, N. S. & Khokhlov, A. R. Investigation of translational motion of poly(ethylene glycol) macromolecules in poly(methacrylic acid) hydrogels. *Macromol. Chem. Phys.*, 200: 2152-2159 (1999).
- [28] Karybiants, N. S., Philippova, O. E., Starodoubtsev, S. G. & Khokhlov, A. R. Conformational Transitions in Poly(methacrylic acid) Gel / Poly(ethylene glycol) Complexes. Effect of the Gel Cross-linking Density. *Macromol. Chem. Phys.*, 197.2373 (1996).
- [29] Oyama, H. T., Tang, W. T. & Frank, C. W. Complex formation between poly(acrylic acid) and pyrene-labeled polyethylene glycol in aqueous solution. *Macromolecules*, 20: 474-480 (1987).
- [30] Oyama, H. T., Tang, W. T. & Frank, C. W. Effect of hydrophobic interaction in the poly(methacrylic acid)pyrene end-labeled poly(ethylene glycol) complex. *Macromolecules*, 20: 1839-1847 (1987).
- [31] Polacco, G., Grazia Cascone, M., Petarca, L. & Peretti, A. Thermal behaviour of poly(methacrylic acid)/poly(N-vinyl-2-pyrrolidone) complexes. *European Polymer Journal*, 36: 2541-2544 (2000).

- [32] Sukhishvili, S. A. & Granick, S. Layered, Erasable Polymer Multilayers Formed by Hydrogen-Bonded Sequential Self-Assembly. *Macromolecules*, 35: 301-310 (2002).
- [33] Scranton, A. B., Klier, J. & Peppas, N. A. Complexation Thermodynamic of Free and Graft Oligomers with Complementary Polymers. *J. Polymer Sci.: Part B: Polymer Physics*, 29: 211-224 (1991).
- [34] Zhao, B. & Brittain, W. J. Polymer brushes: surface-immobilized macromolecules. *Prog. Polym. Sci.*, 25: 677-710 (2000).
- [35] Zhang, D. & Ortiz, C. Synthesis and single molecule force spectroscopy of graft copolymers of poly(2-hydroxyethyl methacrylate-g-ethylene glycol). *Macromolecules*, 37: 4271-4282 (2004).
- [36] Qin, S., Matyjaszewski, K., Xu, H. & Sheiko, S. S. *Macromolecules*, 36: 605-612 (2003).
- [37] Djalali, R., Li, S.-Y. & Schmidt, M. *Macromolecules*, 35: 4282-4288 (2002).
- [38] Cheng, G., Boker, A., Zhang, M., Krausch, G. & Muller, A. H. E. Amphiphilic Cylindrical Core-Shell Brushes via a "Grafting From" Process Using ATRP. *Macromolecules*, 34: 6883-6888 (2001).
- [39] Desvergne, S., Heroguez, V., Gnanou, Y. & Borsali, R. Polymacromonomers: Dynamics of Dilute and Nondilute Solutions. *Macromolecules*, 38: 2400-2409 (2005).
- [40] Heinegard, D. & Oldberg, A. Structure and biology of cartilage and bone matrix noncollagenous macromolecules. *FASEB J.*, 3: 2042-2051 (1989).
- [41] Bansil, R., Stanley, E. & LaMont, J. T. MUCIN BIOPHYSICS. *Annu. Rev. Physiol.*, 57: 635-57 (1995).
- [42] Restrepo, A. S. & Ju, L.-K. Poly(methacrylic acid) grafted with poly(ethylene glycol) and n-dodecane as pH-sensitive surfactants for water-in-oil fermentations. *Ind. Eng. Chem. Res.*, 42: 4296-4302 (2003).
- [43] Poe, G. D., Jarrett, W. L., Scales, C. W. & McCormick, C. L. Enhanced coil expansion and intrapolymer complex formation of linear poly(methacrylic acid) containing poly(ethylene glycol) grafts. *Macromolecules*, 37: 2603-2612 (2004).

- [44] Jones, M.-C., Ranger, M. & Leroux, J.-C. pH-sensitive Unimolecular polymeric micelles: Synthesis of a novel drug carrier. *Bioconjugate Chem.*: 774-781 (2003).
- [45] Dean, D., Han, L., Grodzinsky, A. J. & Ortiz, C. Compressive Nanomechanics of Opposing Aggrecan Macromolecules. *Journal of Biomechanics*, 39: 2555-2565 (2006).
- [46] Dean, D., Han, L., Ortiz, C. & Grodzinsky, A. J. Nanoscale conformation and compressibility of cartilage aggrecan using micro-contact printing and atomic force microscopy. *Macromolecules*, 38: 4047-4049 (2005).
- [47] Carrot, G., Hilborn, J. G., Trollsas, M. & Hedrick, J. L. Two General Methods for the Synthesis of Thiol-Functional Polycaprolactones. *Macromolecules*, 32: 5264-5269 (1999).
- [48] Carrot, G., Hilborn, J., Hedrick, J. L. & Trollsas, M. Novel Initiators for Atom Transfer Radical and Ring-Opening Polymerization: A New General Method for the Preparation of Thiol-Functional Polymers. *Macromolecules*, 32: 5171-5173 (1999).
- [49] Shaltiel, S. Thiolytic of some dinitrophenyl derivatives of amino acids. *Biochem. Biophys. Res. Commun.*, 29: 178-83 (1967).
- [50] Zhang, D., Macias, C. & Ortiz, C. Synthesis and solubility of (mono-) end-functionalized poly(2-hydroxyethyl methacrylate-g-ethylene glycol) graft copolymers with varying macromolecular architectures. *Macromolecules*, 38: 2530-2534 (2005).
- [51] Matyjaszewski, K. & Xia, J. Atom Transfer Radical Polymerization. *Chem. Rev.*, 101: 2921-2990 (2001).
- [52] Krishnan, R. & Srinivasan, K. S. V. Homo and block copolymers of tert-butyl methacrylate by atom transfer radical polymerization. *Euro. Poly. J.*, 40: 2269-2276 (2004).
- [53] Wang, C., Ravi, P., Tam, K. C. & Gan, L. H. Self-Assembly Behavior of Poly(methacrylic acid-block-ethyl acrylate) Polymer in Aqueous Medium: Potentiometric Titration and Laser Light Scattering Studies. *J. Phys. Chem. B*, 108: 1621-1627 (2004).

- [54] Karanam, S., Goossens, H., Klumperman, B. & Lemstra, P. Controlled Synthesis and Characterization of Model Methyl Methacrylate/tert-Butyl Methacrylate Triblock Copolymers via ATRP Macromolecules. *Macromolecules*, 36: 3051 (2003).
- [55] Wang, X. S. & Armes, S. P. Facile Atom Transfer Radical Polymerization of Methoxy-Capped Oligo(ethylene glycol) Methacrylate in Aqueous Media at Ambient Temperature. *Macromolecules*, 33: 6640-6647 (2000).
- [56] Wang, X. S., Malet, F. L. G., Armes, S. P., Haddleton, D. M. & Perrier, S. Unexpected Viability of Pyridyl Methanimine-Based Ligands for Transition-Metal-Mediated Living Radical Polymerization in Aqueous Media at Ambient Temperature. *Macromolecules*, 34: 162-164 (2001).
- [57] Coullerez, G. r., Carlmark, A., Malmstrom, E. & Jonsson, M. Understanding Copper-Based Atom-Transfer Radical Polymerization in Aqueous Media. *J. Phy. Chem.*, 108: 7129-7131 (2004).
- [58] Perrier, S., Armes, S. P., Wang, X. S., Malet, F. & Haddleton, D. M. *J. Polym. Sci., Part A: Polym. Chem.*, 99: 1696-1707 (2001).
- [59] Neugebauer, D., Zhang, Y., Pakula, T., Sheiko, S. S. & Matyjaszewski, K. Densely-Grafted and Double-Grafted PEO Brushes via ATRP. A Route to Soft Elastomers. *Macromolecules*, 36: 6746-6755 (2003).
- [60] Sant, V. P., Smith, D. & Leroux, J.-C. Novel pH-sensitive supramolecular assemblies for oral delivery of poorly water soluble drugs: preparation and characterization. *J. Control. Release*, 97: 301-312 (2004).
- [61] Ranger, M., Jones, M.-C., Yessine, M.-A. & Leroux, J.-C. From Well-Defined Diblock Copolymers Prepared by a Versatile Atom Transfer Radical Polymerization Method to Supramolecular Assemblies. *J. Polym. Sci., Part A: Polym. Chem.*, 39: 3861-3874 (2001).
- [62] Krishnan, R. & Srinivasan, K. S. V. Poly(ethylene glycol) Block Copolymers by Atom Transfer Radical Polymerization-Synthesis, Kinetics and Characterization. *J. Macromol. Sci., Part A: Pure and Applied Chemistry*, 42: 495-508 (2005).
- [63] Ali, M. M. & Stover, H. D. H. Well-Defined Amphiphilic Thermosensitive Copolymers Based on Poly(ethylene glycol monomethacrylate) and Methyl

- Methacrylate Prepared by Atom Transfer Radical Polymerization. *Macromolecules*, 37: 5219-5227 (2004).
- [64] Begum, R. & Matsuura, H. Conformational properties of short poly(oxyethylene) chains in water studied by IR spectroscopy. *J. Chem. Soc., Faraday Trans.*, 93: 3839-3848 (1997).
- [65] Fang, Z. & Kennedy, J. P. Novel Block Ionomers: I. Synthesis and Characterization of Polyisobutylene-Based Block Anionomers. *J. Polymer Sci. A Polymer Chem.*, 40: 3662-3678 (2002).
- [66] Kwon, S.-K., Choi, W.-J., Kim, Y.-H. & Choi, S.-K. Synthesis of Amphiphilic Poly(alkyl methacrylate-*b*-methacrylic acid) by Group Transfer Polymerization and Selective Hydrolysis. *Bull. Korean Chem. Soc.*, 13: 479-482 (1992).
- [67] Shin, H. S. et al. Structural Comparison of Langmuir-Blodgett and Spin-Coated Films of Poly(*tert*-butyl methacrylate) by External Reflection FTIR Spectroscopy and Two-Dimensional Correlation Analysis. *Langmuir*, 18: 5523-5528 (2002).
- [68] Wilbur, J. L., Kumar, A., Kim, E. & Whitesides, G. M. Microfabrication by microcontact printing of self-assembled monolayers. *Adv. Mater.*, 6: 600-604 (1994).
- [69] Seog, J. et al. Direct measurement of glycosaminoglycan intermolecular interactions via high-resolution force spectroscopy. *Macromolecules*, 35: 5601-5615 (2002).
- [70] Bell, C. L. & Peppas, N. A. *Biomaterials*, 17: 1203-1218 (1996).
- [71] Ulman, A. & Tillman, N. Self-Assembling Double Layers on Gold Surfaces: The Merging of Two Chemistries. *Langmuir*, 5: 1418-1420 (1989).
- [72] Rixman, M., Dean, D. & Ortiz, C. Nanoscale Interactions Between Human Serum Albumin and Low Density Surfaces of Poly(ethylene oxide). *Langmuir*, 19: 9357-9372 (2003).
- [73] R. Konradi, H. Zhang, Biesalski, M. & Ruhe, J. in *Polymer Brushes* (eds. Advincula, R., Brittain, B., Caster, K. & Ruhe, J.) 249-270 (Wiley-VCH Verlag GmbH & Co. KGaA, Weinheim, Germany, 2004).
- [74] Zhang, H. & Ruhe, J. *Macromolecules*, 38: 4855-4860 (2005).

- [75] Holappa, S., Kantonen, L., Winnik, F. M. & Tenhu, H. Self-complexation of poly(ethylene oxide)-block-poly(methacrylic acid) studied by fluorescence spectroscopy. *Macromolecules*, 37: 7008-7018 (2004).
- [76] Khutoryanskiy, V. V., Dubolazov, A. V., Nurkeeva, Z. S. & Mun, G. A. pH Effects in the complex formation and blending of poly(acrylic acid) with poly(ethylene oxide). *Langmuir*, 20: 3785-3790 (2004).
- [77] Kizhakkedathu, J. N., Norris-Jones, R. & Brooks, D. E. Synthesis of Well-Defined Environmentally Responsive Polymer Brushes by Aqueous ATRP. *Macromolecules*, 37: 734-743 (2004).
- [78] Wesley, R. D. et al. Hydrodynamic Layer Thickness of a Polybase Brush in the Presence of Salt. *Langmuir*, 16: 4467-4469 (2000).
- [79] Guo, X. & Ballauff, M. Spherical polyelectrolyte brushes: Comparison between annealed and quenched brushes. *Phys. Rev. E*, 64: 051406 (2001).
- [80] Wu, T., Gang, P., Genzer, J., Szleifer, I. & Vlcek, P. in *Polymer Brushes* (eds. Brittain, B., Advincula, R., Ruehe, J. & Caster, K.) (Wiley & Sons, 2003).
- [81] Currie, E. P. K., A. B. Sieval, Fleer, G. J. & Stuart, M. A. C. *Langmuir*, 16: 8324-8333 (2000).
- [82] Ryan, A. J. et al. *Faraday Discussions*, 128: 55-74 (2005).
- [83] Kaholek, M., W.-K. Lee, B. LaMattina, Caster, K. & Zauscher, S. in *Polymer Brushes* (eds. Advincula, R., Brittain, B., Caster, K. & Ruhe, J.) 381-402 (Wiley-VCH Verlag GmbH & Co. KGaA, Weinheim, Germany, 2004).
- [84] Kaholek, M., Lee, W.-K., LaMattina, B., Caster, K. C. & Zauscher, S. Fabrication of stimulus-responsive nanopatterned polymer brushes by scanning-probe lithography. *Nano Letters*, 4: 373-376 (2004).
- [85] Kaholek, M. et al. Stimulus-responsive poly(N-isopropylacrylamide) brushes and nanopatterns prepared by surface-initiated polymerization. *Chem. Mater.*, 16: 3688-3696 (2004).
- [86] de las Heras Alarcon, C., T. Farhan, V. L. Osborne, Huck, W. T. S. & Alexander, C. *J. Materials Chemistry*, 15: 2089-2094 (2005).

- [87] Hyun, J., Lee, W.-K., Nath, N., Chilkoti, A. & Zauscher, S. Capture and Release of Proteins on the Nanoscale by Stimuli-Responsive Elastin-Like Polypeptide "Switches". *J. Am. Chem. Soc.*, 126: 7330-7335. (2004).
- [88] Granville, A. M., Boyes, S. G., Akgun, B., Foster, M. D. & Brittain, W. J. Thermoresponsive behavior of semifluorinated polymer brushes. *Macromolecules*, 38: 3263-3270 (2005).
- [89] Lemieux, M. et al. Reorganization of Binary Polymer Brushes: Reversible Switching of Surface Microstructures and Nanomechanical Properties. *Macromolecules*, 36: 7244-7255 (2003).
- [90] LeMieux, M. C. et al. Ultrathin binary grafted polymer layers with switchable morphology. *Langmuir*, 20: 10046-10054 (2004).
- [91] Julthongpiput, D., Lin, Y.-H., Teng, J., Zubarev, E. R. & Tsukruk, V. V. Y-shaped polymer brushes: nanoscale switchable surfaces. *Langmuir*, 19: 7832-7836 (2003).
- [92] Lin, Y.-H., Teng, J., Zubarev, E. R., Shulha, H. & Tsukruk, V. V. In-situ observation of switchable nanoscale topography for Y-shaped binary brushes in fluids. *Nano Letters*, 5: 491-495 (2005).
- [93] Balamurugan, S. et al. Thermal Response of Poly(N-isopropylacrylamide) Brushes Probed by Surface Plasmon Resonance. *Langmuir*, 19: 2545-2549 (2003).
- [94] Zhang, H. & Ito, Y. pH Control of Transport through a Porous Membrane Self-Assembled with a Poly(acrylic acid) Loop Brush. *Langmuir*, 17: 8336-8340 (2001).
- [95] Galaev, I. Y. & Mattiasson, B. "Smart" polymers and what they could do in biotechnology and medicine. *Trends in Biotechnology*, 17: 335-340 (1999).
- [96] Huber, D. L., Manginell, R. P., Samara, M. A., Kim, B.-I. & Bunker, B. C. Programmed adsorption and release of proteins in a microfluidic device. *Science*, 301: 352-354 (2003).
- [97] Hyun, J., Lee, W.-K., Nath, N., Chilkoti, A. & Zauscher, S. Capture and release of proteins on the nanoscale by stimuli-responsive elastin-like polypeptide "switches". *J. Am. Chem. Soc.*, 126: 7330-7335 (2004).

- [98] Leckband, D. Measuring Forces that Control Protein Interactions. *Ann. Rev. Biophys. Biomol. Structure*, 29: 1-26 (2000).
- [99] Ye, M., Zhang, D., Han, L., Tejada, J. & Ortiz, C. Synthesis, preparation, and conformation of stimulus-responsive end-grafted poly(methacrylic acid-g-ethylene glycol) layers. *Soft Matter*, 2: 243-256 (2006).
- [100] Vezenov, D. V., Noy, A., Rozsnyai, L. F. & Lieber, C. M. Force titrations and ionization state sensitive imaging of functional groups in aqueous solutions by chemical force microscopy. *J. Am. Chem. Soc.*, 119: 2006-2015 (1997).
- [101] Heitz, C., Rawiso, M. & Francois, J. X-ray scattering study of a poly(methacrylic acid) sample as a function of its neutralization degree. *Polymer*, 40: 1637 (1999).
- [102] Dean, D., Seog, J., Ortiz, C. & Grodzinsky, A. J. Molecular-level theoretical model for electrostatic interactions within polyelectrolyte brushes: applications to charged glycosaminoglycans. *Langmuir*, 19: 5526-5539 (2003).
- [103] Devereux, O. F. & de Bruyn, P. L. *Interaction of plane-parallel double layers* (MIT Press, Cambridge, MA, 1963).
- [104] Ohshima, H. Electrostatic repulsion between two parallel plates covered with polymer brush layers. *Colloid Polym. Sci.*, 277: 535-540 (1999).
- [105] Manning, G. S. Limiting laws and counterion condensation in polyelectrolyte solutions. I. Colligative properties. *J. Chem. Phys.*, 51: 924-930 (1969).
- [106] Ohshima, H. Electrostatic repulsion between two parallel plates covered with polymer brush layers. *Colloid Polym. Sci.*, 277: 535-540 (1999).
- [107] Sharp, K. A. & Honig, B. Calculating total electrostatic energies with the nonlinear Poisson-Boltzmann equation. *J. Phys. Chem.*, 94: 7684-7692 (1990).
- [108] Shestakov, A. I. & Milovich, J. L. Solution of the nonlinear Poisson-Boltzmann equation using pseudo-transient continuation and the finite element method. *J. Colloid Interface Sci.*, 247: 62-79 (2002).
- [109] Verwey, E. J. W. & Overbeek, J. T. G. *Theory of the Stability of Lyophobic Colloids* (Elsevier, Amsterdam, 1948).
- [110] Israelachvili, J. N. *Intermolecular and surface forces* (Academic Press, London, 1992).

- [111] Bhattacharjee, S. & Elimelech, M. Surface element integration: a novel technique for evaluation of DLVO interaction between a particle and a flat plate. *J. Colloid Interface Sci.*, 193: 273-285 (1997).
- [112] de Gennes, P. G. Polymers at an interface: a simplified view. *Adv. Colloid Interface Sci.*, 27: 189-209 (1987).
- [113] Dhinojwala, A. C., L; Granick, S. Critique of the friction coefficient concept for wet (lubricated) sliding. *Langmuir*, 12: 4537-4542 (1996).
- [114] Klein, J. K., E; Mahalu, D; Perahia, D; Fetters, LJ. Reduction of Frictional Forces between Solid-Surfaces Bearing Polymer Brushes. *Nature*, 370: 634-636 (1994).
- [115] Klein, J. K., E; Perahia, D; Mahalu, D; Warburg, S. Interfacial Sliding of Polymer-Bearing Surfaces. *Faraday Discussions*, 98: 173-188 (1994).
- [116] Kampf, N. G., JF; Jerome, R; Klein, J. Normal and shear forces between a polyelectrolyte brush and a solid surface. *Journal of Polymer Science Part B - Polymer Physics*, 43: 193-204 (2005).
- [117] Raviv, U. G., S; Kampf, N; Gohy, JF; Jerome, R; Klein, J. Lubrication by charged polymers. *Nature*, 425: 163-165 (2003).
- [118] Kobayashi, M. T., Y; Hosaka, N; Kaido, M; Suzuki, A; Yamada, N; Torikai, N; Ishihara, K; Takahara, A. Friction behavior of high-density poly(2-methacryloyloxyethyl phosphorylcholine) brush in aqueous media. *Soft Matter*, 3: 740-746 (2007).
- [119] LeMieux, M. L., YH; Cuong, PD; Ahn, HS; Zubarev, ER; Tsukruk, VV. Microtribological and nanomechanical properties of switchable Y-shaped amphiphilic polymer brushes. *Advanced Functional Materials*, 15: 1529-1540 (2005).
- [120] McNamee, C. Y., S; Higashitani, K. Preparation and characterization of pure and mixed monolayers of poly(ethylene glycol) brushes chemically adsorbed to silica surfaces. 23: 4389-4399 (2007).
- [121] Ogletree, D. F., Carpick, R. W. & Salmeron., M. Calibration of frictional forces in atomic force microscopy. *Rev. Sci. Instrum.*, 67: 3298-3306 (1996).
- [122] Han, L., Dean, D., Ortiz, C. & Grodzinsky, A. J. Lateral Nanomechanics of Cartilage Aggrecan Macromolecules. *Biophysical Journal*, 92: 1384-1398 (2007).

- [123] Hutter, J. L. & Bechhoefer, J. Calibration of atomic-force microscope tips. *Rev. Sci. Instrum.*, 64: 1868-1873 (1993).
- [124] Han, L., Dean, D., Ortiz, C. & Grodzinsky, A. J. Lateral Nanomechanics of Cartilage Aggrecan Macromolecules. *accepted by Biophysical Journal* (2006).
- [125] Ostuni, E., Chapman, R. G., Holmlin, R. E., Takayama, S. & Whitesides, G. M. D. Survey of structure-property relationships of surfaces that resist the adsorption of protein. *Langmuir*, 17: 5605-5620 (2001).
- [126] Stenberg, E., Persson, B., Roos, H. & Urbaniczky, C. Quantitative-Determination of Surface Concentration of Protein with Surface-Plasmon Resonance Using Radiolabeled Proteins. *Journal of Colloid and Interface Science*, 143: 513-526 (1991).
- [127] He, X. M. & Carter, D. C. Atomic-Structure and Chemistry of Human Serum-Albumin. *Nature*, 358: 209-215 (1992).
- [128] Malamud, D. & Drysdale, J. W. Isoelectric Points of Proteins - Table. *Analytical Biochemistry*, 86: 620-647 (1978).
- [129] Peters, T. Serum-Albumin. *Advances in Protein Chemistry*, 37: 161-245 (1985).
- [130] Kiselev, M. A., Gryzunov, Y. A., Dobretsov, G. E. & Komarova, M. N. The size of human serum albumin molecules in solution. *Biofizika*, 46: 423-427 (2001).
- [131] Gianazza, E., Firgerio, A., Astrua-Testori, S. & Righetti, P. G. *Electrophoresis*, 5: 310 (1984).
- [132] Curry, S., Mandelkow, H., Brick, P. & Franks, N. Crystal structure of human serum albumin complexed with fatty acid reveals an asymmetric distribution of binding sites. *Nature Structural Biology*, 5: 827 (1998).